

**THE INFLUENCE OF THE SHORT-CHAIN FATTY ACID BUTYRATE ON
“SIGNAL TRANSDUCER AND ACTIVATOR OF TRANSCRIPTION 3” (STAT3)
AND SELECTED INFLAMMATORY GENES IN THE COLON CARCINOMA CELL LINE
CACO-2 CULTURED IN 2D AND 3D**

Inaugural dissertation to receive the degree Dr. med.
at the Faculty of Medicine
of the Julius-Maximilian-University of Würzburg

by Katharina Läsker
born in Lutherstadt Wittenberg



Würzburg, December 2021

Referee: Prof. Dr. med. Andreas Geier

Co-referee: Prof. Dr. rer. nat. Elke Butt-Dörje

Dean: Prof. Dr. med. Matthias Frosch

Day of the oral examination: 22nd November 2022

The doctoral candidate is a physician

**„DAS EXPERIMENT, DEM NICHT EINE THEORIE, D.H. EINE IDEE VORAUSGEHT,
VERHÄLT SICH ZUR NATURFORSCHUNG
WIE DAS RASSELN EINER KINDERKLAPPER ZUR MUSIK.“**

Justus Freiherr von Liebig (1803 - 1873),

German Chemist

Table of Contents

	<i>Page</i>
1. Introduction	1 - 23
1.1. Research in the field of intestinal dysbiosis-associated diseases – an overview ..	1 - 2
1.2. The role of a western diet and the Metabolic Syndrome	2 - 3
1.3. The role of short-chain fatty acids (SCFAs)	4 - 11
1.3.1. SCFAs and their positive effects on intestinal barrier elements	5 - 6
1.3.2. SCFA kinetics in health and disease	6 - 7
1.3.3. Functions of intestinal epithelial cells (IECs) within the intestinal barrier	7 - 11
1.3.4. A short introduction of NFκB	11
1.4. Butyrate and its known modes of action	12 - 17
1.4.1. Histone-deacetylase inhibition	12 - 14
1.4.2. Association with PPARγ	14
1.4.3. SCFA-receptor signaling	15 - 16
1.4.4. The activation of p38 MAPK	17
1.5. STAT3 – a central transcription factor within the intestinal barrier	18 - 22
1.5.1. OSM and OSMR	21
1.5.2. Additional immunologic contribution of STAT3 in the intestine	22
1.6. Aim of the study	23
2. Methods and Materials	24 - 53
General considerations	24 - 25
2.1. Cell culture and Cell culture assays	25 - 36
CACO-2 cell line	25 - 26
For this study..., splitting and passaging..., freezing and thawing of cells	26 - 27
Incubation assays	27 - 36
2.1.1. Sodium butyrate incubation assays	29 - 30
2.1.2. TSA incubation assays	30 - 32
2.1.3. SB 202190 and SB 203580 incubation assays	32 - 33
2.1.4. 2D/3D cell culture assays	33 - 36

2.2. RNA-extraction	36 - 38
2.3. cDNA-synthesis	38 - 39
2.4. Quantitative polymerase-chain-reaction (qPCR)	39 - 43
Dilution of the cDNA	39
Primer design	39 - 40
CT-value and housekeeping genes	40 - 41
qPCR	41 - 43
2.5. Protein electrophoresis/ SDS-PAGE	43 - 45
2.6. Western blot	45 - 47
2.7. Immunodetection	47 - 49
2.8. Simultaneous detection of several signaling molecules and reprobing of membrane.....	49
2.9. Data analysis and statistics	49 - 53
3. Results	54 - 93
3.1. Butyrate's effects on STAT3 in CACO-2 cells	54 - 66
3.1.1. Butyrate significantly increases pS727-STAT3 in CACO-2 cells	54 - 55
3.1.2. Time-dependency of pS727-STAT3 elevation and p38 MAPK activity	56 - 57
3.1.3. Butyrate increases total STAT3 protein	57 - 58
3.1.4. Butyrate significantly increases <i>hSTAT3</i> gene expression	59
3.1.5. Butyrate modulates STAT3 mainly via HDAC inhibition	60 - 63
3.1.6. Butyrate-caused pS727-STAT3 elevation is connected to p38 MAPK activity	63 - 66
3.2. Effects of a short-term cytokine stimulation on butyrate-caused changes of STAT3	67 - 74
3.2.1. Effects of TNF α and OSM on pS727-STAT3	67 - 69
3.2.2. Summary of effects of TNF α and OSM on total STAT3 protein	70
3.2.3. Butyrate significantly increases <i>hOSMRβ</i> gene expression	70 - 74
3.2.4. Butyrate attenuates the susceptibility of CACO-2 cells towards TNF α	75
3.3. Butyrate effects on <i>hSOCS3</i> expression	76 - 79
3.3.1. Butyrate downregulates <i>hSOCS3</i> expression in CACO-2 cells after 24h	76 - 77
3.3.2. Butyrate attenuates TNF α -induced <i>hSOCS3</i> expression	78
3.3.3. OSM has no influence on <i>hSOCS3</i> expression after 1 and 4h of exposure	78 - 79

3.4. Comparison of gene expression between a 2D and a 3D cell culture system	80 - 94
3.4.1. Butyrate increases <i>hCXCL-8</i> and decreases <i>hCCL-2</i> expression	80 - 81
3.4.2. Butyrate attenuates TNF α -induced cytokine expression and reduces I κ B protein	82 - 83
3.4.3. OSM has no effect on <i>hCXCL-8</i> and <i>hCCL-2</i> expression after 4h in 2D	84
3.4.4. Increase of <i>GPR109A</i> mRNA expression in a 3D cell culture	85 - 86
3.4.5. Differential cytokine mRNA expression in a 2D versus a 3D setting	87 - 94
<i>hCXCL-8</i>	88 - 89
<i>hCCL-20</i>	90 - 91
<i>hTNFα</i>	92 - 93
<i>hCCL-2</i>	93 - 94
4. Discussion	95 - 116
4.1. Butyrate increases pS727-STAT3 in CACO-2 cells via HDAC inhibition	95 - 106
4.1.1. An elevation of total STAT3 protein contributes to the pS727-STAT3 fraction	97
4.1.2. Possible role of phosphatase inhibition by HDAC inhibitors	97 - 100
4.1.3. Possible apoptosis induction including PKC δ activation	100 - 101
4.1.4. An activation of p38 MAPK is essential for the pS727-STAT3 elevation	101 - 106
4.1.4.1. Possible activation of a p38 MAPK upstream kinase	103 - 104
4.1.4.2. Possible support of p38 MAPK-activating signaling pathways	104 - 105
4.1.4.3. Possible role of AMPK activation	105
4.1.4.4. Possible inhibition of p38 MAPK dephosphorylation	105 - 106
4.1.4.5. Possible activation by GPR signaling	106
4.2. Butyrate effects on <i>hOSMRβ</i> expression	107 - 108
4.3. Butyrate effects on <i>hSOCS3</i> expression	108 - 109
4.4. Butyrate effects on cytokine- and GPR109A expression the significance of a 3D environment	110 - 112
4.5. Conclusions and Outlook	113 - 116
5. Summary/ Zusammenfassung	117 - 119
6. List of references	120 - 129

Appendix

- I List of scientific abbreviations and acronyms**
- II List of figures**
- III List of tables**
- IV Danksagung**

1. Introduction

1.1. Research in the field of intestinal dysbiosis-associated diseases – an overview

A disturbed host-microbiome mutualism (syn. dysbiosis) coinciding with a weakening of the intestinal barrier accompanies the development of a wide range of human chronic inflammatory and metabolic diseases. Some of them increasingly emerge in the course of adverse lifestyle and diet habits in industrial and developing countries [1]. These comprise the Metabolic Syndrome [2], Non-alcoholic fatty liver disease (NAFLD) and Steatohepatitis (NASH) [3, 4], Inflammatory bowel diseases (IBDs) [5-9], Atherosclerosis [10] and Colon- and Hepatocellular Carcinoma [11, 12].

It is long-time known that the successful symbiosis with the intestinal microbiome, which consists of a huge number of bacteria, fungi and protozoa especially concentrated in the large intestine [13, 14] plays an important role in the maintaining of the human host's health. It positively affects the immune system and metabolism in multiple respect, partly via the production of bioactive molecules [15]. This is tried to use therapeutically: Predating modern microbiome research, first kinds of fecal transplantation in humans had already been carried out in China during the 4th century, addressing the treatment of colitis [16]. Nowadays, prebiotics are in usage to promote the proliferation of beneficial bacteria, with success in the complementary treatment of the Metabolic Syndrome [17] and IBDs [5].

The numerous modulating effects exerted by intestinal bacteria have been systematically proven in animal studies, e.g. in germ-free mice [18] or mice which were colonized with a microbiome of reduced diversity [19].

Molecular microbiome research reaches back to the 1970's and made increasingly advances post-millennium, especially since molecular biologic methods have improved [20, 21]. Research in that field overall reveals the important influence of microbiome-produced bioactive substances like short-chain fatty acids (SCFAs) on cell physiology [22, 23]. From special interest is how SCFAs modulate the function of intestinal epithelial cells (IECs) [24, 25] since IECs directly participate in the immune modulation at the

intestinal barrier [26]. For instance, they deliver leucocyte-attracting cytokines. For further information see chapter 1.3.3.

Besides a shift in the intestinal microbiome composition, the perception of a “dysbiosis” comprises a change in the bacterial production and intestinal incorporation of SCFAs [25], which is further described in chapter 1.3.2.

Butyrate is a quantitatively significant representative of the SCFA class of substances. Its beneficial influence on the intestinal barrier has already been proven in animal- [27, 28] and human studies [29]. For instance, Butyrate was shown to modulate the cytokine excretion by IECs *in vitro* [30] and *in vivo* [31].

Butyrate and other SCFAs exert their effects via several molecular mechanisms. Some of them are summarized in chapter 1.4. Among others, Butyrate modulates the function of gene transcription factors which are centrally involved in the proliferation and immunomodulation of IECs. To name are NFκB, which is introduced in the chapters 1.3.4. and 1.4., and Signal transducer and activator of transcription 3 (STAT3) (see chapter 1.5.). Therapeutic approaches targeting NFκB and STAT3, e.g. in the therapy of IBD or colon cancer (rev. in [32] and [33]), show the clinical relevance of these mechanisms. However, due to a possible resistance to therapy or unpredictable side effects, the therapeutic use of the naturally evolving or artificially designed molecules in this context is still limited. Therefore, a deeper understanding of the biochemical mechanisms is of high interest.

1.2. The role of a western diet and the Metabolic Syndrome

To date, the question of whether to regard a dysbiosis as a cause or a consequence of the observed metabolic and immunologic changes in dysbiosis-associated diseases cannot finally be answered. It rather exists a vicious circle of interconnected disease elements which is exemplified in Figure 1.

In any case, the functionality of the intestinal barrier is of high significance in disease prevention. Because of the strengthening effects of SCFAs on the gut barrier (see chapter 1.3.1.), a total or relative lack of these molecules promotes an increased gut permeability and a disposition towards chronic unresolved inflammation. Such a lack

occurs at higher frequency in human populations favoring a so-called “western diet” [34, 35]. It is high-caloric and lacks in complex carbohydrates like pectin, inulin and starch which are substrates of SCFA-producing bacteria in the large intestine. The lack of SCFAs also negatively affects energy uptake [36] and fat- and glucose metabolism [17, 37]. An exemplarily symptom complex is reflected in the Metabolic Syndrome and in certain interrelated diseases. The Metabolic Syndrome encompasses a variety of symptoms that can be traced back to a chronically increased nutritional energy balance. Among them are a central obesity and a hepatic and systemic insulin resistance. Accompanying failures in vascular, hepatic and immune cell function lead to a weakening of the intestinal barrier from the tissue side and, in turn, promote the manifestation of an intestinal dysbiosis in the sense of a vicious circle (Fig. 1) [11, 38].

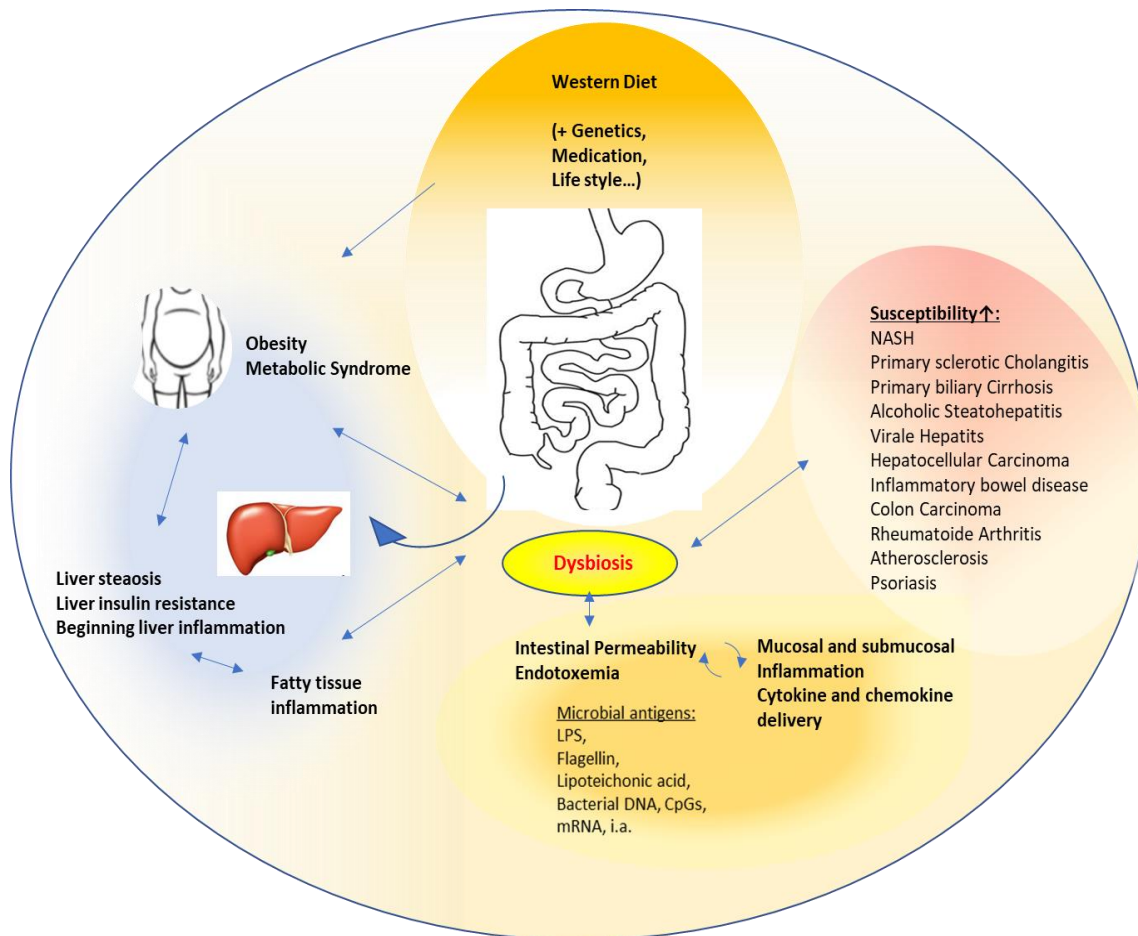


Fig. 1: Interdependent dysbiosis-contributing conditions and connected disease susceptibilities.

Adverse lifestyle habits (including a complex carbohydrate-lacking “western diet”) cause metabolic changes and chronic inflammatory processes in different organs (e.g. intestine, liver and fatty tissue). These result in the manifestation of a dysbiosis and a weakening of the intestinal barrier (so-called “leaky gut”), including an increased transintestinal passage of microbial antigens (= endotoxemia). Under these conditions, the susceptibility for the development of several diseases is increased, e.g. Non-alcoholic Steatohepatitis (NASH), Colon Carcinoma and Inflammatory bowel disease.

1.3. The role of short-chain fatty acids (SCFAs)

SCFAs are byproducts of intestinal bacterial fermentation of starch and other complex carbohydrates - mainly derived from plant components - within the colon and distal ileum. They comprehend carbonic acids consisting of two to six carbon ions within their carbonic chain. These include acetic acid (C2), propionic acid (C3), butyric acid (C4), valeric acid (C5) and caproic acid (C6) [39]. They can also origin from bacterial fermented food. E.g., acetic acid exists in vinegar and butyric acid in milk products. Some bacterial

strains (e.g. Roseburia and Faecalibacterium prausnitzii that are members of the Firmicutes-Clostridiales spp.) are especially capable to produce butyric acid because they express the enzyme butyryl-CoA acetate transferase that extends acetyl-CoA to butyryl-CoA, whereas e.g. acetate is produced by most of the bacteria (rev. in [40]). In addition to their favourable effects on fat- and glucose metabolism [17, 37, 41], SCFAs also positively affect many features of the gut barrier.

1.3.1. SCFAs and their positive effects on intestinal barrier elements

Besides being the most important energy source for enterocytes, SCFAs exert many more functions to positively modulate the immune system and the barrier elements of the intestinal epithelium:

First, SCFAs support the general function, proliferation and steady turnover of IECs. Especially butyric acid can cover up to 70% of the IECs' energy need gained by β -Oxidation [42]. Apart from that, SCFAs and their salts like sodium butyrate (Fig.2) have been shown to improve mucus- and tight junction quality [43-45]. Furthermore, they promote the production of IL-18 and bactericidal agents by IECs [46, 47] and directly support the reaction of cells belonging to the innate immune system. E.g., they strengthen the phagocytotic activities of macrophages [48]. SCFAs are also important to elicit activated mesenterial lymphocytes and innate immune cells, like neutrophils and macrophages, to the lamina propria of the intestinal mucosa [49]. Kim et al. especially emphasized the meaning of SCFA-receptor signaling (see 1.4.3.) in IECs (i.e. via GPR43 and GPR41) for the chemoattraction of neutrophils and the creation of a proinflammatory cytokine milieu that was essential for the early pathogen defense in an artificially generated ileitis by Citrobacter rodentium infection in mice [50]. Thus, SCFAs have a decisive influence on the strengthening of the "first-line" barrier function at the intestinal mucosal interface [46, 51].

At the same time, SCFAs also exert immunoregulatory and recovering effects on IECs [52] and other immunocompetent cells. This is ,e.g., known for DCs [53], macrophages [48, 54-56] and T-lymphocytes [27, 57]. Anti-inflammatory reactions are normally

initiated in concert with inflammatory processes [38, 58] in order to avoid an excessive tissue damage.

1.3.2. SCFA kinetics in health and disease

While comparatively low SCFA levels occur in the portal and systemic blood circulation [59], their total amount in the proximal colon normally reaches 70 – 140 mM/kg feces within the European population [60] with a distribution of about 60 – 20 – 20 for the predominant SCFAs: acetic acid, propionic acid and butyric acid, respectively. The affinity of SCFA-receptors is adapted to local physiological amounts [56].

SCFAs and their salts (like sodium butyrate, Fig. 2b) are weak acids. Their pKa is about 4,8 and the great majority (more than 90 %) occurs in the deprotonated – ionized – state in the presence of the more basic pH (5,5 – 6,5) in the lower small intestine and colon [61]. Therefore, absorption into enterocytes via membrane-intrinsic transport proteins is much more likely than passive diffusion as the charged ion cannot passively passage through the lipid bilayer of the cell membrane. The more intraluminal pH-values drop, the more passive diffusion is observed.



Fig. 2: Molecular structure of a) butyric acid and b) sodium butyrate

SCFAs form salts like sodium butyrate. The deprotonated form of the salt dominates in the alkaline pH of the large intestinal lumen. Na⁺ = sodium ion.

Besides the total lack of SCFAs, which can be accelerated by a “western diet” and by a chronic shift in the intestinal microbiome composition, also the intestinal incorporation of SCFAs can be decreased, especially in the case of chronic inflammation [25]. This can cause a relative increase of SCFAs in the intestinal lumen [62], which might affect the epithelium also in a negative way, since in cell culture assays, butyrate’s positive effects

on the barrier function of enterocytes were partly dose-dependent. Using an *in vitro* model of the CACO-2 monolayer, Peng et al. found a barrier-strengthening influence of butyrate at concentrations of 2 mM, whereas concentrations of 8 mM were significantly disruptive [63]. Recent stool content measurements revealed an increase of SCFAs in the feces of gamma-proteobacteria-dominated microbiome carriers [64]. The same applies to the feces of patients suffering from chronic intestinal inflammation [65]. Accordingly, the amount of SCFAs in the feces of patients that suffer from Non-alcoholic steatohepatitis (NASH) was elevated [66]. It could be shown that intestinal SCFA transport proteins get down-regulated during chronic inflammation [65].

1.3.3. Functions of intestinal epithelial cells (IECs) within the intestinal barrier

The intestinal barrier is formed by a monolayer of IECs arranged on connective tissue structures (lamina propria) and is penetrated by immune cells (Fig. 3). The tissue homeostasis of the intestine is characterized by a steady epithelial cell turnover (every 24 to 96 hours [67]) and constant tissue repair processes, including cell proliferation, -differentiation, and -apoptosis. It is also marked by the balance between immune defense against pathogens on the one hand and immune tolerance towards microbial symbionts and nutritional components on the other hand [68]. The permeability of the monolayer is a characteristic defining how soluted substances like salts and particles can pass through. It depends on the expression of specific barrier elements by IECs, like a stable mucus layer and intercellular protein bridges (so-called “tight junctions”).

The modulation of innate immune cell functions and the recruitment and differentiation of neutrophils, dendritic cells, macrophages and cells of the adapted immune system – i.e. lymphocytes – into either effector- (e.g. Th1-, Th2-, Th17- , ILC3-cells [69], IgA-producing plasma-cells) or regulatory (= anti-inflammatory) subtypes (e.g. Treg- cells) is crucial for the manifestation of a context-adapted and effective immune reaction [40]. Intestinal epithelial cells (IECs) have an important role in this by at least two mechanisms:

- 1.) The formation of a first line barrier between the intestinal lumen and the submucosa that also guarantees a polar antigen-sensing.
- 2.) The integration of environmental signals and the communication with neighboring immune- competent cells.

The communication between IECs and surrounding immune cells happens mainly via the paracrine secretion of signal molecules (e.g. cytokines, chemokines) and the modulation of the cellular receptor distribution. Situation-dependently (exemplified in the Figures 3-5), IECs can deliver proinflammatory or regulatory cytokines and factors like CXCL-8, CCL-2, CCL-20, IL-10, TSLP or TGF β [58]. The composition of this “cytokine-cocktail” contributes to the milieu that governs lymphocyte differentiation [70].

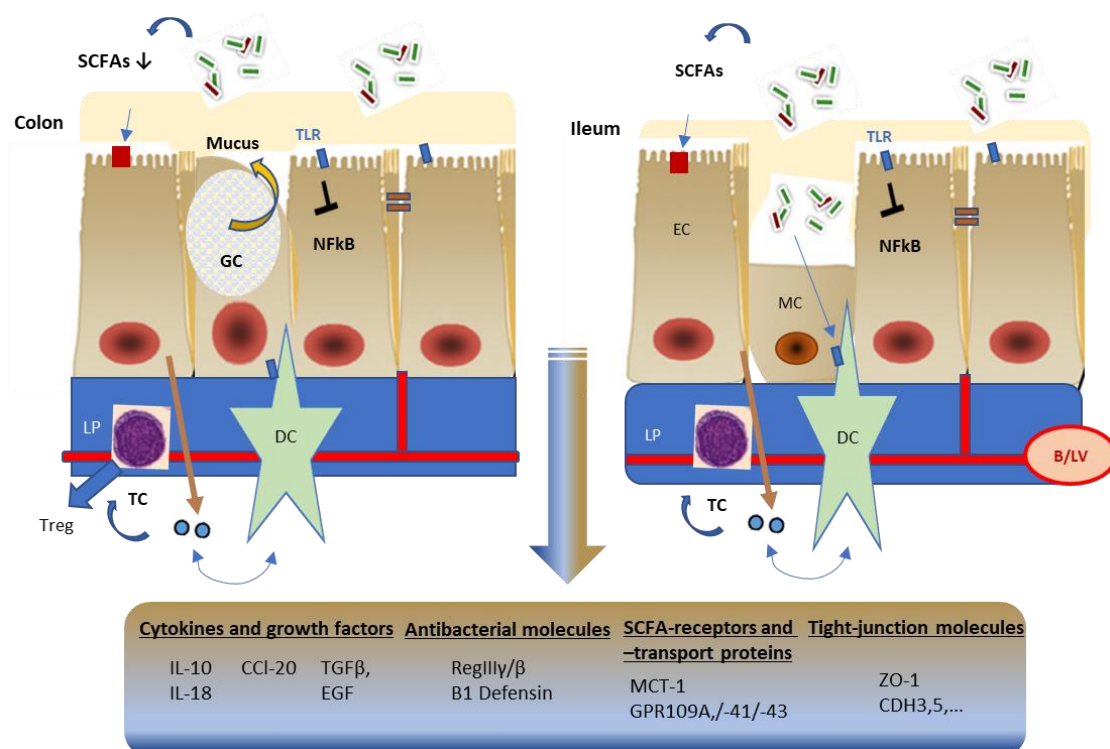


Fig 3: Homeostasis. In the state of homeostasis, there is a balance between tissue repair and antimicrobial activity. Additional abbreviations/ symbols: \equiv = tight junction complex, LP = Lamina propria (connective tissue of the mucosa) and submucosal tissue that contains blood- and lymph capillaries, connective tissue fiber producing fibroblasts and immune cells), DC = dendritic cell, TC = T-cell, TLR = Toll-like receptors, B/LV = blood- and lymph vessels, CCL-20 = T-cell attracting chemokine, EC = enterocyte, $\bullet\bullet$ = cytokines, \blacksquare = SCFA-receptor, microbiome = microbiome, \perp = blocking/deactivating.

In the state of homeostasis (Fig. 3), there is a balance between tissue repair and antimicrobial activity. The sensing of commensal microbiota by Toll-like receptors (TLRs) in the apical membrane of IECs leads to the predominant production of the tolerance-promoting cytokines TGF- β and IL-10. This enables the differentiation of T cells into regulatory subtypes (Treg.), which manifest an anti-inflammatory, tolerant and regenerating environment. TGF- β and EGF support continuous tissue renewal processes. Simultaneously, NF κ B-mediated proinflammatory cytokine production is suppressed. ECs express IL-18 that leads to a feedback loop with immune cells towards the production of antibacterial agents (RegIII, β 1-Defensin) and to the support of tissue restitution as well [71]. SCFA-carrier like MCT-1 and SCFA-sensing receptors like GPR41, GPR43 and GPR109A are continuously expressed by IECs.

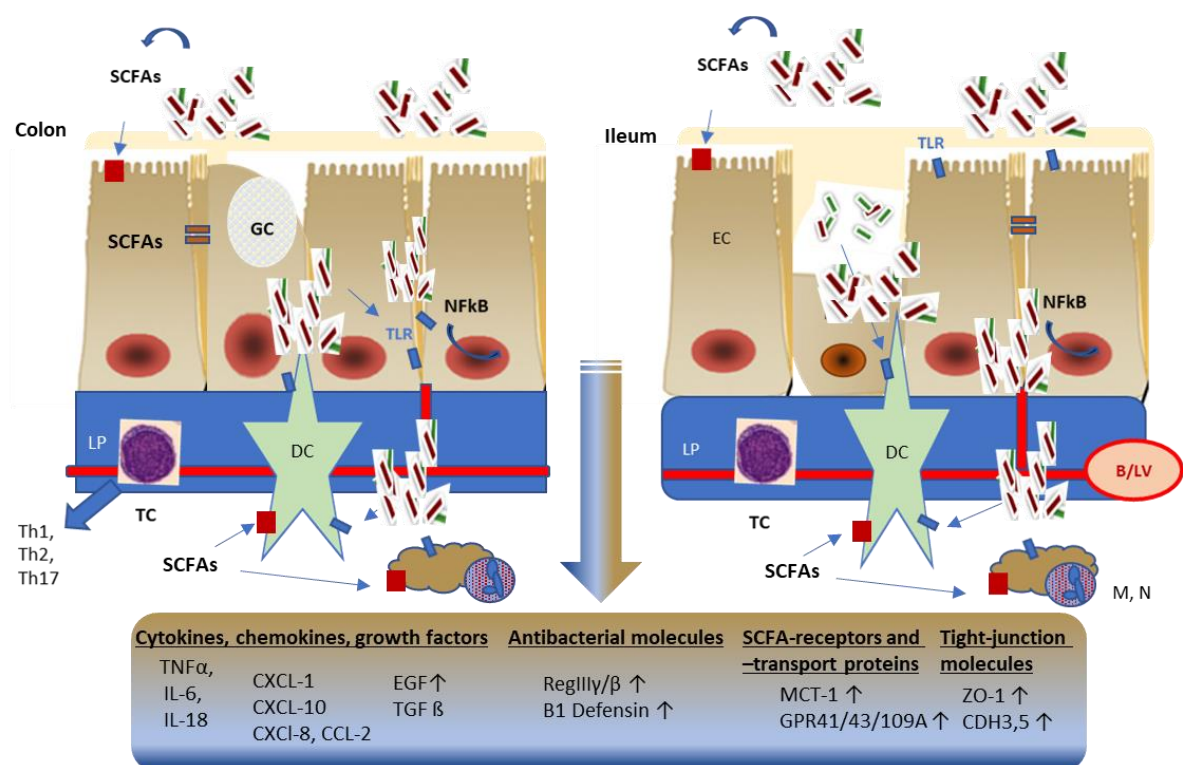



Fig. 4: Acute inflammation and recovery. Acute infection activates proinflammatory and pro-survival signaling pathways in IECs. Additional abbreviations and symbols: M = monocytes/macrophages, N = neutrophils, ZO-1 + CDH3,5 = Zonulin-1 + Cadherins 3,5 (proteins of tight junction complexes),  = dysbiotic microbiome.

The baso-lateral sensing of microbial antigens in the acute infection (Fig. 4) activates proinflammatory and pro-survival signaling pathways in IECs, leading to the plasmatic liberation of NFκB and to the subsequent expression of neutrophil-, monocyte- and lymphocyte-attracting chemokines and cytokines (e.g. IL-6, CLL-2, TNFα, CXCL-8, CXCL-1), which finally promote the differentiation of T-cells into effector-subtypes (Th1, Th2, Th17). The transfer of SCFAs by transport proteins is initially strengthened, promoting the IEC-governed acute immune reactions by a variety of mechanisms, including the fortification of tight junctions and mucus sphere as well as the forcing of IL-18- and antimicrobial peptide production by IECs. At the same time, SCFAs also exert immunoregulatory and recovering effects on IECs and other immunocompetent cells. These processes are normally initiated parallel to the acute-inflammation state, as the return to homeostasis is essential to maintain tissue integrity [38, 58].

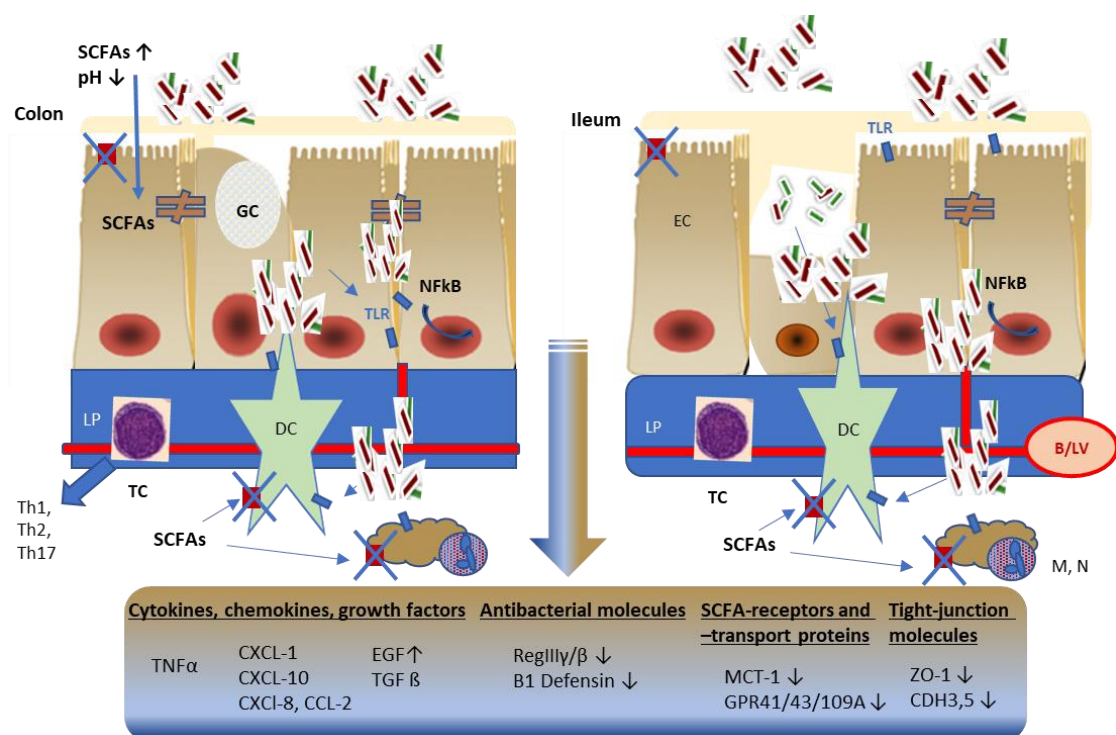


Fig 5: Chronic inflammation. A dysbiosis has established, including a higher proportion of mucus-degrading bacteria. Displayed is the invasion of bacteria, respectively the transepithelial passage of microbial antigens towards the lymph- and blood stream (=endotoxemia). The downregulation of SCFA receptors inhibits the influence of SCFAs on the immune regulation. E.g., the tight junction protein- and mucus production is decreased.

In the state of chronic inflammation (Fig. 5), the inflammatory reaction is not effective and inflammation-limiting processes are insufficient. Inflammatory processes dominate over tissue recovery. The mucus layer is thinned and SCFAs as well as bacteria get access to the cell surface at higher concentrations. The reactive downregulation of receptors and transport proteins for SCFAs inhibits their cellular uptake and sensing by IECs. Thus, they lose their immune modulative influence. Tight-junction proteins and the production of antibacterial agents are decreased and the transepithelial passage of microbial antigens towards the blood- and lymph stream is elevated (= endotoxemia). SCFAs accumulate in the intestinal lumen, the pH value drops. In combination with a prolonged cell-metabolic switch of energy production from β -Oxidation towards Glycolysis (that is characteristic for a proinflammatory environment [72]) it leads to an additional intracellular elevation of SCFA-levels, which can be cell destructive.

The reviews by L.W. Peterson et al. [26], Y. Goto et al. [73], J.M. Wells [74] or P. Gonçalves [75] give an overview of important aspects in the communication of IECs with other cells of the intestinal immune system.

1.3.4. A short introduction of NF κ B

The transcription-factor NF κ B will become relevant in the discussion of SCFA effects on IEC functions and regarding the interference with STAT3. It is, e.g., activated by TLR-, IL-1 β -R and TNFR signaling (TNF α - and TNFR signaling is described in [76] and [77]) and downstream of mitogen activated protein (MAP) kinase pathways (e.g. p38 MAPK, JNK or ERK pathway). In the inactive situation it is bound to I κ B in the cytosol. When activated, it is released through phosphorylation and proteasome-degradation of I κ B. It then enters the nucleus and primarily initiates the transcription of proinflammatory genes. In IECs, e.g. cytokines like IL-6, IL-8, IL-11 and IL-31, as well as anti-apoptotic proteins like Bcl-xl and survivin are, hence, upregulated. NF κ B is also involved in SCFA-receptor expression. Situation-dependently, NF κ B signaling pathways either promote cell proliferation or -apoptosis. Normally, NF κ B induces the expression of its own binding protein I κ B, which contributes to the limitation of NF κ B mediated gene transcription.

1.4. Butyrate and its known modes of action

Butyrate has been shown to influence the differentiation and function of many cell types, including IECs and intestinal immune cells (rev. [60]) Butyrate enemas attenuated inflammatory symptoms in both, experimental colitis in animal models [27] as well as in human patients suffering from inflammatory bowel disease [29]. Furthermore, butyrate application ameliorated symptoms of the Metabolic Syndrome [17, 36, 37].

Butyrate exerts its effects mainly via two distinct molecular mechanisms:

- 1) Signaling via membrane-anchored SCFA-receptors (see the chapter 1.4.3.) and
- 2) via the inhibition of histone deacetylases (HDACs) (see chapter 1.4.1.).

By HDAC-inhibition [78], butyrate can e.g. affect gene transcription and the function of transcription factors. This is further described in chapter 1.4.1.

The regulation of cholesterol- und triglyceride metabolism is partly dependent on the activity of isoforms of the transcription factors of the PPAR-family. Butyrate has been shown to interplay in this regulatory circuit (see chapter 1.4.2.).

Alone or in combination with Vitamin D, butyrate exerts anticancerogenic effects by stimulating the differentiation and apoptosis of colorectal cancer cells *in vitro*, which is connected to butyrate's function as an HDAC inhibitor and its influences on the TGF β - and p38 MAPK signaling pathway [79-81] (see chapter 1.4.3.).

1.4.1. Histone deacetylase inhibition

In vitro assays showed the anti-inflammatory effects of butyrate at the signal transduction level. The central transcription factor NF κ B which transduces inflammatory signals to gene transcription (e.g. in conjunction with the cytokine TNF α , signaling via the TNFR, see chapter 1.3.4.), is affected by butyrate in a controversial manner: In *in vitro*-stimulated CACO2-cells, Luhrs et al. saw that the cytosolic liberation of NF κ B and its translocation into the nucleus was augmented by butyrate incubation which was partly traced back to a decreased degradation of the cytosolic NF κ B-binding protein I κ B [52]. The NF κ B-suppressing effect was also confirmed by *in vivo* studies in men after the application of butyrate enemas [31, 82]. In other tumor cell lines, Lin et al. showed an

increased *in vitro* activation of NFκB regulated genes after TLR- and TNFR activation under the influence of butyrate [83]. Likewise, Adam et al. showed a prolongation of TNFα-induced NFκB's DNA-binding in HeLa cells [84]. The underlying mechanism was found to be the cytosolic histone deacetylase inhibitor function of butyrate.

Transcription factors like NFκB and STAT3 often form complexes with enzymes that support the DNA-binding and the gene transcription process. They often interact with histone acetyl transferases (HATs). HATs acetylate lysine residues at histones, which are DNA packing proteins. After acetylation, the lysine residues lose their mutual chemical attraction. That leads to an opening of chromatin segments for a better gene accessibility. Important HATs are CREB-binding protein (CBP) and p300 [78].

The antagonists of HATs are histone deacetylases (HDACs) that remove the acetyl-groups and keep the balance between accessibility and closure of genes [78].

The acetyl-group movements enabled by HATs and HDACs are even more numerous at the level of transcription factors and other proteins directly [85]. p53 and retinoblastoma protein are examples for HDAC-regulated proteins. They are central regulators of cell cycle progression. Further, subunits NFκB (p65) [86] and STAT3 [87] are directly regulated as well. Acetylation is then a kind of posttranslational modification that affects the function of these proteins by e.g. modulating their promotor affinity [84, 88] and association with co-factors. Several research groups like Lee et al. [89] or Grivennikov et al. [90] could show an interaction of STAT3 and NFκB based on the acetylation level. The actions of HATs and HDACs significantly contribute to the regulation of basic cellular functions like proliferation, differentiation and apoptosis [91], fat- and glucose metabolism [92-94] and immune response [95, 96].

Cousens et al. named butyrate and propionate as “non-competitive pan-HDAC inhibitors” [97]. In the case of butyrate, inhibition is proven except for HDAC 6, -10 and the members of the third group of HDACs (Sirtuins) [78]. HDACs comprise up to date 18 members that are divided into 4 subgroups according to their Zn²⁺- or NAD⁺ dependency and their chemical relationship to yeast HDACs [98]. Many natural evolving [99] as well as the nowadays artificially designed HDAC inhibitor molecules block the active centrum

of the HDAC enzyme [92]. Contrarily, butyrate seems to block a functionally important region at HDACs different from that. Davie et al. presumed, that 2 butyrate molecules could bind in a hydrophobic cleft of the HDAC enzyme which is located apart from the substrate binding site and is used by Trichostatin A (= TSA, a bacteria-derived natural HDAC inhibitor with a similar spectrum of HDAC inhibition as butyrate, introduced in chapter 2.1.2) [78].

Many of butyrate's cellular effects on IECs could be traced back to its function as an HDAC-inhibitor: e.g. cell cycle arrest, differentiation and apoptosis in tumor cells. That can be partly explained by the reactivation of initial silenced tumor suppressor genes [100-102] and the vitamin D-receptor gene [79, 103].

In immune cells, IL-10 expression and the differentiation of T cells into regulatory subtypes by gene induction of the *FOXP3*-locus is supported by HDAC-inhibition [40].

In certain situations, like inflammation and increased proliferation (e.g. also in cancer progression) cells become rather dependent on glucose- than on fatty acid metabolization [104]. This is referred to as "Warburg effect". This effect, combined with the downregulation of SCFA receptors, then pronounces the significance of HDAC inhibition by SCFAs for cell functionality. In this context, the increased sensitivity of tumor cells like CACO-2 towards butyrate's proapoptotic effects has to be mentioned. Indeed, Cousens et al. described a dose-dependent acceleration of histone-acetylation by butyrate [97].

1.4.2. Up-regulation of VDR and association with PPAR γ

Another mechanism of modifying gene transcription in colonocytes is butyrate's association with isoforms of the peroxisome proliferator-activated receptor- (PPAR-) family, in particular PPAR γ . PPARs are intranuclear transcription factors that have been shown to play a role in fat- and glucose metabolism-regulating gene expression as well as in inflammatory processes [105]. PPAR γ is expressed in adipocytes, monocytes, macrophages and IECs [106]. Butyrate i.a. relieves the binding of coactivators like CBP (CREB binding protein) to the molecule. Apart from that, the expression of PPAR γ is upregulated in the presence of butyrate.

1.4.3. SCFA-receptor signaling

Another important effector mechanism of SCFAs is the signaling via membrane-anchored G-protein coupled receptors. Representatives are GPR43 (free fatty acid receptor 2 or FFAR2) and -109A (hydroxy carboxylic acid receptor 2 or HCAR2) which have also a special affinity to propionate (GPR43) and butyrate (both) [39]. Their abundance includes various cell types [107], e.g. T-cells (GPR43), dendritic cells (GPR109A) and IECs (both).

Upon ligand binding, GPRs recruit small G-proteins that transduce the signal into the cytoplasm, mainly via generating second messenger molecules like cAMP, IP3 and calcium ions. Hence, downstream of SCFA receptor activation, the activity of several enzymes like PKA and PKC δ is regulated, the inflammasome can be activated (important for IL-18 delivery [51]) and there exists a transactivation potential for mTOR [70] and mitogen-activated protein (MAP) kinase pathways, like p38 MAPK [108].

In acute inflammation in mouse models, GPR43 and GPR109a in both, IECs as well as in intestinal immune cells, were indispensable for an adequate myeloid cell migration and an effective anti-infectious immune reaction [46]. Furthermore, GPR activation in IECs supports wound healing and the production of antimicrobial peptides [46]. In human dendritic cells, GPR109A-ligand-binding leads to an activation of retinol acid synthetase and thus, indirectly to the stimulation of regulatory T cell development [109] (1.3.). A *gpr109a* knockout leads to a reduced Treg population in the ileum of mice [53]. Zimmerman et al. found the expression of genes upregulated in *mGPR109a*-deficient colon-epithelial cells of mice, that encode for SMAD proteins that inhibit TGF β signaling [57]. These facts implicate that GPR109A is essentially involved in “first-line” barrier strengthening, chronic inflammation counteracting and differentiation promoting, anti-cancerogenic effects in IECs.

One common way of negative regulation of SCFA receptor signaling is the β -arrestine-driven endocytosis of the ligand-/receptor complex [110].

Apart from that, β -arrestines seem to fulfil multimodal functions as intranuclear recruiters of transcription co-factors to modify gene transcription and as linker proteins that combine SCFA receptors with MAP kinases [111].

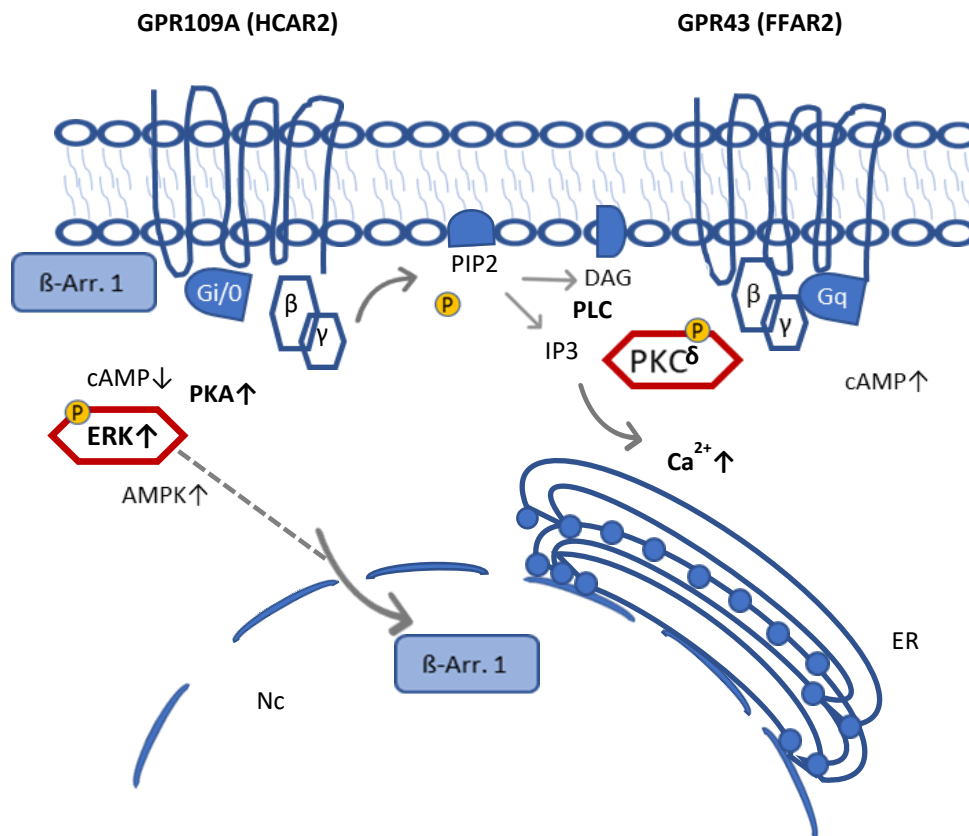


Fig.6: GPR signaling and connections with MAP kinases. Displayed are some connections between SCFA receptor signaling and the activation of MAP kinase pathways like ERK as well as the activation of other kinases like AMPK and PKC δ . The small G-proteins fulfil distinct functions upon receptor activation. The Gi/o part of the GPR109A receptor inhibits the Adenylate cyclase. The following decrease of cyclic AMP (cAMP) leads to the activation of Protein kinase A (PKA), EGFR kinase (ERK) and AMP kinase (AMPK). The $\beta\gamma$ -subunit of the small G-protein activates the membrane-located Diacylglycerol (DAG) and liberates Calcium (Ca²⁺) out of ER-stores which activates Protein kinases C (PKCs) like PKC δ . The Gq associated β -Arrestine 1 (β -Arr.1) is supported by active ERK in its gene-transcriptional functions. Additional abbreviations and symbols: Nc = Nucleus, ER = endoplasmic reticulum.

1.4.4. The activation of p38 MAPK

P38 MAPK is one member of the mitogen-activated protein kinase (MAPK) family, which also comprises the extracellular signal-regulated kinase ERK 1/2 and c-Jun NH2-terminal kinase (JNK). MAP kinases are serine/threonine kinases that catalyze the phosphorylation of serine and/or threonine residues at proteins. P38 MAPK is one of several kinases which is assumed to take part in the phosphorylation of the serine727-residue of STAT3 (also see chapter 1.5.).

The p38 MAPK pathway can be triggered by multiple cell stress-causing conditions, such as oxidative stress or temperature oscillation. It is involved in SCFA receptor signaling (1.4.3.) and is also activated in the course of cytokine- and growth factor receptor activation. Known activating ligands are e.g. TGF β , IL-1 β and TNF α . P38 MAPK activation requires its phosphorylation at 2 threonine/tyrosine residues mediated by superior kinases. These are referred to as MAP-kinase kinases (MKKs or MEKs, especially MEK3 and MEK6) which are, in turn, previously phosphorylated by MAP-kinase kinase kinases (MKKKs, especially MKKK1). P38 MAPK is involved in proinflammatory cell reactions and situation-dependently supports either apoptosis, differentiation or survival of cells.

E.g. Daniel et al. found the butyrate-caused p38 MAPK activation and also the butyrate-induced TGF β /SMAD3 signaling involved in the cell differentiation of CACO-2 cells [80], [81]. The activated p38 MAPK subsequently phosphorylates other gene transcription-modifying proteins like heat shock protein (HSP) 27, which is an anti-apoptotic factor, or MK2 (mitogen kinase activated protein 2) which can stabilize the mRNAs of cytokines like IL-6, TNF α and CXCL-8 (via phosphorylation of tris-tetra-prolin) [112].

In our assay, the p38 protein isoform p38 α is detected by specific antibodies.

P38 α is one of four protein isoforms which have an alternating expression profile between different tissues and organs. P38 α is ubiquitously expressed, e.g. in immune cells, liver- and lung tissue, heart, pancreas and intestine.

1.5. STAT3 – a central transcription factor within the intestinal barrier

STAT3 is a ubiquitous, central transcription factor in immunological, cell survival- and wound healing processes [113]. It belongs to a family of transcription factors, also containing STAT1, 2, 4, 5A, 5B and 6. It can be activated by cytokines of the IL-6- and IL-10 family [69] as well as downstream of growth factor [114] and TLR signaling [115]. Thus, it integrates inflammatory and proliferative cell stimuli. Cell type- and context-dependent, STAT3 is known to induce e.g. the expression of acute phase genes in hepatocytes [116], antibacterial peptide genes in IECs [117], and to promote cancer progression [118].

The STAT3-activating cytokines are ligands of different hetero-dimeric, -tetrameric or -hexameric receptors which have binding sites for tyrosine-kinases of the Janus kinase (JAK) family in common. Receptor activation leads to the recruitment and activation of the JAKs, a phosphorylation of receptor tyrosine residues and a subsequent recruitment and phosphorylation of STAT3 monomers at tyrosine- (Y-) residues at position 705. The Y705-phosphorus group enables the homo-dimerization of STAT3 monomers, or the hetero-dimerization with e.g. STAT5 monomers, which is often, but not necessarily, needed for transcriptional functionality (Fig. 8). After activation of growth factor receptors (e.g. EGFR) the Y705-phosphorylation of STAT3 often includes the activation of the src-tyrosine kinase instead of the JAKs.



Fig. 7: Structural organization of STAT3. After Heinrich et al. [119]; displayed is the DNA-binding domain in the middle of the molecule as well as the SH2-(receptor-binding and dimerization) domain as well as the tyrosine (Y) and the serine (S) phosphorylation sides at the c'-terminus.

STAT3 molecules obtain a phospho-tyrosine affinity at their SH2-structural domain. After binding at phosphorylated tyrosine residues of intracellular receptor units, associated tyrosine kinases from the Janus kinase subtype (mainly JAK1 and JAK2) phosphorylate STAT3 monomers at the tyrosine residue Y705 (light blue segment in Fig.

7 and Fig. 8). This causes a conformation change in the SH2 region followed by the STAT3 separation from the receptor and the forming of STAT3 dimers by bidirectional attraction of the SH2 domains to the opposite phospho-tyrosine (Y)705 residue (Fig. 8b). From the two main phosphorylation sites at STAT3 (Y705 and S727), the Y705 phosphorylation is often supposed to be important for the dimerization, nuclear immigration and DNA-binding of STAT3. The S727 phosphorylation typically follows tyrosine phosphorylation as cellular response to several cytokines and growth factors [120], but also occurs independently [121, 122]. In literature, its detailed significance is yet controversial. Already in the 90th, researchers found both transcription functionality supporting as well as inhibiting effects of pS727-STAT3 [121], [123]. In the case of ERK-mediated serine727-phosphorylation, the S727-phosphorus group inhibited Y705-phosphorylation [121]. More recently, also mitochondrial and calcium regulating functions of pS727-STAT3 have been discovered [124]. In the mitochondrion, pS272-STAT3 seems to exert effects on enzymes of the oxidative chain, thereby increasing ATP production from oxidative phosphorylation [125]. Its relevance for the cellular outcome seems to be cell type-dependent. Especially, cancer cell types are differentially specialized on varying survival strategies. For instance, Ras-mutated cells seem to profit by a higher proportion of mitochondrial pS727-STAT3 [126, 127] whereas, in src-mutated cells like CACO-2 cells, the dual phosphorylation of STAT3 both at Y705 and S727 residues, seems to have major priority for cell survival [128, 129].

The phosphorylation at serine727-residues (red segment in Fig. 7) is often supposed to be required for STAT3's full transcriptional effectivity [130] but could also terminate STAT3's DNA-binding [121, 131] and accelerate its export to cytoplasm [123]. Dependent on cell type and activation mode, serine727-phosphorylation is accredited to different serine/threonine kinase members. p38 MAPK (further introduced in chapter 3.4.), JNK and ERK as well as PKC isoforms and mTOR have been shown to be involved in this process [132]. Thereby, several of the named kinases can be transactivated in the course of receptor signaling. It is shown for SCFA receptors in chapter 1.4.3. It also counts for STATs-activating growth factor- and cytokine receptors, like the OSMR [133] (chapter 1.5.1.). The general structure and signaling of the receptor dimer is shown in Figure 8.

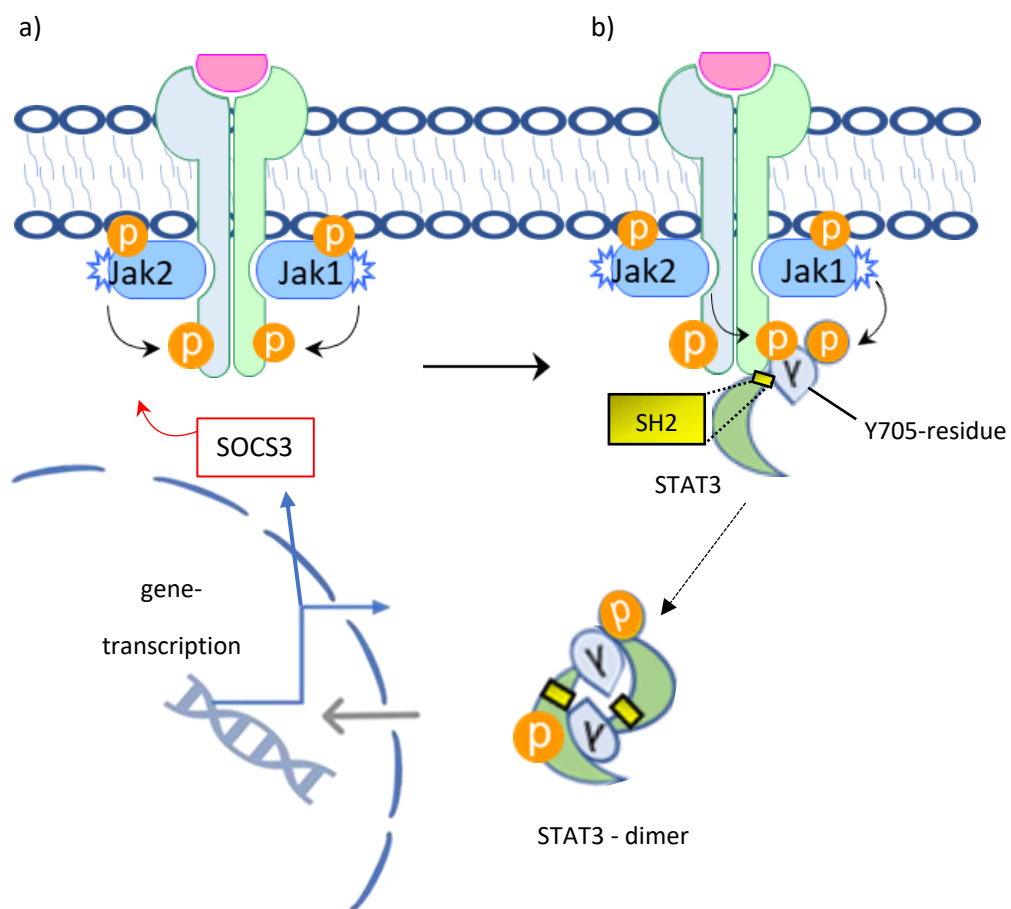


Fig. 8: Signaling via the JAK/STAT pathway. Displayed is the activation of the gene transcription factor *STAT3* in response to cytokine receptor activation. After being tyrosine phosphorylated by receptor-associated Janus kinases (*Jak1* and *2*), *STAT3* forms homo- or heterodimers and translocates into the nucleus. The cooperation with certain transcription co-factors leads to the transcription of *STAT3* dependent gene clusters. *SOCS3* is a co-regulated inhibitor of the signaling cascade. In case of the *OSMR*, the binding of *OSM* (red ligand) would lead to dimerization of the receptor subunits *gp130* (light blue) and *OSMR β* (light green), their reciprocal phosphorylation at tyrosine motifs and subsequent recruitment and tyrosine-phosphorylation of *STAT3* monomers.

The transcriptional activity of *STAT3* leads to its parallel negative feedback regulation, for instance via the transcriptional induction of the inhibitory protein *SOCS3* (Fig. 8a), that binds to *GP130* and inhibits *JAK*'s tyrosine kinase activity. Another negative feedback mechanism is the cytoplasmatic activation of phosphatases *SHP1*, *SHP2* or protein inhibitor of activated *STAT* (*PIAS*). Both can dephosphorylate and deactivate the *JAKs* or the phospho-*STAT3* protein directly and, thus, terminate the *STAT3* signal [119].

1.5.1. OSM and OSMR

STAT3 has been found constitutively activated in intestinal and peripheral T-cells, lamina propria myeloid cells, and IECs of patients suffering from inflammatory bowel disease (IBD) [134, 135]. In assays based on murine STAT3 knockout models a strong evidence occurred that activated STAT3 has an essential impact on the integrity of the intestinal barrier. Mice which are lacking STAT3 in their IECs (Stat3 Δ IEC -mice) are much more susceptible to gut epithelial damage in DSS-induced artificial colitis [69, 136] or during *Citrobacter rodentium* infection [137]. Welte et al. showed that a lack of STAT3 in hematopoietic cells of mice leads to the development of Crohn`s disease-like symptoms [138].

In accordance with that, the STAT3 activating IL-6-type cytokine, Oncostatin M (OSM), was more abundant and the OSM-receptor subunit OSMR β was more expressed in the intestinal mucosa of patients suffering from IBD [139]. A current opinion suggests a recovering and pro-defensive role of OSM in the etiopathology of IBD [140]. OSM seems to be compensational increased in the situation of unresolved inflammation. This was observed in the case of mutations in genes that encode pattern recognition receptors (PRR), immune defense regulating cytokines like IL-23 or the Vit.-D receptor [69]. Fitting the findings that ascribe a decisive immunologic input at tissue interfaces to the OSM-STAT-pathway, an OSMR knockout in the adipose tissue of high fat-fed mice exacerbated fatty tissue inflammation [141]. In humans, OSM is known to signal via two different receptor dimers. The LIF receptor complex consists of GP130 and LIFR, the OSM receptor (OSMR) complex contains GP130 and an OSMR β (OSM receptor β) unit instead. In case of receptor activation, Janus-kinases (JAKs) are activated and phosphorylate STAT3 monomers at tyrosine705 residues, hence, increase pY705-STAT3 protein (Fig. 8). While the OSMR subunit GP130 is ubiquitously expressed, the expression of the OSMR β subunit varies among tissues. In colon carcinomas, OSMR β was shown to be epigenetically silenced by promotor methylation [142], which is even used for diagnostic purpose [143].

1.5.2. Additional immunologic contribution of STAT3 in the intestine

Intestinal STAT3 also plays a role in the signaling of other cytokines present in the intestinal mucosa, for example CCL-2, CXCL-8, IL-17, IL-22 and IL-31 [69, 133, 144, 145]. CCL-2, also referred to as monocyte-chemoattractant protein 1, attracts monocytes and lymphocytes to tissues during inflammation. It is especially abundant in the intestinal mucosa of patients suffering from inflammatory bowel diseases like Crohn's disease. CCL-2 induces the IL-6- and TNF α production by myeloid cells [145].

CXCL-8 is a neutrophil-attracting and the wound healing-promoting cytokine. Beside by NF κ B (see Fig. 3), it can also be induced by IL-31R signaling and the subsequent activation of STATs. Butyrate was shown to increase the IL-31R- and the IL-31-expression in HCT116 colon carcinoma cells [144].

STAT3 seems to exert its immunologic contribution at different levels:

Levy and Elinav et al. [24] as well as Daïen and Marcia et al. [146] described the outstanding importance of IL-22-induced activation of STAT3 in IECs regarding the generation of antibacterial substances like RegIII β . They underlined the importance of this bactericidal-substance production in maintaining the composition of the intestinal microbiota and the prevention of a dysbiosis, which was also confirmed by others [147], [148], [149].

Besides, STAT3 activation in lymphocytes promotes IL-22 and IL-17 production and, thus, the mature of Th17- as well as Th2-cells [70], [136]. In myelocytes, STAT3 contributes to the development of immunologic tolerance towards microbes and limits proinflammatory immune reactions [150]. Due to a steady influence of growth factors, among other causes, STAT3 is constitutively activated in diverse tumors and tumor cell lines. Besides apoptosis prevention in these cells, this circumstance also accounts for tumor molecular mimicry, also referred to as "tumor immune escape" [151], [152], [153]. Beside the common, complete form of the molecule, there also exist splice or posttranslational processing variants of STAT3, e.g. STAT3 β , which lacks the S727-residue and has an own panel of functions (rev. in [124]).

1.6. Aim of this study

STAT3 is a central transcription factor, involved in immune modulation and wound healing processes within the intestinal epithelium. The development of synthetic molecules which function as modulators of STAT3 is currently a matter of research concerning new therapies of dysbiosis-associated diseases like colon cancer and inflammatory bowel disease [154, 155].

To explore the influence of butyrate on modifications of STAT3 known to be involved in its transcriptional activity in intestinal epithelial cells (IECs), different biochemical and functional aspects are investigated. A special focus will be laid on STAT3's phosphorylation at serine residue at position 727 of the molecule (pS727-STAT3). It can exert transcription promoting as well as inhibiting effects.

p38 MAPK is one of several possible serine kinases conducting this protein modification. In especially designed cell culture assays, p38 MAPK is blocked to study this impact.

The influence of HDAC-inhibition on changes of pS727-STAT3 and total STAT3 is, as well, investigated, both at the protein and the gene transcription level.

Furthermore, the influence of short-and middle term inflammatory cytokine stimuli (1 to 4 hours) both on the butyrate effects on intestinal STAT3 as well as on the gene transcription of cytokines in intestinal epithelial cells is studied.

One of the limitations of the common CACO-2 cell model which forms the basis for most of the here conducted experiments, is the low expression of butyrate receptors like GPR109A. Considering a hypothesized impact of butyrate receptor signaling on the outcome of experiments in IECs, comparative assays are carried out in cells cultured in 3D instead of traditional 2D. To this end, we take usage of the "sis-muc" intestinal model, provided by the Fraunhofer institute of tissue engineering Würzburg. This more physiological cell culture model has so far not been investigated in the context of butyrate-mediated signal transduction in intestine-derived cells.

2. Methods and Materials

General considerations

To investigate how a physiological concentration of butyrate bears on STAT3 in intestinal epithelial cells, it was focused on the well-established cell culture model of CACO-2 colon carcinoma cells. An overview of the special properties of this cell line is given in chapter 2.1. The here used physiological concentration of 5 mM sodium butyrate, added with the cell culture medium, was determined by referring to experiences in former studies. Concentrations of 2 to 5 mM butyrate salts had been shown to resemble best the contact with the surface of colonic epithelial cells under physiological conditions, when also liquid- and mucus solubility of butyrate had been considered.

The butyrate effects on STAT3 were analyzed with and without the influence of simultaneous short-term inflammatory stimuli (see the application of OSM or TNF α in the cell culture assays of 2.1.).

To discriminate the portion of the different modes of action exerted by butyrate regarding changes in both the total protein amount of STAT3 and STAT3's phosphorylated states, the medium in the cell culture assays was partly complemented with:

- 1.) Trichostatin A (TSA) instead of sodium butyrate, to verify the influence of HDAC inhibition on the results (chapter 2.1.2.).
- 2.) molecular blockers of p38 MAP-kinase activity (SB202190 and SB203580) to study the influence of p38 MAPK activation in the context of STAT3 modification (chapter 2.1.3.).

The changes in the protein concentration of distinct forms of STAT3 were estimated using the techniques of SDS-page and Western blot analysis (chapters 2.5. and 2.6.).

Specific protein detecting antibodies, directed against epitopes of the total STAT3 protein, respectively those evolving after serine727- or tyrosine705-phosphorylation, allowed to distinguish between the amounts of the single states of phosphorylated STAT3 in relation to the total STAT3 protein amount (chapter 2.7.). Tubulin was likewise

detected and served as reference protein for the total protein amount contained in a sample.

To estimate the portion which butyrate had on the STAT3-expression at a gene-transcription level or on the expression of the negative feedback protein SOCS3, qPCR was consulted (chapter 2.4.).

As the activation of the butyrate receptors like GPR109A is known to have an influence on several elements of the intestinal barrier as well, including the activation of members of the mitogen activated protein kinase family like p38 MAPK in IECs in downstream signal transduction pathways, this was considered also. A disadvantage of the CACO-2 cell culture model is the relatively low receptor expression of butyrate receptors in CACO-2 cells (see chapter 2.1.).

To accomplish a higher butyrate receptor expression, CACO-2 cells were additionally seeded on a 3D porcine scaffold membrane in a transwell system (chapter 2.1.4). The intention of this approach was to better resemble the physiological crypt-villus formation and 3D-arrangement of the epithelial cells as well as to provide a nearly physiological molecular connective tissue fiber structure. Additionally, the “humanified” milieu is further complemented through the two given chambers in the transwell system, that allow a differentiated apical/basal medium supply. Subsequently, the GPR109A expression of the so treated CACO-2 cells could be compared using qPCR (2.4.) with that of cells that had been seeded on the commonly used cell culture plate.

2.1. Cell culture and cell culture assays

CACO-2 cell line

An overview of CACO-2 characteristics is given in [156]. When differentiated after confluence, CACO-2 cells form stable tight junction complexes and show an apical membranous brush border with microvilli. Although there are many similarities CACO-2 cells share with normal enterocytes, there are also variations, e.g. concerning the gene expression profile of agent-transport proteins, receptor proteins and cytokines [84]. Examples for this, that are presumably worth to mention in conjunction with this thesis,

are the underrepresentation of butyrate transporter like SMCT-1 [157], the butyrate receptors like GPR109A and GPR43 [158] and the OSM receptor [142].

For this study,

the human colon adenocarcinoma cell line CACO-2 was purchased from CLS, Eppelheim. Used CACO2 cells were within the 56th to 64th passage (also see “Splitting and passaging of cells”). CACO2-cells were cultured in T75 (75 cm²) culture flasks in high glucose (4.5 g/l D-Glucose) Dulbecco`s Modified Eagle Medium (DMEM), supplemented with 10 % fetal calf serum (FCS), 1 % natrium-pyruvate, 1 % non-essential amino acids (NEAA) and 1 % Penicillin/Streptavidin. The cultivation took place in a clean incubator at 37 °C and 5 % CO₂.

At 80 % confluence, cells were either divided into smaller portions (1 Mio. cells) and moved into new culture flasks for reproduction (also see “splitting and passaging of cells”) or into cryo-tubes for storage (also see “freezing and thawing of cells”) or were seeded at 230.000 cells per well in 24-well-culture plates for the incubation assays.

The seeding of the cells and the addition of the incubation supplements was conducted under sterile conditions within a laminar airflow cabinet. All used materials and solutions were sterilized by autoclaving or sterile filtering. Greater amounts of solution or medium were warmed up in a 37°C water pool before being added to avoid oscillations in temperature.

Splitting and passaging of cells:

After bringing a new purchased cell line into culture, the cells attach at the surface of the culture flask and start mitosis until they reach confluence (= all-sided cell-cell contact). Then they stop to proliferate and differentiate into matured cells of their original tissue. It is necessary to keep cells in a proliferative, not differentiated state to equalize them in maturation at the beginning of an assay. To this end, when reached about 80 % of confluence, the cells are frequently “passaged”, that means they are

detached and distributed into smaller amounts which are transferred into new culture flasks. The number of the “passage” declares how often this process was conducted after bringing the new purchased cell line into culture for the first time.

To detach cells from the culture material they are incubated in 3 ml Trypsin for 10 min within the incubator, after having shortly (a few seconds) been washed in 2 steps, first in 5 ml PBS (cell buffer) and then in 4 ml Trypsin to eliminate cell detritus. In order to stop the Trypsin-generated removal-process, 7 ml DMEM is added after the 10 min-incubation time, and cells are counted in a Geiger-chamber. Therefore, cells are stained by mixing a small amount of the cell suspension 1:4 with Trypan-blue within an Eppendorf-tube by carefully up- and down- pipetting. After counting, the main cell solution is centrifuged for 5 min at 1000 rpm. The supernatant is removed, and the remaining cell pellet is resuspended in the appropriate amount of DMEM and it is preceded as previously described.

Freezing and thawing of cells:

Cells which should be stored were quickly frozen at -80°C in aliquots à ~ 4 Mio cells in a special freezing medium, containing approximately 1/11 DMSO in DMEM + supplements (table 1).

The process of thawing had to be carried out very quickly to prevent the absorption of the cell poison DMSO by the cells. Therefore, the cryo-tubes were shortly warmed (< 1 min) in the 37°C water pool and then decanted into minimum 5 ml DMEM for dilution of DMSO, centrifuged (5 min at 1000 rpm) and resuspended in DMEM + supplements, afterwards being cultured as previously described.

Incubation assays:

CACO-2 cells that had reached 80% confluence were seeded either on 24-well-plates (for the assays described in chapter 2.1.1.-2.1.3.) or, additionally, in a transwell system (further described in 2.1.4.). During differentiation, cells were maintained in a volume

of 2 ml DMEM plus supplements (see “For this study”, page 26) which was renewed every 2 days. The assays described in 1.2.1.-1.2.3. were conducted 3 separate times for cells that had differentiated over a period of 5 days and 1 time for 24 days differentiated cells. The 3D-assay described in 2.1.4. was conducted one time with for 21 days differentiated cells. For each run, cells were independently thawed and cultured. Usually, cells adhered at the surface of the cell culture plate and reached confluence within 24 hours. At the beginning of each assay, all cells were treated equally with a simultaneous medium change. An appropriate solvent control was carried along in the respective negative controls (e.g. aqua dest. in the case of butyrate). At the end of each assay, DMEM + supplements were quickly removed, and the cells were washed with ice-cold PBS (cell buffer). Then, cells were harvested either in ice-cold PBS or left on the culture material and were then either dry-frozen at -80°C for later RNA-analysis (described in chapter 2.2. to 2.4.) or lysed in ice-cold Laemmli buffer (for recipe see table 1) and stored at -20°C for later protein analysis (described in chapter 2.5. to 2.7.).

Table 1: Cell culture medium and -agents

Name of the agent	Special information/ cat.no.	Manufacturer/ buffer prescription
DMEM high glucose*	+ 4.5g/l D-Glucose D5796-500 ml	Sigma Aldrich, now Merck KGaA, Darmstadt GER
L-Glutamine-Solution	200 mM, G7513-100 ml	Sigma Aldrich, now Merck KGaA, Darmstadt GER
Fetal bovine serum (FBS)	FBS superior S 0615	Biochrom GmbH, Berlin, GER
Penicillin/Streptomycin	P0781-100ML	Sigma Aldrich, now Merck KGaA, Darmstadt GER

Non-essential amino acids	M-7145	Sigma Aldrich, now Merck KGaA, Darmstadt GER
Dimethyl-sulfoxide (DMSO)	A3672,0250	Applichem, Darmstadt
Trypan Blue Stain	T10282	Invitrogen™ (Thermo Fisher, Carlsbad, CA, USA)
Trypsin-EDTA solution	T3924	Sigma Aldrich, now Merck KGaA, Darmstadt GER
Dulbecco's Phosphate buffered Saline (DPBS) (pH 7.4 – 7.6)		Sigma Aldrich, now Merck KGaA, Darmstadt GER
Laemmli Buffer working aliquot (lasting for 5 wells/samples)	<ul style="list-style-type: none"> • 0.8 ml of the stock solution, containing: 60 mM Tris-HCl pH 6,8; 2 % SDS, 10 % Glycerin, 0.02 % Bromophenol Blue • 0.2 ml 50 mM TCEP, added shortly before usage 	
Cell-freezing medium:	<ul style="list-style-type: none"> • 8.64 ml DMEM* • 2.4 ml FBS • 960 µl DMSO 	

2.1.1. Sodium butyrate incubation assays

Confluent cells were incubated with 5 mM sodium butyrate (abbreviation “B” in Fig. 9) for 48 hours before exposing to any additional stimulus. Solvent controls were carried along that were exposed to an equivalent of sterile filtrated aqua dest. (which was the butyrate solute agent), added to the culture medium. To simulate an inflammatory state, 10 ng/ml TNF α (TNF) or 20 ng/ml OSM were added as depicted in Fig. 9 and cells

were harvested after 15 min or 1h, for both agents respectively. Cells were harvested for both, RNA-analysis and protein analysis.

TNF α and OSM are proinflammatory cytokines, mainly expressed by macrophages, fibroblasts and lymphocytes. Recombinative produced molecules were obtained from PeproTech GmbH, Hamburg, and were stored in low-binding tubes at - 20°C according to the manufacturer's instructions.

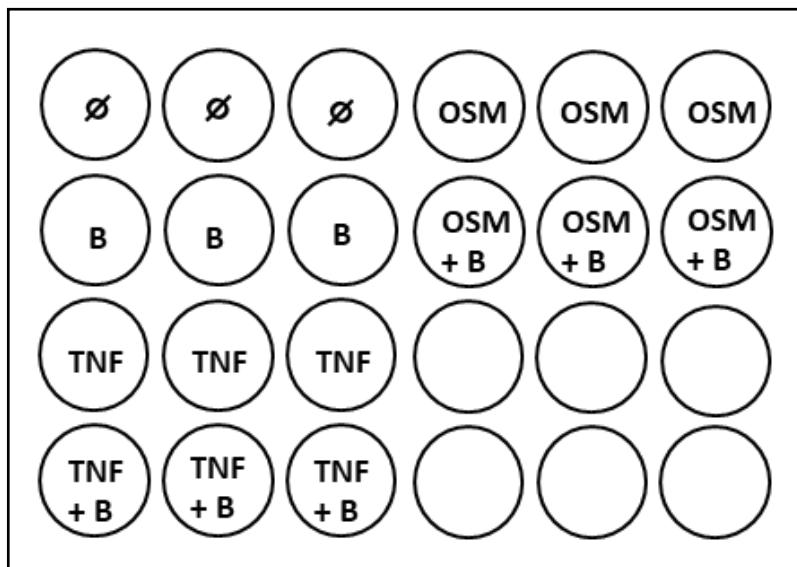


Fig. 9: Sodium butyrate incubation assays. Two identically prepared culture plates were used simultaneously. Cells on one of the plates were harvested after 15' of TNF α (= TNF)-, respectively OSM-stimulation, cells on the other plate after 1h of stimulation with these agents. The unstimulated controls (= \emptyset) and those cells which had been exposed to a single butyrate (= B) stimulus were harvested simultaneously with the TNF/OSM-samples on the same plate.

2.1.2. TSA incubation assays

In order to explore the portion of butyrate's HDAC-inhibition effect on the results, butyrate was replaced by 400 nM Trichostatin A (TSA). While the HDAC inhibitory effects of butyrate in CACO-2 cells had been most distinct after 48 hours of exposure in former conducted assays, the presence of TSA had been shown to be more effective after 24h and causes cell death of CACO-2 cells after 48h. Therefore, experiments were

respectively completed and finished after butyrate- or TSA exposure for both points in time - 24 and 48h (see chapter 2.1.1. and 2.1.2.). Cells were, again, harvested for RNA- and protein analysis.

TSA is an antifungal antibiotic that is derived from *Streptomyces* species and is known for its HDAC-inhibitory effects in mammalian cells that resemble those of butyrate's. Lyophilized TSA was acquired from *Cell Signaling Technology*[®] and was resuspended in Ethanol (EtOH) according to the manufacturer's instructions. An appropriate amount of the solute agent EtOH was carried along in the respective negative controls. The cell viability was evaluated morphologically by light microscopy (see Figure 21, page 62). The experimental setup is depicted in Fig. 10.

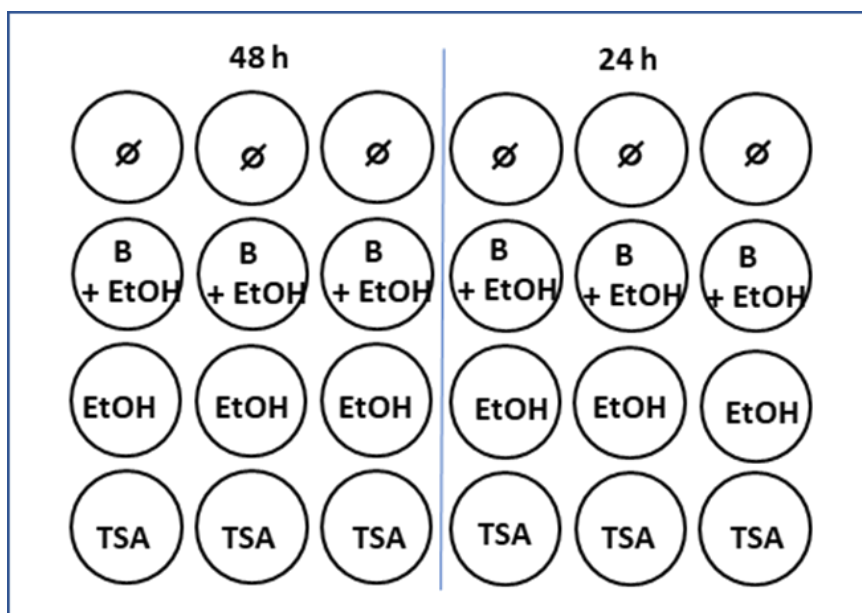


Fig. 10: TSA incubation assays. Symbols: ∅ = unstimulated control, EtOH = Ethanol, TSA = Trichostatin A, B = (sodium-) butyrate. Two identically prepared culture plates were used simultaneously. Where indicated, cells were treated with 5 mM sodium butyrate or 400 nM TSA for 24h, respectively 48h. EtOH was carried along as TSA solvent control. After the incubation period, cells of one plate were harvested in Laemmli buffer for protein analysis. Cells of the other plate were dry frozen for later qPCR analysis.

Table 2: Cytokines and agents

Agent	Description/ cat. No.	Manufacturer
Sodium-Butyrate (B)	Butyric acid Sodium salt Cat.no. 303410-5g/ 100g	Sigma Aldrich, St. Louis, MO
Oncostatin M (= OSM)	Cat.no. 300-10 227 a.a.	PeptoTech GmbH, Hamburg
*Tumor necrosis factor alpha (= TNF or TNF α)	2018-00-A-L	Knoll AG, Ludwigshafen
Trichostatin A (TSA)	Cat.no. 9950 – 1mg	Cell Signaling Technology Frankfurt, GER

*kindly provided by Prof. Dr. D. Männel, Regensburg

2.1.3. SB 202190 and SB 203580 incubation assays

To determine the influence of p38 MAPK activity on butyrate's ser727-phosphorylatory effect on STAT3, the p38 MAPK activity was blocked by SB202190 or SB203580 which were added in a 10 μ M- concentration to the cell culture medium, 30 minutes prior to butyrate exposure. Both blockers are exchangeable and inhibit the enzymatic activity of p38 MAPK by binding in the catalytic center of the enzyme.

SB202190 and SB203580 were acquired from Axon Medchem, Groningen, had been dissolved in DMSO and stored at -20°C, according to the manufacturer's instructions. An equivalent amount of DMSO was carried along as solvent control. The experimental setup is displayed in Fig. 11.

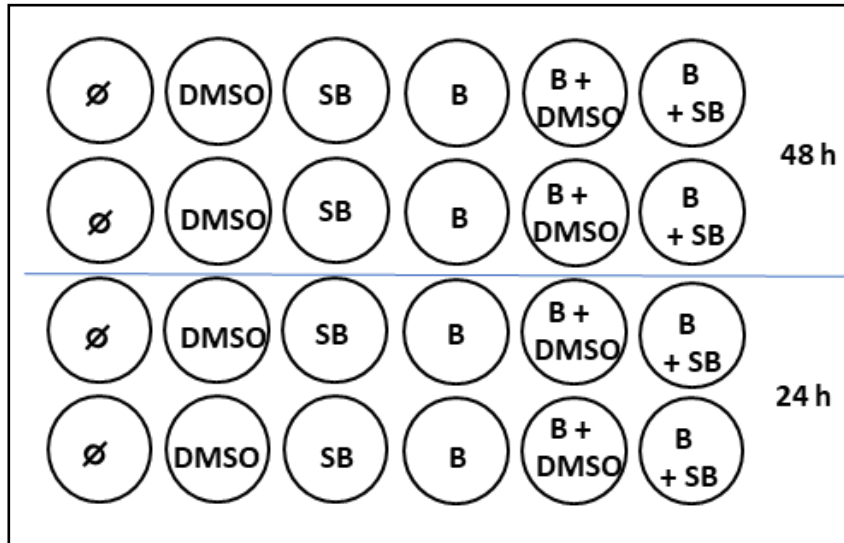


Fig. 11: SB202190 and SB203580 incubation assays. The butyrate incubation in the upper part of the cell culture plate started 24 h earlier than in the underpart. SB-202190 (= SB) was added 30' previous to the addition of butyrate to guarantee the best possible blocking of the P38 MAPK activity during butyrate influence. An equivalent of DMSO was carried along as solvent control for SB 202190. Finally, cells were harvested for protein analysis.

Full cell lysates underwent Western blot analysis (see chapter 2.6.) and a known substrate of p38 MAPK, MK2 and its activated, phosphorylated form p-T222-MK2 as well as total STAT3 and pS727-STAT3 protein were detected as it is explained in chapter 2.7.

2.1.4. 2D/3D cell culture assays

By using the “sis-muc” porcine 3D-scaffold membrane model of the CACO-2 monolayer which was provided by the Fraunhofer institute for tissue engineering Würzburg [159], a more “humanized” milieu and a more physiological cell differentiation was pursued. For the 2D/3D-cell culture assays, CACO2 cells were seeded either on the common 24-well plates (“2D-setting”) or on a connective tissue matrix which was derived from fragments of the small intestine of a pig. Thus, it well resembles the crypt-villus-structure of the human small intestine and provides a porcine extracellular fiber network as basis layer for the 3D-arrangement of the CACO-2 cells that is similar to the conditions IECs would experience on the basal lamina/submucosa in the human

intestine. The previously decellularized connective tissue matrix functions as 3D scaffold for the CACO-2 cells and is affixed in an anergic plastic frame that is set in a 12-well-plate chamber in the sense of a transwell system (Fig. 12a). The system allows a two-sided (apical/basal) medium contact and, hence, a polar adapted medium composition.

Cells were seeded with a density of 300.000 cells per well or per scaffold membrane. After a 21 days-maturation period, cells were incubated with 5 mM butyrate for 48 hours. In the 3D-setup, 0.5 ml of the cell culture medium was filled in the upper chamber. It reached the cells from apical and contained the same butyrate and/or TNF α concentration used in the 2D-setting. 1.5 ml of the cell culture medium was filled in the lower chamber and reached the cells from basal. This basal medium volume was left unattended except for the regular medium change. After the incubation period, cells that should represent the inflammatory state were apically stimulated with 10 ng/ml TNF α for 4h (Fig. 12c). In the 3D setup, the stimulation was carried out only from the upper chamber.

At the end of the assay, cells were harvested and dry-frozen at -80°C as previously explained for subsequent RNA-or protein analysis. The cells on the scaffolds were left on their surface and dry-frozen together with the membrane at -80°C as well.

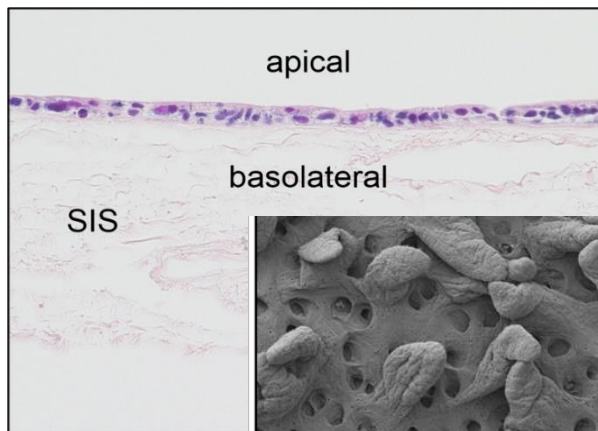
a)



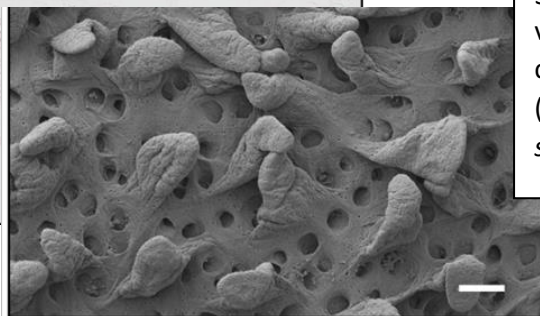
Plastic frame with the affixed decellularized matrix (left hand side) and the upper part of the frame that will be subsequently set onto the underpart to hold the membrane tight.

Readily prepared membrane containing frame, placed in a slot of the 12-well plate, spoiled by cell culture medium.

b)



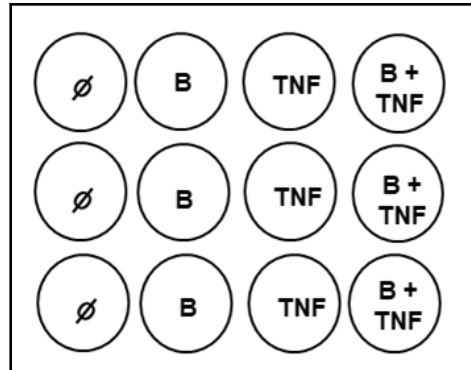
CACO-2 monolayer ("muc" like "mucosa") on the underneath (basal) located submucosa which is formed by decellularized porcine connective tissue fiber ("SIS" like "small intestinal submucosa").
(light microscopic)



3D-structure of the crypt-villus-architecture of the connective tissue scaffold.
(electron microscopic, scale bar: 100 μm)

c)

3D



2D

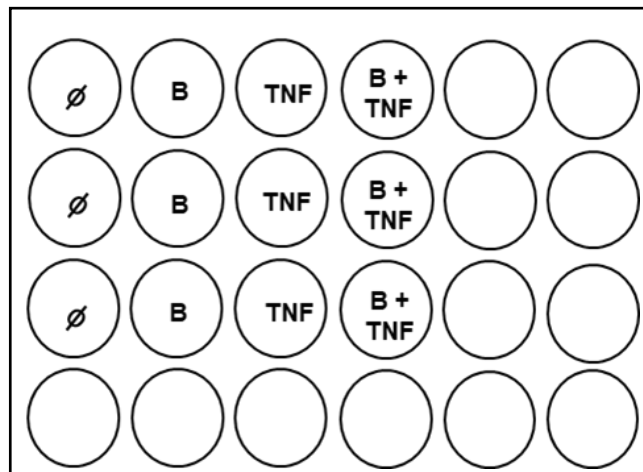


Fig. 12: 2D/3D cell culture assays. Displayed are a) macroscopic and b) microscopic pictures of the “SIS-MUC” 3D- cell culture model. In c), the 2D/3D experimental arrangement is visualized. Where indicated, cells were incubated with 5 mM butyrate for 48h. Afterwards, cells that should represent the inflammatory state were additionally stimulated with 10 ng/ml TNF α for 4h.

2.2. RNA extraction

For the mRNA analysis, cells were lysed and the total RNA was separated from cell detritus, proteins and DNA. All the working steps, described in more detail in the next paragraphs, were conducted within a very clean environment and with special working

material like eppendorf tubes and pipette tips prepared for the use in RNA extraction. In addition, reagents and cell material were preferably kept in low temperatures to avoid the destruction of the fragile RNA by enzymes that occur ubiquitously (= RNases).

As part of the cell culture assays described in 2.1.1., 2.1.2. and 2.1.3., the obtained RNA was purified by using the RNeasy Mini-Kit from Qiagen. The samples, previously stored at -80°C, were thawed on ice and the RNA isolation was conducted according to the slightly modified manufacturer's protocol as follows.

In order to disrupt the cells, 350µl of a mixture of β-Mercaptoethanol and lysis buffer in a ratio of 1:100 was added to every sample. After a short incubation, cell material was scratched from the surface and transferred into an RNase-free 1.5ml reaction tube. Then, each sample was thoroughly vortexed, transferred onto a shredder spin column placed onto a 2ml collection tube and centrifuged at 15,000 rpm for two minutes. The homogenized lysates were mixed with 350µl of 70 % ethanol each by up-and down pipetting until the respective mixture was completely transparent. This procedure led to an RNA precipitation which enabled the following RNA-binding to the desalt silica membrane in the RNeasy spin columns, to which the samples were transferred next. Each loaded spin column with the RNA-binding membrane was, again, placed onto a 2ml collection tube and then centrifuged at 11,000 rpm for 15 seconds. The flow-through was discarded. For DNA digestion, 50 µl of the previously prepared DNase I-stock solution (see table of materials) was placed directly in the middle of each upper spin column membrane and slowly penetrated the membrane during an incubation time of 15 minutes at room temperature. After that, three washing cycles followed by using the proper, with ethanol prepared buffer substances, centrifuging and discarding the flow-through, according to the manufacturer's instructions. Finally, the RNA was eluted in 25 µl RNase-free water placed in the middle of each upper membrane, washing the membrane out in a last centrifuge cycle (11,000 rpm for 1 minute).

For the purification of the RNA in the 3D-cell culture assays in 2.2.4., the NucleoSpin®RNA- isolation kit from Macherey-Nagel was used. A mechanic destruction of the cells by shredder columns, like previously described, was missing. Instead, the cell destruction happened chemically by adding the lysis buffer which had been completed

with 1/44 TCEP (8 μ l TCEP with 350 μ l lysis-buffer). TCEP hydrochloride solution was obtained from Sigma Aldrich, St. Louis, MO. The following working steps were as those in 2.1.1.-2.1.3., including the DNA-digestion step, except for using the reagents and spin columns of the Machery-Nagel kit and adding 80% ethanol to the lysate for the RNA-precipitation. The cell-carrying scaffold membrane was lysed by using the double amount of prepared lysis buffer (700 μ l buffer with 16 μ l TCEP per sample). The incubating time for the lysis was 5 minutes. After that, the samples were thoroughly vortexed and centrifuged at 11,000 rpm for 1 minute before transferring the lysate to the spin columns. Since the capacity of the spin columns is 400 μ l, the samples were transferred in two steps à 350 μ l respectively, with a centrifuge step inbetween, always discarding the flow-through in the collection tubes.

Measurement of the RNA concentration:

At the end, the concentration of the eluted RNA was measured with Nanodrop systems 2000 and Nanodrop 2000/2000c v1.4.2-Software (Thermo Fisher Scientific, Waltham). RNA-concentrations in 2.1.1.-2.1.3. resulted between 116 and 347 ng/ μ l, in 2.1.4. it were between 30 and 122 ng/ μ l. The RNA was stored at -80°C for later usage.

2.3. cDNA synthesis

To convert the isolated RNA into cDNA, 600 ng total RNA of each sample (350 ng in the 2D/3D assays) was diluted in RNase free water up to the equalized end-volume of 10.5 μ l. Afterwards, each RNA-solution was carefully mixed by up-and down-pipetting with 9.5 μ l cDNA-synthesis reagent mixture. That contained 0.5 μ l RTase (RT = reverse transcriptase), 2 μ l 10x RT-buffer, 0.8 μ l 25x random nucleotides (100 mM), 2 μ l 10x random primer and 4.2 μ l RNase-free water. The High Capacity cDNA Reverse Transcription Kit from Applied Biosystems, Foster, was used. After thawing the kit reagents on ice, the random primer mix as well as the RT-buffer were vortexed and the random nucleotides were gently mixed by up-and down-pipetting before usage. The single 20 μ l reaction volumes (RNA-template + cDNA-synthesis reagent mixture) were transferred into small, low binding, RNase-free reaction tubes. All tubes were put into a

thermocycler (peqSTAR Thermocycler, Peqlab Biotechnologie, Erlangen) programmed as follows: 25°C during the first 10 minutes, 37°C during the next 120 minutes (RT-reaction), 85°C during the last 5 minutes (deactivation of reverse transcriptase), storage at 8°C. The definitive storage of the cDNA took place at -20°C.

2.4. Quantitative polymerase chain reaction (qPCR)

Dilution of the cDNA:

The cDNA obtained during the assays described in 2.1.1. – 2.1.3. was diluted 1:3, that from the 3D-assays in 2.1.4. 1:1 in RNase-free water, before subjecting it to the qPCR-reaction to amplify and quantify the cDNA of genes we were interested in.

Primer design:

Primers are short, nucleotide single strand-corresponding starting sequences for the amplifying enzyme, which is explained below in more detail (see the paragraph “qPCR”). The respective forward- and backward primers were designed with the *primer3plus* software, *Primer Express 3.0* (Applied Biosystems, Foster) or *PerlPrimer v1.1.21* in combination with the *NCBI primer blast* tool. Special attention was paid to the including of splice variants and to the excluding of sequence polymorphisms. To exclude the amplification of remaining DNA fragments in the sample, the primers were designed to span two exons with an intermediate intron as long as possible, or to overlap the border between an exon and an intron. As the intron is excised in the course of the RNA development, the transcript of the full DNA lasts much longer and, in contrast to the RNA-amplification, does not come to an end until one PCR-cycle is finished. The primer sequence was modified with the primer test tool according to the laboratory-internal established standard annealing temperature of 58-60°C. Afterwards, the readily designed primers were acquired from *Eurofins Genomics, Munich* or *Microsynth, Basel*. Before using the primers on a larger scale, their efficacy had been tested (an example is given in Fig. 13 and 14). To this end, the primers were diluted 1:4, 1:16, 1:64 and 1:256

in RNase-free water and the respective gene expression was measured by qPCR. The resulting CT values showed a linear decrease of cDNA amplification. The declination coefficient was 3.3 ideally.

CT value and housekeeping genes

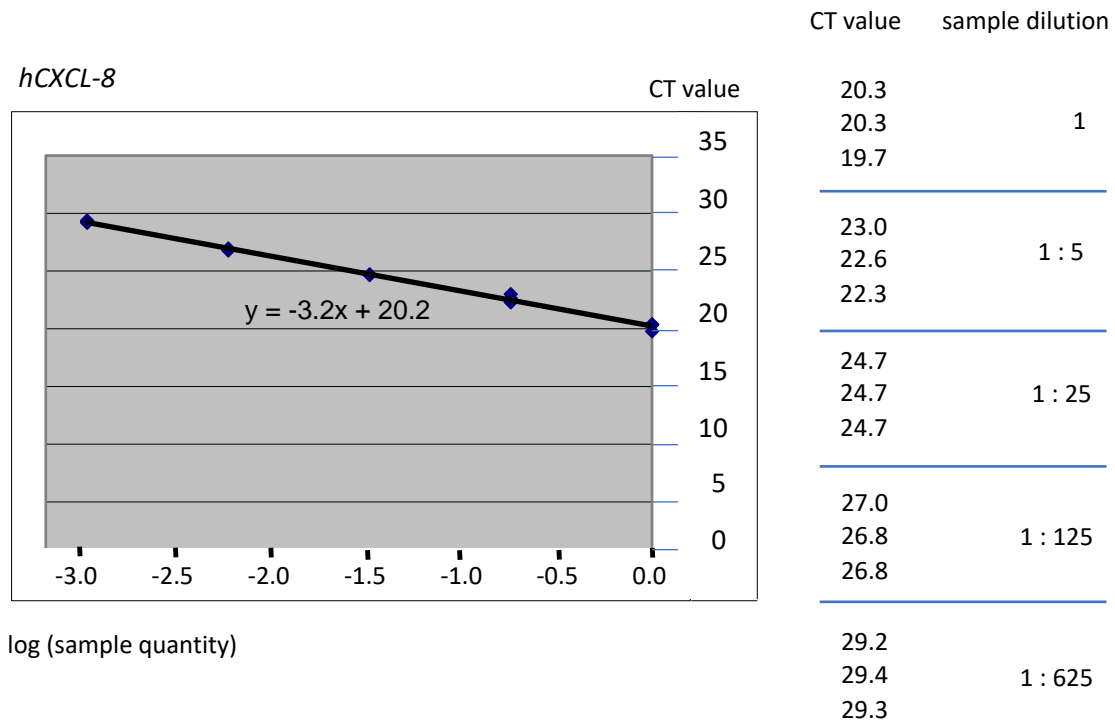


Fig. 13: Measurement of the primer efficacy, by using the example of primer against *hCXCL-8*, the linear increase of the CT value with logarithmic decrease of the sample quantity is illustrated.

The CT value (= cycle threshold value) is a theoretically set value within the exponential part of the cDNA replication curve that represents the number of needed PCR cycles after which a defined level of SYBR-green-cDNA complex fluorescence is reached. It is a value that allows the conclusion of the cDNA concentration of the examined gene in the sample and to compare it with the concentration of the same gene-cDNA in other samples. To correct for the bias caused by a, between the samples differing total gene amount, a quotient is calculated based on one to three reference genes. These reference genes, also referred to as “housekeeping genes”, are known to be relatively constantly expressed in the cells, irrespective of external conditions. In this examination, *hRPLPO*

(*human RPLP0*) and *hHPRT* (*human HPRT*) were used as housekeeping genes. Fig. 14 shows an example of an amplification plot with CT values.

SYBR-green is a cyanin colorant which emits light with a wave length of $\lambda = 521$ nm (green) in complex with double-stranded DNA.

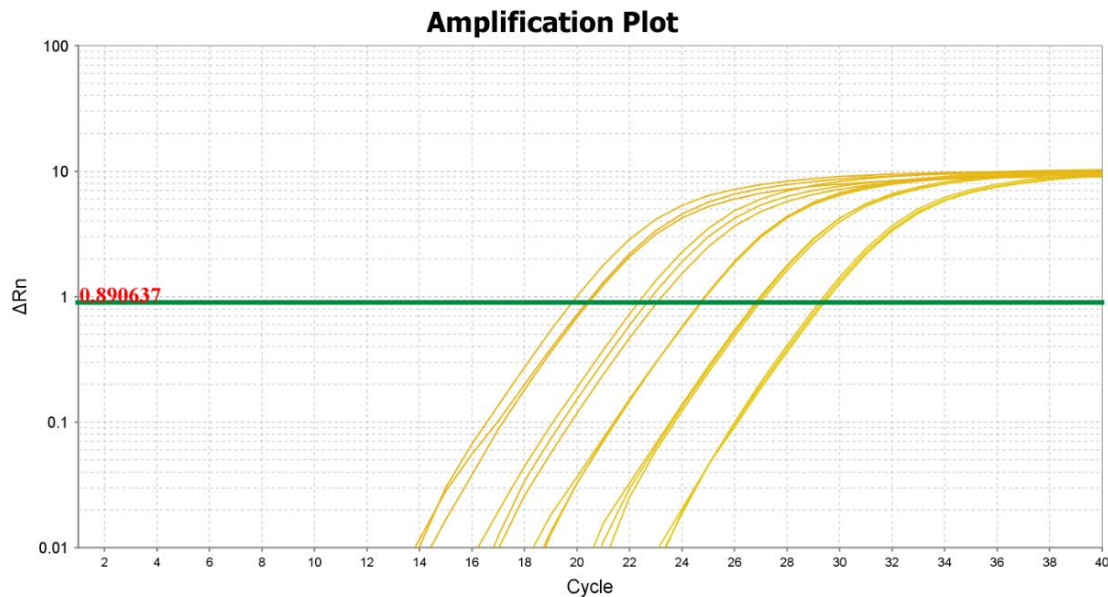


Fig. 14: PCR amplification plot. Showing *hCXCL-8* expression at different primer dilution steps.

qPCR:

The quantitative polymerase chain reaction (= qPCR) is a method to amplify, detect and quantify traces of specific cDNA sequences within a sample. As part of that, a quantitatively equalized cDNA sample is completed with the SYBR Select mastermix and previously designed short corresponding starting sequences (= primer), consisting of 18 to 26 ribonucleotides to amplify the sense and the anti-sense strand of the cDNA (forward and reverse primer, respectively). The SYBR select mastermix contains the SYBR-green nucleotide strand intercalating substance, the Taq polymerase and the Taq polymerase buffer. The primer facilitate the binding of the Taq polymerase to the cDNA. The Taq polymerase is a heat-stable DNA polymerase discovered in the bacterial species *thermophilus aquarius* that catalyses the elongation of the primer-initiated cDNA

double strand. It is also contained in the SYBR Select mastermix. Its ideal working temperature has been found to be about 70° C.

For the starting reagent, an equivalent amount of forward and reverse primer of the respective target gene was mixed with the 6-fold of ultra-pure (DNA-free) water and the 10-fold of SYBR Select mastermix within an DNase-free PCR reaction tube. In 2 corresponding wells of the PCR plate, 9 µl of the so-prepared starting reagent were mixed with 1 µl of the equalised cDNA template to be examined. The cDNA sample had been thawed on ice and well vortexed before adding. As negative control (NTC = non-template control), for every measured gene 2x 1 µl of ultra-pure water was supplemented to the primer-containing master mix instead.

The loaded PCR plate was covered with an adherent, transparent plastic film and centrifuged at high speed for a few seconds before being placed in the PCR device. The heating program was defined according to the PCR plate arrangement and the primer-annealing temperature. After starting the PCR program, the heating steps took place in a series of cycles comprising a double-strand breaking heating-time at the beginning (97°C), a primer-annealing phase (60°C), a longer temperature peak (70°C) as synthesizing-temperature for the Taq polymerase. Afterwards, the procedure started again from the beginning.

Used PCR system: *ViiA7 Real-Time PCR System + ViiA7 v1.2.1-Software (Applied Biosystems, Foster)*. Used PCR kit: *SYBR Select Master Mix (Applied Biosystems, Foster)*.

Table 3: Primer sequences

hHPRT_forward hHPRT_reverse	TGGGAGGCCATCACATTGTA AGCAGGTCAGCAAAGAATTTATAGC
hRPLP0_forward hRPLP0_reverse	CATCTACAACCCTGAAGTGCTTGAT CAATCTGCAGACAGACAGTGGC
hOSMR_forward	TGTCTGGAGAATTGTGAGCTTG

hOSMR_reverse	CATGCAGTTTTGATAATGGCTTC
hSOCS3_forward hSOCS3_reverse	AGACTTCGATTCGGGACCA AACTTGCTGTGGGTGACCA
hSTAT3_forward hSTAT3_reverse	CCCTTGGATTGAGAGTCAAGA AAGCGGCTATACTGCTGGTC
hCXCL8_forward hCXCL8_reverse	GTGGACCACACTGCGCC CAGTTTTCTTGGGGTCCAG
hCCL2_forward hCCL2_reverse	CAGCCAGATGCAATCAATGC CAGCTTCTTTGGGACACTTGC
hGPR109A_forward hGPR109A_reverse	CCGATCCAGAATGGCGG GAACATGGCTTCGTGCCACT

2.5. Protein electrophoresis/ SDS-PAGE

The SDS-PAGE (sodium-dodecyl-sulfat polyacrylamide gelelectrophoresis) is a method to isolate single proteins depending on their molecular size. It is based on electrochemical and mechanical processes. The gel matrix consists of acrylamid molecules that polymerize in a radical reaction to a 3-dimensional network. The pores inbetween that network are the smaller the higher the acrylamid portion is. The electrical voltage in the electrophoresis chamber leads to a slowly movement of the proteins through the gel matrix to the anode of the electrical system. Depending on their size, the proteins are more or less hindered in that movement by the pores of the gel with the smallest protein molecules being the least affected. To achieve an exact protein isolation (depending on amperage and time), two differently concentrated acryamid gel matrices were put in a row for the proteins to pass through (= discontinuous

gelelectrophoresis named after Laemmli). As part of this, the protein samples were pipetted into the slots of a smaller region of 3% acrylamid “collecting” gel (pH 6,8), which proteins passed before the following, 10%-polyacrylamid-containing “seperating” gel (pH 8,8). The ingredients of the collecting gel were *3,4 ml ultra-pure water (= AMPUVA®), 830 µl 30% acrylamid, 630 µl 2M TrisHCl (pH 6.8), 50 µl 10% SDS, 40 µl 20% APS, 5 µl TEMED*. The greater pores and the lower pH of the collecting gel (leaving proteins in the uncharged form), led to a comparatively slower passage and concentration of the proteins at the border between the two gel matrices. The separating gel contained the following ingredients: *5.9 ml ultra-pure H₂O, 5.0 ml 30% acrylamid, 3.8 ml 1.5 M TrisHCl (pH 8.8), 150 µl 10% SDS, 75 µl 20 % APS, 12 µl TEMED*.

The seperating gel was prepared first and quickly filled into the electrophoresis chamber. APS and TEMED were supplemented at the very end of the mixing procedure, because they induce the polymerization within a few seconds. A sharp border of the gel matrix was achieved by pipetting isopropanol on the surface at the beginning of the polymerization process. The seperating gel had been fully polymerized after 30' at room temperature. Then, the isopropanol was removed and the collecting gel mixture was filled onto the surface. It fully polymerizd within 1.5 hours at room temperature. During that time, a comb was set into the matrix to form the slots for the later pipetting of the protein samples.

The 30% acrylamide/BIS solution (37.5:1) was obtained from Bio-Rad Laboratories GmbH, Hercules, CA, USA (cat. no. #1610158). For other agents see table 4.

The SDS in the gel overcomes the positive charged portions of the protein molecules and equalizes the protein molecules in a negative charge. It ameliorates the protein migration to the anode of the electrophorese system. Glycin (which is a component of the Running buffer) is charged at the pH of 8.8 in the separating gel, which is essential to finish the protein collection and to start the separation process.

The proteins, which had been denaturated and stored in Laemmly buffer were now shortly heated at 95°C for 5 minutes to destroy possible renewed waterbridge bindings. After removing the comb, the protein samples were pipetted into the slots at equal amounts. As a scale, the following standardized protein ladder was pipetted into the

first slot: *“PageRuler Plus” prestained Protein Ladder, Thermo Fisher Scientific (Waltham).*

At 300 V, 30 mA and 150 W, the proteins were separated in the electric field for one and a half to two hours in the electrophoresis chamber, filled with 1x Running buffer.

2.6. Western blot

The Western blotting technique with the subsequent immunodetection (chapter 2.7.) of the blotted proteins allows a semi-quantitative comparison of the protein amount between different samples. It usually follows the gel electrophoresis and includes the fixation of the isolated proteins onto a blot membrane. For this purpose, the proteins are vertically transferred onto the membrane by the usage of a defined electrical voltage within a Western blotting chamber. To form a closed electrical circuit the following working steps were carried out:

The membrane to be blotted was cut to a size of 12 x 5 cm, shortly activated in methanol (5'') and afterwards impregnated in the anode-II-buffer for 15'. The protein-containing separating gel was incubated with cathode buffer for 5'. To keep orientation, the left upper corner of the gel was cut and thereby marked. 10 layers of filter paper (Whatman®) were cut to the same size as the membrane; four of them were impregnated in anode-I-buffer and two of them in anode-II-buffer. Then, these six were layered onto the anode of the blotting chamber, avoiding any air bubbles. The anode-II-buffer-impregnated membrane was placed onto that stack, followed by the protein-containing gel and the four remaining Whatman papers that had been likewise saturated in cathode-buffer before. The stack was carefully smoothed out, avoiding any destruction of the gel. After setting the cathode cover to close the electric circuit, the proteins were blotted on the membrane at 0.8 mA/ cm² gel (48 mA for the size of 12 x 5 cm) for 1h.

Afterwards, the membrane was gently removed, cut at the upper left corner to mark the blotted side and shortly washed in 1x TBS-T to remove remaining blotting buffer and to prevent it from drying out.

Table 4: Western blot and electrophoresis buffers and reagents

Name of the buffer solution:	Ingredients for solution in AMPUVA®:
Anode-I-buffer (2000 ml)	300 mM Tris (72.68 g/ 2000 ml), 20% (v/v) Methanol (400 ml/ 2000 ml)
Anode-II-buffer (2000 ml)	25 mM Tris (6.057 g/ 2000 ml), 20% (v/v) Methanol (400 ml/ 2000 ml)
Cathode-buffer (2000 ml)	40 mM 6-Aminohexanoic-acid (10.49 g/ 2000 ml), 20% (v/v) Methanol (400 ml/ 2000 ml)
10 x TBS-T (pH 7,6) (2000 ml)	1.37 M NaCl (160,12 g/ 2000 ml), 200 mM Tris (48,46 g/ 2000 ml), 1% Tween (20 ml/ 2000 ml)
10 x Running buffer (2500 ml)	0.25 M Tris (75,63 g/ 2500 ml), 1.92 M Glycin (360 g/ 2500 ml), 0.1% SDS (w/v) (25 g/ 2500 ml)
20% SDS-solution (10 ml)	2 g SDS /10 ml

Agent	Description/ Cat. no.	Manufacturer
Ammoniumperoxodisulfat	(APS)/ A2941,0100	AppliChem GmbH, Darmstadt, GER
6-Aminohexanoic acid	3113.3	Roth, Karlsruhe, GER
Glycerin (>99.5 %)	A3092	AppliChem GmbH, Darmstadt, GER
Hydrochloric acid (37 %)	fuming/ 4625.1	Roth, Karlsruhe, GER
Methanol (≥99.8%)	32213-2.5L-M	AppliChem GmbH, Darmstadt, GER
NaCl	131659.1214	AppliChem GmbH, Darmstadt, GER
SDS ultrapure (≥99 %)	A1112,0500	AppliChem GmbH, Darmstadt, GER
TEMED (≥99 %)	2367.3	Roth, Karlsruhe, GER

Tris ($\geq 99.9\%$)	A2264,1000	AppliChem GmbH, Darmstadt, GER
Tween [®] 20 BioChemica	A1389,0500	AppliChem GmbH, Darmstadt, GER

2.7. Immunodetection

Immunodetection is the analysis of protein compounds with the help of antibodies. The first antibodies specifically bind to short amino acid sequences (= epitopes) of a defined protein. The secondary antibodies bind the constant region of the first antibodies and were, in our study, coupled to an enzyme (horseradish peroxidase = HRP) that transforms a substrate which results in the emission of light.

Unspecific hydrophobic binding sites on the membrane were at first blocked by incubating the membrane in 10% BSA (bovine serum albumin) for 20 minutes on a shaking device. After that, the membrane was briefly washed twice in 1x TBS-T before adding the first antibodies to detect the membrane-blotted proteins. The incubation with the first antibody took place overnight at 4°C on a shaking device.

After being washed three times in 1x TBS-T (15', 5', 5'), the membrane was incubated with the secondary antibody for one hour at room temperature. After another three washing steps in 1x TBS-T the membrane was incubated in a 1:1 mixture of Luminol and peroxide solution for one minute. HRP catalyses the oxidation of Luminol- di-anions by hydrogen peroxide. During the following chemical transitions a bluish light is emitted (= chemiluminescence). The chemiluminescence detection was carried out via the usage of *Chemi Doc[™] MP Imaging System (170-8280) from Bio-Rad*. The software used was *Image Lab v5.2.1. from Bio-Rad*.

Reagents used: *ECL Western Blotting Detection Reagent, GE Healthcare, Amersham, cat.no.: RPN2106; Albumin Fraktion V (BSA) (pH 7,0), AppliChem, cat.no.: A6588,0250*. The antibodies were obtained from *Cell Signaling Technology[®], Danvers, USA* (Table 5). The first antibodies were maintained in 5% BSA at 5 °C. The secondary antibodies were maintained in 1x TBS-T at 5 °C.

Table 5: Antibodies

Antibodies (concentration):	CST-No.:	Species and preparation:
α -STAT3 (pY705) (1:2000)	9145S	mouse monoclonal, 2,5 μ l in 5 ml 5% BSA
anti-tubulin (1:5000)	2148S	mouse monoclonal, 1 μ l in 5 ml 5% BSA
α -STAT3-(pS727) (1:1000)	9134L	rabbit polyclonal, 5 μ l in 5 ml 5% BSA
anti- α -P-p38 MAPK (1:1000)	4511S	rabbit monoclonal, 5 μ l in 5 ml 5% BSA
anti- α -p38 MAPK (1:1000)	9212S	rabbit monoclonal, 5 μ l in 5 ml 5% BSA
anti- α -STAT3 (1:2000)	9139S	mouse monoclonal, 2,5 μ l in 5 ml 5% BSA
anti- α -pT222-MK2 (1:1000)	3044S	rabbit polyclonal, 5 μ l in 5 ml 5% BSA
anti-rabbit (1:4000), HRP-coupled	7074S	3 μ l in 12 ml 1x TBS-T
anti-mouse (1:4000), HRP-coupled	7076S	3 μ l in 12 ml 1x TBS-T
anti- GAPDH (1:5000)	5174S	rabbit monoclonal, 1 μ l in 5 ml 5% BSA
anti- P-I κ B α (1:2000)	9242S	rabbit polyclonal, 2.5 μ l in 5 ml 5% BSA

anti- MK2 (1:1000)	3042S	rabbit polyclonal, 5 μ l in 5 ml 5% BSA
--------------------	-------	--

2.8. Simultaneous detection of several signaling molecules and reprobing of membrane

If possible, e.g. due to different molecular weights, two different signaling molecules were detected simultaneously from one cell lysate by cutting the Western blot membrane into two fragments. The upper fragment was used to detect the higher molecular weight protein, the lower to detect the lower molecular weight protein. To evaluate total protein irrespective of the phosphorylation status, the membranes were incubated in 30 ml stripping buffer (2g SDS dissolved in 100 ml 10x TBS-T) supplemented with 280 μ l Mercaptoethanol (99%) at 70 °C for 25', washed and reprobed with antibodies detecting the total protein. To prove equal loading of individual lanes the membranes were stripped again and incubated with antibodies detecting the house-keeping protein tubulin.

2.9. Data analysis and statistics

Western blot results

The raw Western blot results, which respectively consist of detected (photographed) light typically arranged in a broad, smooth band, were analyzed using the ImageLab software. Specifically, this entails employing the ImageLab tools "Crop", "Lanes and bands", "Analysis table" and "relative Quant" to ascertain the mean location of the light along the x- and y-axis and to express its intensity in a decimal term, which represents the amount of protein in the sample. Since one is interested in the protein (total STAT3 and pS727-STAT3) *concentration*, the sample size needed to be determined as well. This was provided here by simultaneously measuring the amount of Tubulin in the respective sample, likewise via Western blot analysis. Subsequently, only the protein-Tubulin ratio

was used for the calculation of the increase of the total STAT3 and pS727-STAT3 concentration, that evolved in sodium butyrate, respectively TSA treated samples in comparison to not treated samples. The latter served as control samples, used to differentiate sodium-butyrate/TSA-related protein production or phosphorylation from possible other causes. To ameliorate measurement errors, each measurement was repeated thrice. The calculation was carried out via the usage of *Microsoft Excel 2010*. First, the mean value ($\langle x \rangle$) of the measurement-vs-control concentrations (x_i) was calculated.

The standard deviation, $SD = \sqrt{\sum (x_i - \langle x \rangle)^2 : (n - 1)}$, of such a data cohort (n = number of elements) was used as an estimate of the measurement uncertainty of an individual datum ($\sigma_i = SD$). Hence, the uncertainty of the mean value is $\sigma_m = \sigma_i / \sqrt{n}$. Since the control samples and treated samples were systematically matched for the calculation of the factor of protein elevation, the measurement error of the solvent controls could be kept unattended (see Fig. 15).

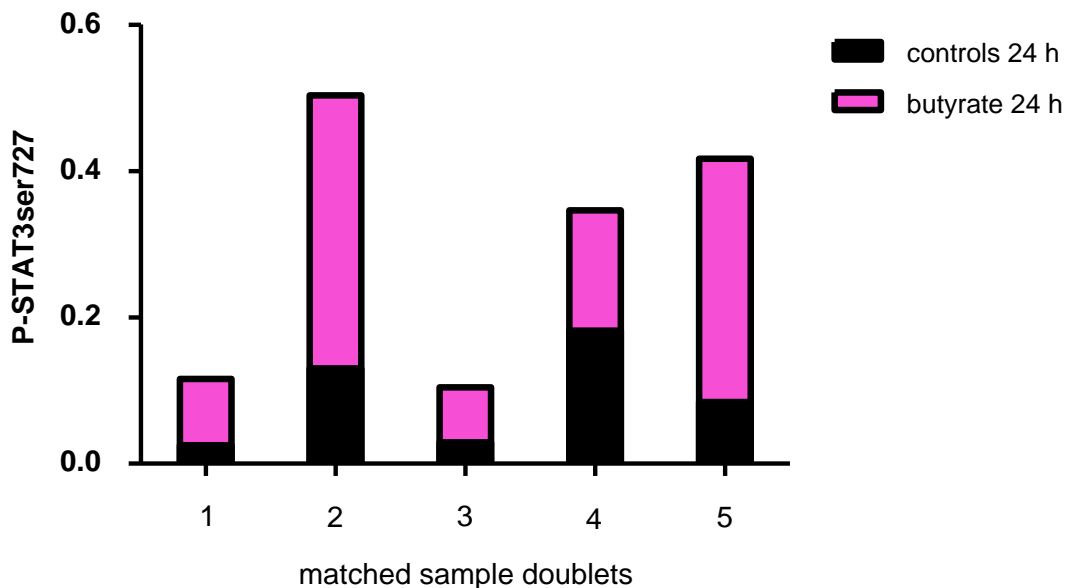


Fig. 15: Matched sample doublets. To calculate the relative difference of the chemiluminescence signal at protein bands, treated samples and control samples were systematically matched. Hence, the measurement error of the control values could be kept unattended. Here, this principle is displayed at the example of the 24-hours butyrate-treated samples ($n=5$).

As alternative verification of the significance of the increase of pS727-STAT3 in the sodium butyrate/TSA-exposed cells compared to the control samples, we performed a one-tailed Mann-Whitney U-test, using the *GraphPad Prism software*. If there had been no clear elevation in protein concentration after butyrate-, respectively TSA exposure, a two-tailed Mann-Whitney U test was applied instead. This was the case with total STAT3 protein after a single butyrate- or TSA-exposure.

We obtained such measurements after 24 hours as well as 50 hours of sodium butyrate incubation and analyzed them both in the above manner.

For those samples that had been treated with sodium-butyrate for 50 hours, above-described procedure was repeated two more times, except for that the samples had been additionally stimulated once with 10 µg/ml TNFα and once with 20 µg/ml OSM during the last hour of butyrate incubation, respectively. The additional stimulation served to assess whether the changes in pS727-STAT3- or total STAT3 concentration were influenced by a defined inflammatory stimulus.

PCR-results

The PCR raw data come in form of the CT values, which had been determined as end results of the PCR process via the *ViiA7 v1.2.1-Software*, and were further processed using *Microsoft Excel 2010*. Based on the CT value, whose meaning is explained in chapter 2.4., page 40, the mRNA concentration of a specific gene product in the treated samples could be related to the mRNA concentration of the same gene product in the respective untreated controls.

Analogous to the protein concentration measurement in the Western blot procedure, the determination of the mRNA concentration involved the normalization of the single results against a stable occurring mRNA (“housekeeping gene”; see chapter 2.4.).

To preclude technical measurement errors, each PCR detection was carried out twice in form of a doubled sample arrangement on the PCR plate. The mean difference of the two single measurements from the mean value of the respective housekeeping gene, the *mean*ΔCT value, was then used for all subsequent calculations.

The calculation of ki_c and ki , which is the divergence of the mRNA concentration in each sample relative to the controls' mean, included the individual determination of $\Delta\Delta CT$. Therefore, the average mean ΔCT of the identically treated control samples was subtracted from the mean ΔCT of each of the control- (for ki_c) and with butyrate, TSA or cytokine-treated samples (for ki). Afterwards, $2^{-\Delta\Delta CT}$ was calculated individually for each control- (for ki_c) and treated sample (for ki), presupposing a duplication of the gene material of interest in every PCR-cycle.

The factor of the mean treated-vs. control mRNA increase (F) was calculated:

$$F = \langle ki \rangle / \langle ki_c \rangle;$$

$\langle ki_c \rangle$ = average of all ki_c and

$\langle ki \rangle$ = average of all ki belonging to identically treated samples in one or more connected assays.

The uncertainty of this factor ($E(F)$) was calculated:

$$E(F) = F * \sqrt{[\sigma_{m_ki_c} / \langle ki_c \rangle]^2 + [\sigma_{m_ki} / \langle ki \rangle]^2};$$

σ_m = sample error of the mean.

In the graphical presentation using the *GraphPad Prism v6 Software*, single relative sample mRNA concentrations were visualized as a multiple of the mean relative control mRNA concentration. The error bars in that graph are the respective sample error of the mean ($\sigma_m \langle ki_c \rangle$, $\sigma_m \langle ki \rangle$). They both differ from $E(F)$, which is the uncertainty of the ratio $F = \langle ki \rangle / \langle ki_c \rangle$.

The significance of the supposed mRNA concentration increase after treatment was calculated on the basis of the mean ΔCT values, using the one-tailed Mann-Whitney U test, if acting on the assumption that target genes of treated samples only progress in one direction. If this was not the case, the two-tailed Mann-Whitney U test was consulted. In the case of $n > 6$, the one- or two-tailed, ungrouped Student's t-test was used situation-dependently.

In the 2D/3D assay described in 2.1.4., the samples had been delivered on two separate PCR runs. To provide comparability, the thresholds of both the gene of interest as well as the housekeeping gene were levelled. Despite of this, the ΔCT values showed a high variance between the two PCR runs. Although a real biological difference among the samples is expected, a loss of primer function cannot be excluded in retrospect. To address this, the $\Delta\Delta CT$ values were calculated by always referring the single mean ΔCT values of treated samples to the respective control values mean out of the same PCR run instead of relating to the average of all control mean ΔCT values.

3. Results

3.1. Butyrate's effects on STAT3 in CACO2-cells

3.1.1. Butyrate significantly increases pS727-STAT3 in CACO-2 cells

To investigate butyrate's effects on the serine727-phosphorylation of STAT3 (pS727-STAT3) in the colon cell line CACO-2, cells were seeded at a density of 230.000 per well into wells of a 24-well plate as described in the methods section. 5 days differentiated cells which formed a confluent monolayer were then incubated with 5 mM sodium butyrate for 24, respectively 50 hours. Afterwards, whole cell extracts were analyzed by SDS-page/Western blot and antibody-based detection of the relevant phosphorus group, as it is explained in chapter 2.7. The quantification of the phosphorylation changes was done on the basis of the chemiluminescence quantification images by the usage of the *Image Lab v5.2.1*-software, as described in chapter 2.9. Three representative examples of the detected bands are displayed in Fig. 16 (a: 50h-butyrate, b: 24h-butyrate incubation). Each Western blot membrane displays the samples of an independently conducted assay, done in triplicates. The quantification plot of the 50h-samples summarizes the results of two independently conducted assays done in triplicates.

In the 24h-sample cohort, the quantification included one experiment done in triplicates (see the Western blot membrane in Fig.16b) and another independently conducted experiment done in duplicatets.

Butyrate exposure significantly elevated pS727-STAT3 protein in CACO-2 cells at both named points in time (Fig. 16). The increase was the most expressed after a 24h-incubation period (up to the 3.8 +/- 0.5-fold of the solvent controls mean; n = 5; p < 0.05) and was, to a lesser extent, also observable after a 50h-butyrate incubation (up to the 2.2 +/- 0.2-fold; n = 6; p < 0.02).

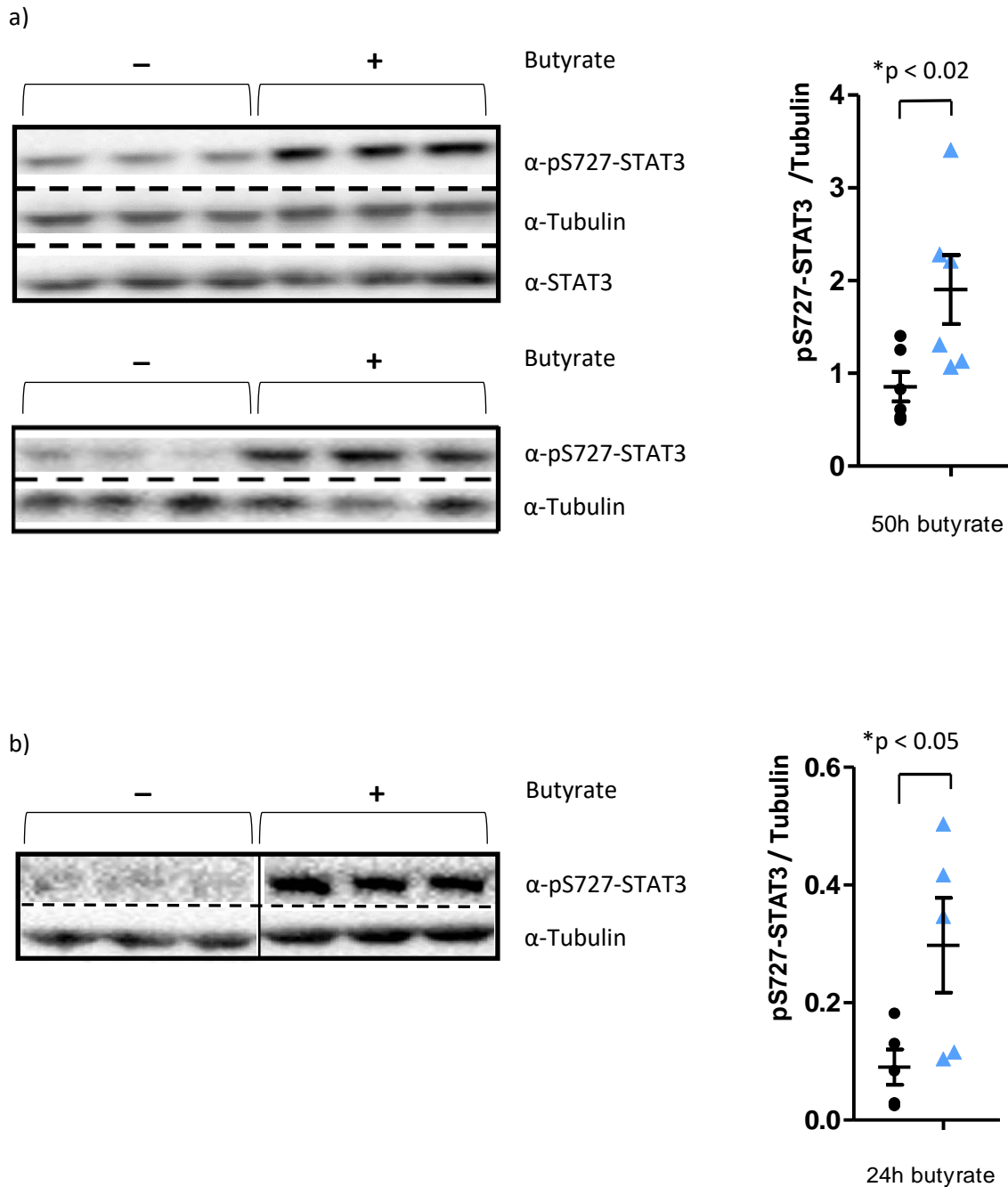


Fig. 16: pS727-STAT3 in the butyrate incubation assays.

5 days-differentiated CACO-2 cells were either left as unstimulated controls or were incubated with 5 mM sodium butyrate for a) 50 hours or b) 24 hours. Full cell lysates were Western-blotted and chemiluminescence-detected for pS727-STAT3. Tubulin served as reference protein for the total protein amount within a sample. Displayed are representative Western blot membranes of 3 independently conducted assays done in triplicates. The quantification graphs of the pS727-STAT3/Tubulin ratios on the right-hand side summarize the results of two independently conducted assays done in triplicates (50h) respectively one experiment done in triplicates and one in duplicates (24h-samples). Black dots represent control values, blue triangles the values of butyrate-treated samples. Black bars show the mean value and the error of the mean. Significance was calculated at the basis of the pS727-STAT3/Tubulin ratios using the one-tailed Mann-Whitney U test of significance.

3.1.2. Time dependency of pS727-STAT3 elevation

To verify the observed points in time as appropriate for recording the butyrate-caused changes of pS727-STAT3, a time-dependent Western blot analysis was added. The observation started at 1 to 7 minutes after the beginning, and comprised the 15, 30, 60 and 75 minutes- as well as the 20-, 24- and 48-hour time points of the butyrate incubation. In addition to the pS727-STAT3 protein, we also investigated possible changes in total STAT3 protein amount since they could contribute to the pS727-STAT3 results. The explanation is, even if the phosphorylation rate of S727-STAT3 stays the same, an increase of total STAT3 would enhance the amount of pS727-STAT3 by providing more molecules to be phosphorylated by the responsive kinases. Total STAT3 was detected with an antibody which also binds to unphosphorylated forms of STAT3 or to STAT3 molecules phosphorylated at other amino acid residues than serine727.

The Western blot results, displayed in Fig. 17, reveal an increase of pS727-STAT3 from 20 hours of butyrate exposure on, which stays until the end of the 48h-observation period. Likewise, the total STAT3 protein is slightly increased during this time of butyrate incubation.

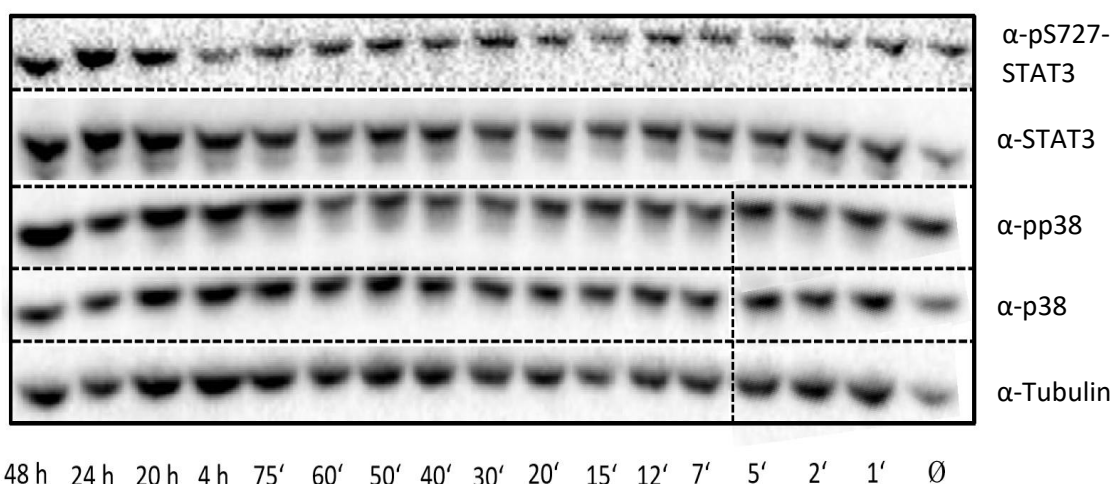


Fig. 17: Time-dependent, butyrate-caused changes of pS727-STAT3, total STAT3 and pp38 MAPK. 5 days differentiated CACO-2 cells were either left in DMEM with an equivalent aqua dest. (\emptyset) or were exposed to 5 mM sodium butyrate for a different duration (from 1' to 48h). Full sample lysats underwent SDS-PAGE electrophoresis and Western blot analysis. Displayed is the Western blot membrane with protein bands, ordered by time of butyrate exposure. Proteins had been detected with indicated antibodies. Because lanes were too diagonal for the graphic, the picture was cut and adapted along the broken lines.

Since the p38 MAPK was formerly assumed to be one of the kinases playing a role in serine727-phosphorylation of STAT3, we also measured its active, phosphorylated form (pp38 = pp38 MAPK) as well as the total p38 MAPK protein (p38) time-dependently in this assay. While the total p38 MAPK protein stayed at the same level when being referred to the matching tubulin signal (which reflects the overall protein amount within a sample), pp38 MAPK was increased from 75 minutes of butyrate exposure on, lasting until the end of the 48h-observation period.

3.1.3. Butyrate increases total STAT3 protein

As already seen in the time-dependent butyrate results above (Fig. 17), an increase of total STAT3 may have contributed to the butyrate-caused elevation of the pS727-STAT3 signal intensity. To further explore this, CACO-2 cells were treated as described in chapter 3.1.2. Full cell lysates underwent Western blot analysis. Total STAT3 protein was detected by a specific antibody (α -STAT3) and subsequently luminescence detected as described in chapter 2.7.

In three independent experiments, carried out in triplicates, twice an upregulation of total STAT3 was observed in response both to 24h and 50(48)h of butyrate treatment. In one out of two quantitatively evaluated 50h-butyrates assays done in triplicates, the intensity of the chemiluminescence signal at α -STAT3-detected protein bands was calculated to be the 1.4 +/- 0.3-fold of the base value; n = 3, p = 0,4 (Fig. 18a). This was not significant at the basis of a 95%-confidence interval using the two-tailed Mann-Whitney U test of significance. However, the increase of total STAT3 contributed to that of pS727-STAT3 with a portion of about 30 % in this example. The other one of the two assays did not show an increase of total STAT3 after an incubation with butyrate for 50h. It is worth to mention, that the Western blot membrane in this example had been stripped twice, which means once more than the one used for the positive example, before detecting α -STAT3. This could have negatively affect the α -STAT3 signal.

After a 24h-butyrates incubation, the increase of total STAT3 protein, normed to tubulin, was up to the 1.2 +/- 0.05-fold of the solvent control in one assay done in biological

triplicates (Fig. 18b). The result did not reach significance on the basis of a 95 %-confidence interval, consulting the two-tailed Mann-Whitney U test ($n = 3$).

On top of the singularly butyrate-treated triplicates, the 50h-observation was widened out on biological triplicates which were additionally stimulated with TNF α or OSM at the very end of the assay (see chapter 3.2.). Butyrate incubation enhanced total STAT3 protein in all of these samples as well. This also applied for the assay displayed in Fig. 18c which did not show a butyrate influence in the singularly butyrate-treated samples.

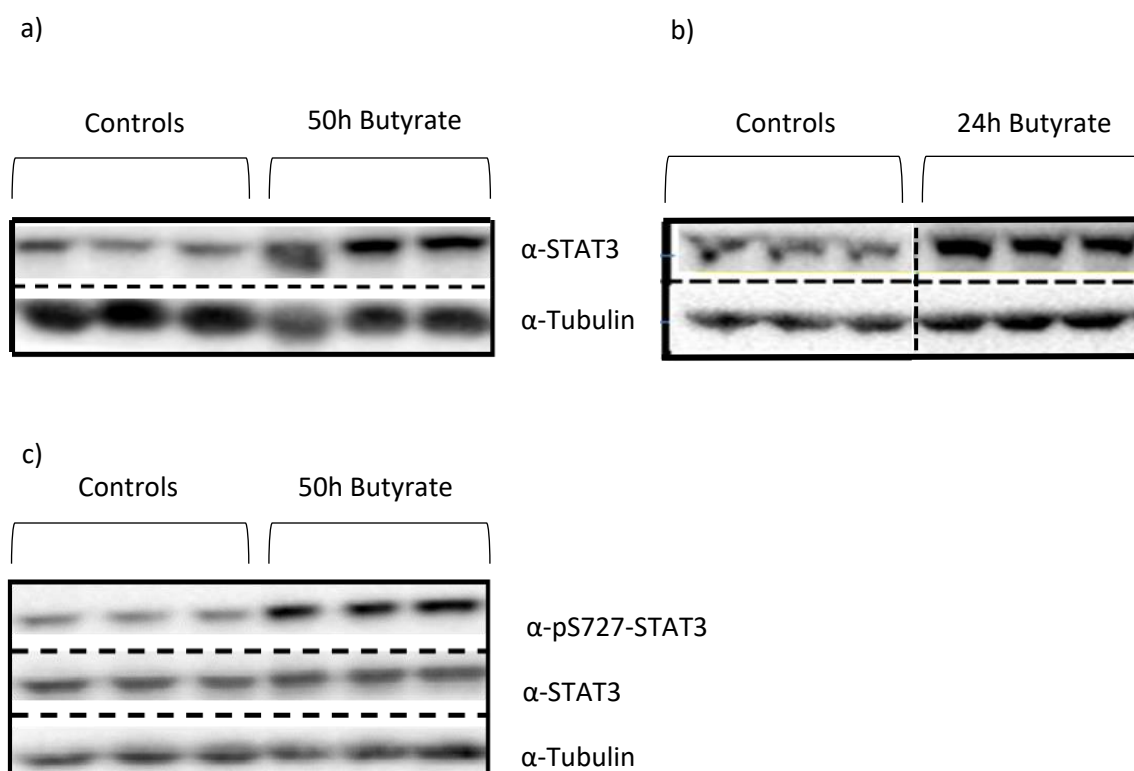


Fig. 18: total STAT3 in the butyrate incubation assays.

5 days differentiated CACO-2 cells were either left as controls or were incubated with 5 mM sodium butyrate for 50h (a and c), respectively 24h (b). Full cell lysates were Western-blotted and luminescence-detected using the indicated first, and HRP-coupled second antibodies (see table 5 in the methods section). Displayed are the Western blot membranes with proteins from 3 independently conducted assays done in biological triplicates. After the detection of pS727-STAT3, the membrane was stripped and reprobed with α -STAT3 antibodies as it is described in chapter 2.8. to detect total STAT3 protein.

3.1.4. Butyrate significantly increases *hSTAT3* expression

qPCR measurement revealed an increase of the expression of the human (h) STAT3 encoding gene (*hSTAT3*) under butyrate influence, both after 24 and 48 hours of exposure (Fig. 19). It reached significance after a 48h-butyrate incubation period. In comparison to a 24h-incubation, the level of significance was mainly reached by the greater sample cohort tested.

This allowed the usage of the two-tailed, unpaired Student's t-test of significance for the 48h-butyrate incubated samples. The mean *hSTAT3*-mRNA elevation was up to the 1.4 +/- 0.04-fold of the base value (n = 9, p < 0.02).

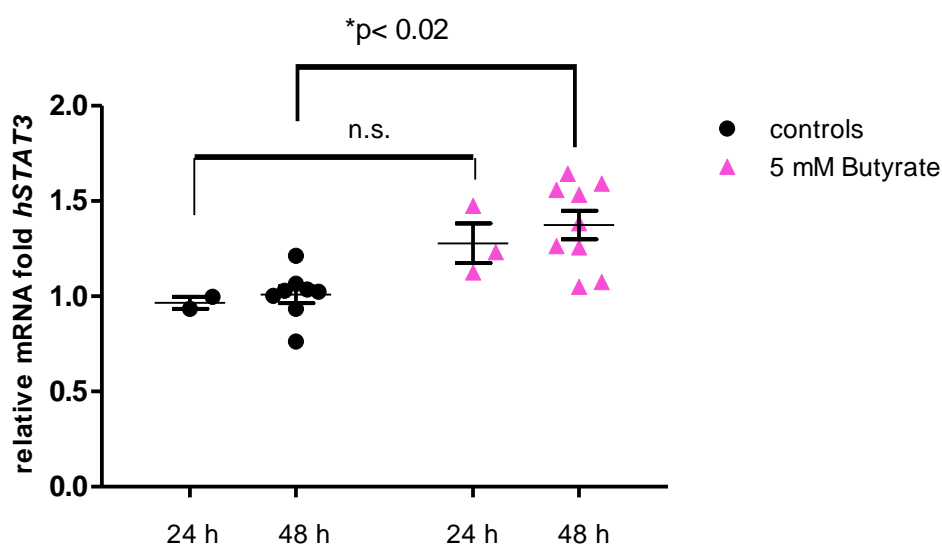


Fig. 19: *hSTAT3* expression in the butyrate incubation assays.

The determination of the *hSTAT3* gene expression via qPCR of CACO-2 cell lysates which were either cultivated in DMEM (controls) or treated with 5 mM sodium butyrate for 24, respectively 48 hours, revealed an elevation of *STAT3* mRNA expression in the course of butyrate exposure. It reached significance after a 48h-butyrate incubation period ($p < 0.02$), mainly due to the greater sample cohort tested. (n.s. = not significant). Significance was calculated by using the two tailed Student's t-test (48h- samples) and the two-tailed Mann-Whitney U test (24h-samples).

3.1.5. Butyrate modulates STAT3 mainly via HDAC inhibition

To investigate the role of HDAC inhibition in the context of butyrate-caused pS727-STAT3 elevation, we replaced butyrate as stimulating agent with 400 nM of the known HDAC inhibitor Trichostatin A (TSA), as described in chapter 2.1.2.

Like butyrate, TSA led to a significant elevation of pS727-STAT3 in CACO-2 cells after 24 hours of incubation. pS727-STAT3 in treated cells was the 2.8 +/- 0.9-fold of the solvent controls mean; n = 3; p < 0.05. This corresponds to a level of pS727-STAT3 elevation which lies between the ones reached by butyrate after 24h and 50h of incubation.

A representative Western blot membrane which shows the pS727-STAT3-detected protein bands as well as the quantification diagram of the chemiluminescence intensity of the single bands (normalized against the tubulin signal) is displayed in Fig. 20.

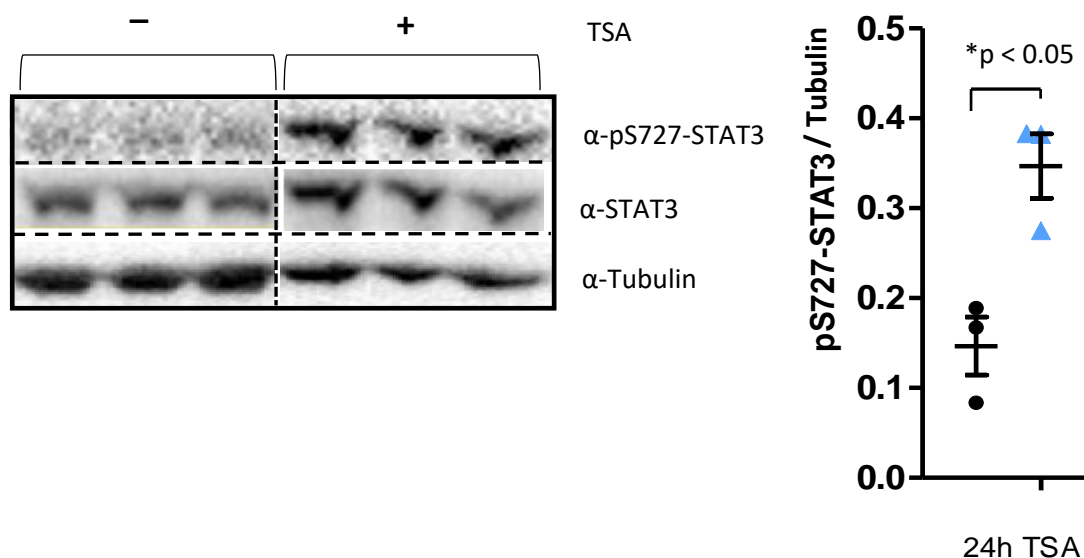


Fig. 20: pS727-STAT3 and STAT3 in the TSA incubation assays.

Displayed is a representative Western blot membrane with the α-pS727-STAT3 and α-STAT3 antibody-chemiluminescence-detected proteins of 3 samples which had been treated with 400 ng/ml TSA for 24 hours, respectively 3 control samples which were exposed to an equivalent amount of Ethanol (the TSA solvent agent). The quantification of the pS727-STAT3/Tubulin ratios is visualized on the right-hand side located graphic (controls = black dots, treated samples = blue triangles). The mean value and the error of the mean are shown (black bars). On the basis of the pS727-STAT3/Tubulin ratios, significance was calculated using the one-tailed Mann-Whitney U test of significance.

Like a 24h-butyrate incubation, also the treatment of CACO-2 cells with 400 nM TSA for 24h slightly increased the total STAT3 protein (Fig. 20). Total STAT3 had been detected with an antibody which also binds to unphosphorylated forms of STAT3 as well as to STAT3 molecules phosphorylated at amino acid residues apart from serine727.

It is worth to mention that, similar to a 24- and 50h-incubation with sodium-butyrate, the incubation of CACO-2 cells with 400 nM TSA for 24 hours did not consistently lead to an increase of STAT3 total protein amount. In one assay done in triplicates, the elevation was up to the 1.3 +/- 0.004-fold of the solvent control. In another assay done in triplicates, no elevation of total STAT3 protein was detectable. The portion of total STAT3 on the pS727-STAT3-elevation was calculated to be 17 % for the 24h-TSA-treated cells in the positive example depicted in the Western blot membrane in Figure 20.

After a TSA-incubation for 48 hours, signs of cell destruction became visible via light microscopy. These comprise the reduction of intercellular spaces, sphere scheme of cells as a sign of detachment from the surface and the increase of cell detritus (Fig. 21).

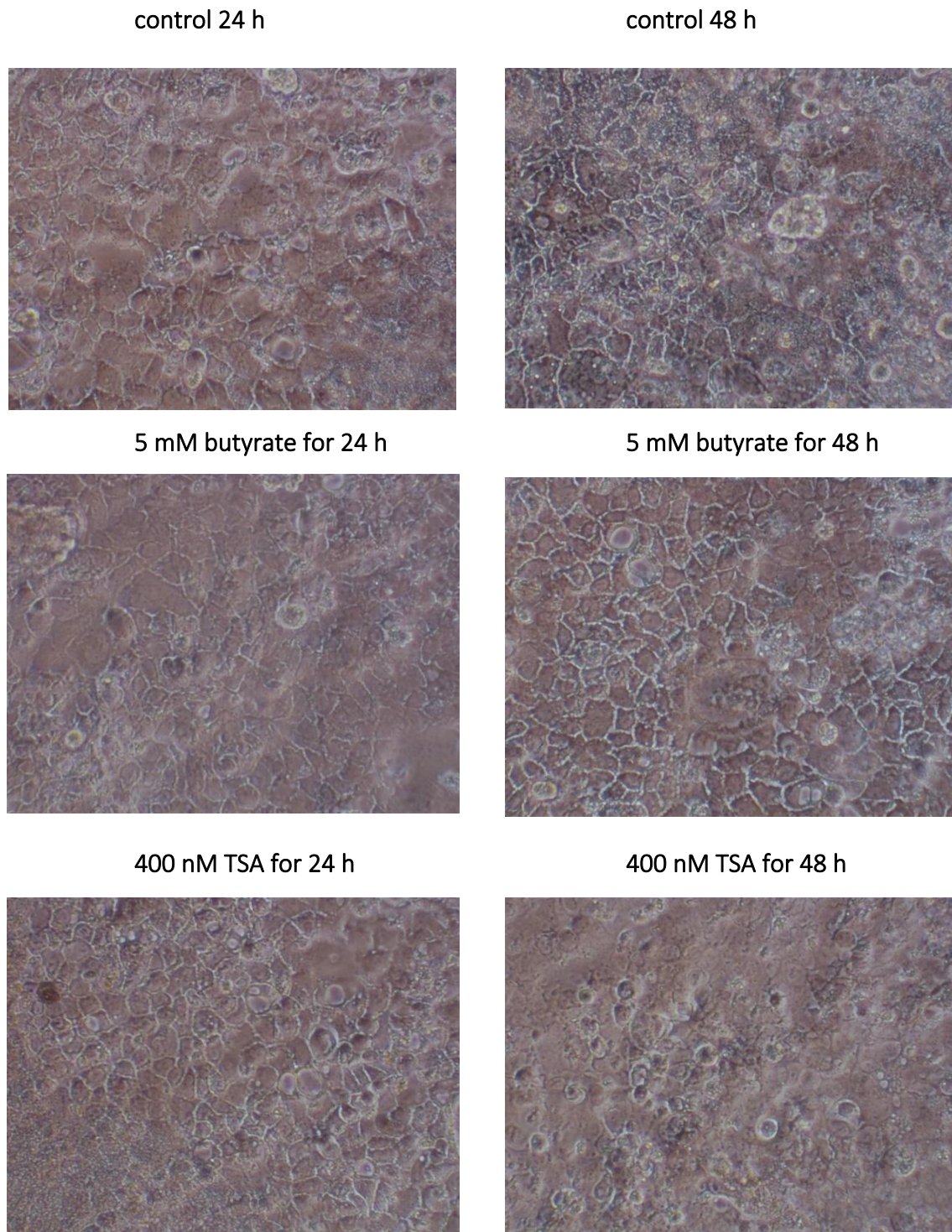


Fig. 21: CACO-2 cell monolayer with or without a butyrate/ TSA treatment, Light microscopic pictures of CACO-2 monolayer, enlargement 200x; After a 48h-TSA incubation period there are signs of cell destruction like invisible intercellular spaces, sphere-scheme of cells and an increase of cell detritus.

The determination of the *hSTAT3* gene expression via qPCR revealed an increase of *hSTAT3* mRNA expression up to the 1.9 +/- 0.3-fold (n = 3, n.s.) after a 24h-incubation of CACO-2 cells with 400 nM TSA (Fig. 22). The expression dropped below the level of the untreated control cohort after 48h of TSA-treatment, probably due to cell destruction which was seen in light-microscopy (Fig. 21).

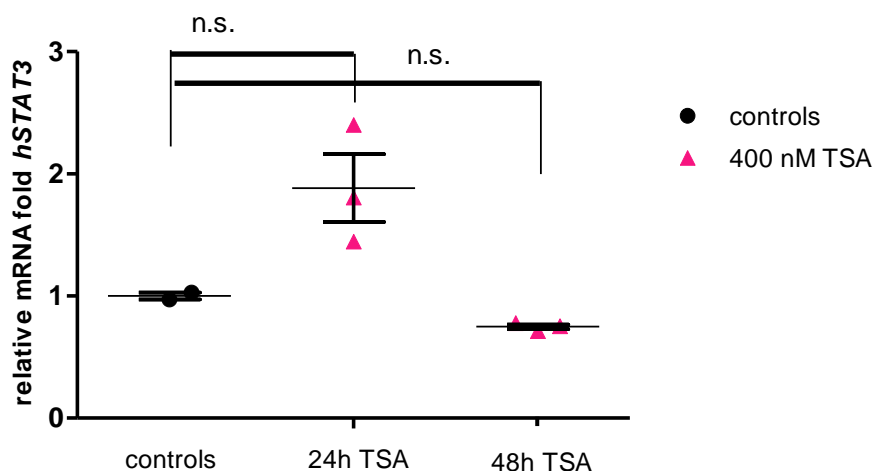


Fig. 22: *hSTAT3* expression in the TSA incubation assays.

5 days differentiated CACO-2 cells were either left as controls or stimulated with 400 nM TSA for 24, respectively 48 hours. Gene expression of *hSTAT3* was determined by qPCR analysis. Displayed are the single, to the mean control value relativated qPCR $2^{-\Delta\Delta CT}$ -values, the mean and the sample error of the mean (black bars). For testing the significance of the results on the basis of the mean ΔCT -values by using the two-tailed Mann-Whitney U test, one more control value was generated by taking the mean value of the control cohort, as the test needed minimum three values per group. n.s. = not significant.

3.1.6. Butyrate-caused pS727-STAT3 elevation is connected to p38 MAPK activity

During butyrate-incubation timeline assays, we already observed an increase of phosphorylated p38 MAPK (pp38 MAPK), occurring in CACO-2 cells after a 75'-lasting exposure to 5 mM sodium-butyrate. pp38 MAPK stayed increased until the end of a 48h-butyrate incubation period (Fig. 17).

p38 MAPK is supposed to be involved in the serine727-phosphorylation of STAT3. To investigate the role of p38 MAPK activity on pS727-STAT3 protein in our assays, we took

usage of the p38 MAPK blocker SB203580 and SB202190. Both block the active centrum of the α -isoform of p38 MAPK and are exchangeable.

Therefore, one of the blockers was supplied to the cell culture medium at a 10 μ M-concentration, 30 minutes previous adding sodium-butyrate. It was left within the culture medium until the end of the assay.

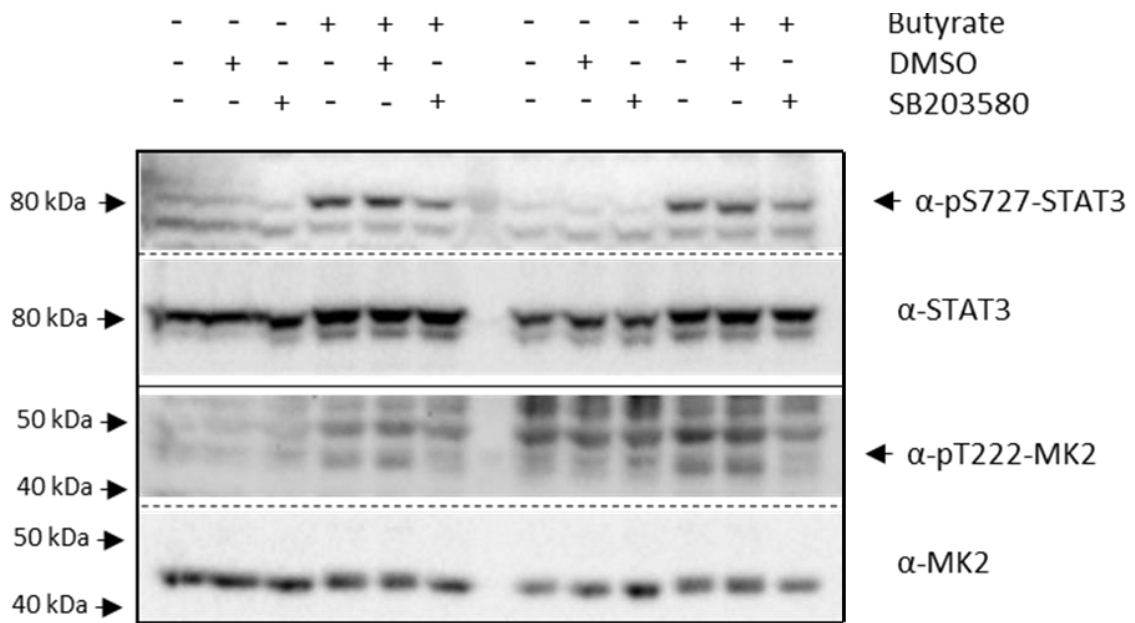
As aforementioned in chapter 1.4.4., mitogen kinase-activated protein (MK2) is a known target of p38 MAPK in IECs. The threonine222-phosphorylated form (pT222-MK2) represents the p38 MAPK-activated form of that enzyme. Therefore, in order to delineate changes of p38 MAPK's enzymatic activity in response to butyrate +/- SB203580, we detected both total MK2 and pT222-MK2, simultaneously focusing on pS727-STAT3 and total STAT3 protein (Fig. 23) via using the Western blot technique and antibody-based chemiluminescence detection.

Butyrate induced T222-MK2-phosphorylation, paralleled to the increase of pS727-STAT3. The usage of SB203580 prevented the butyrate-induced elevation of both pS727-STAT3 protein and pT222-MK2 (Fig. 23a).

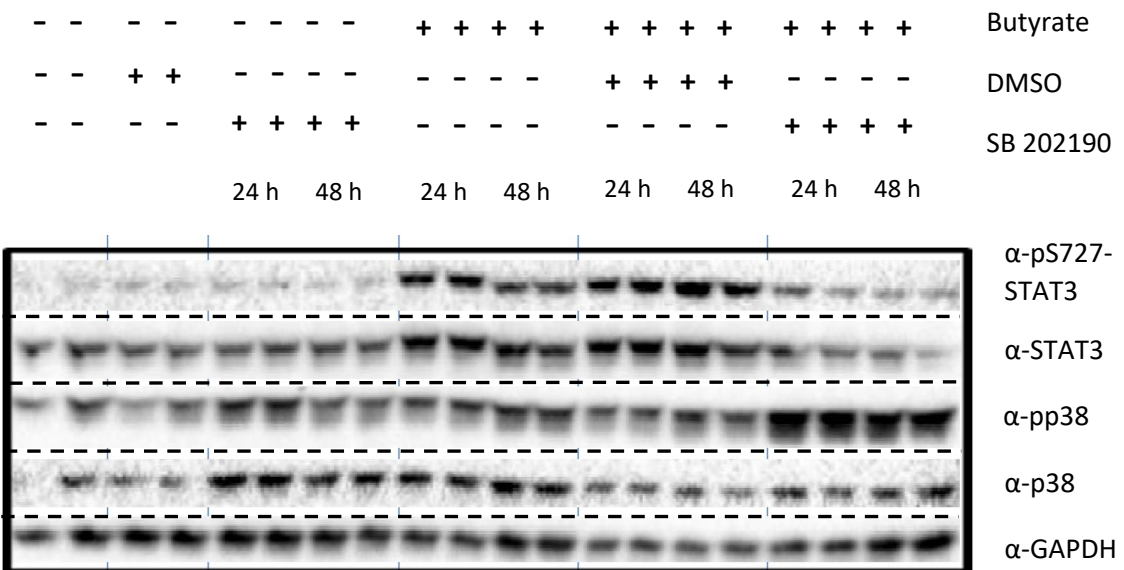
Delineable from the light intensity at p38 MAPK protein bands, p38 MAPK blockade using SB202190 led to an enhancement of phosphorylated p38 MAPK (pp38 MAPK), both after a 24- and a 48h-observation period (Fig. 23b-d). It is noteworthy that the increase of pp38 MAPK was the more pronounced when a p38 MAPK blocker was combined with a 5 mM-butyrate incubation. This could indicate an activation of a p38 MAPK-upstream kinases by butyrate, which is discussed in chapter 4.1.4.a.

A contemporaneous prevention of total STAT3 elevation by SB202190, which was observable in one of the assays done in triplicates (Fig. 23b), could not be reproduced in two further assays (Fig. 23 a,c,d).

a)



b)



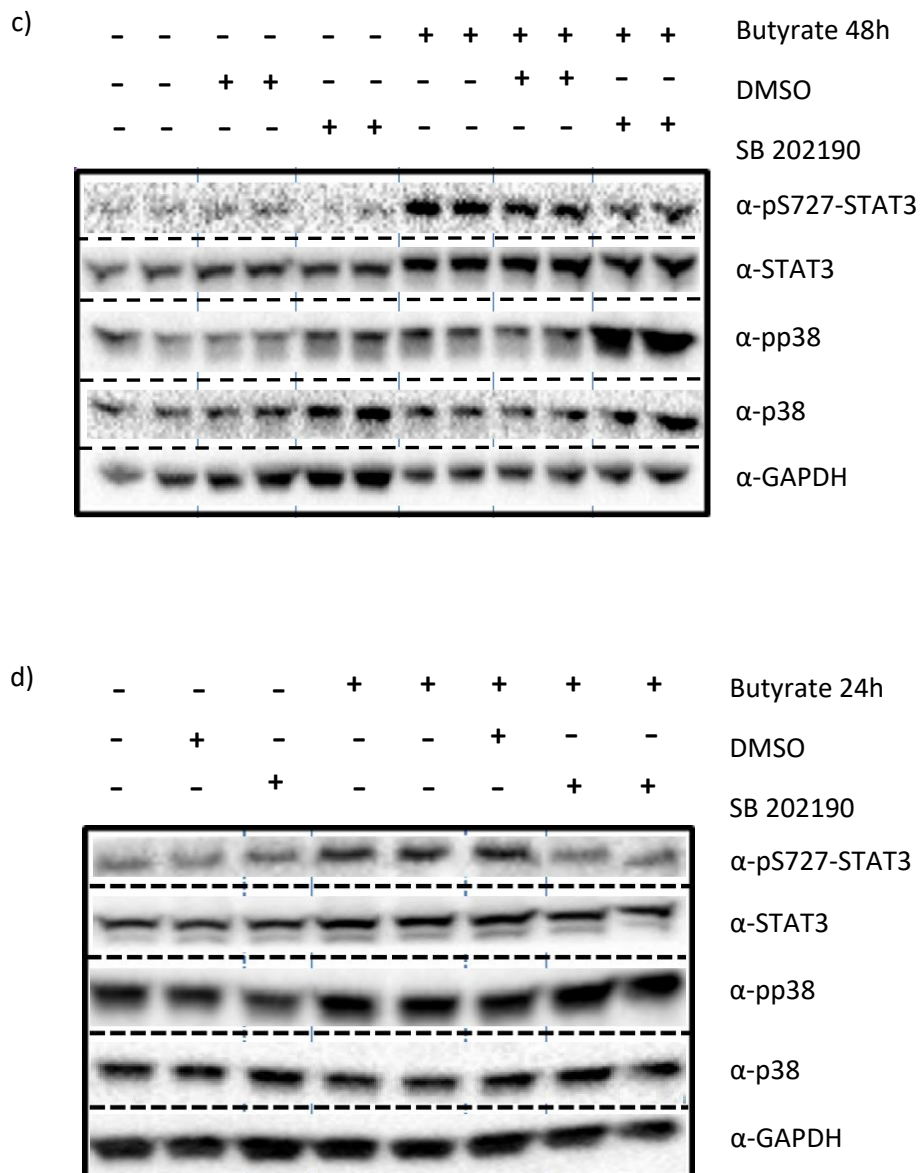


Fig. 23: pS727-STAT3 in the SB202190 and SB203580 incubation assays.

5 days differentiated CACO-2 cells were either left in DMEM or incubated with 5 mM sodium-butyrate for 48 (Fig. 23a,b,c) or 24 hours (Fig. 23 b,d). In one sample cohort of each assay, butyrate incubation was preceded by the 30'-treatment with a p38 MAPK blocker, SB203580 or SB202190, at a concentration of 10 μ M. The solvent controls were exposed to DMEM containing an equivalent amount of DMSO instead. Cell lysates underwent Western blot protein analysis. GAPDH served as reference protein for the total protein amount. Samples which were detected in the Western blot membrane in Fig. 23a originate from two assays done in triplicates. Same samples also served for the western blot analysis in the Figure 24 b and c.

3.2. Effects of a short-term cytokine stimulus on butyrate-caused changes of STAT3

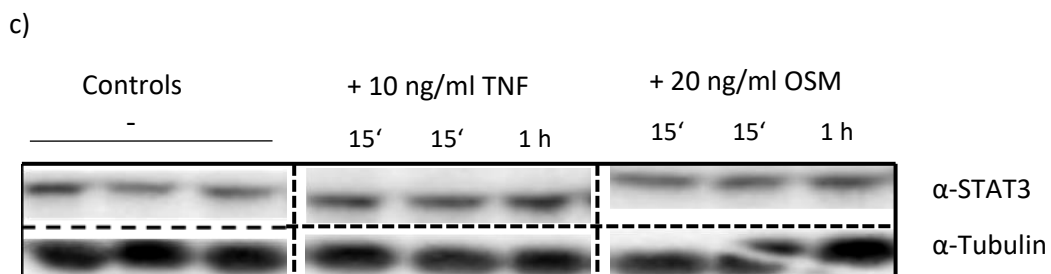
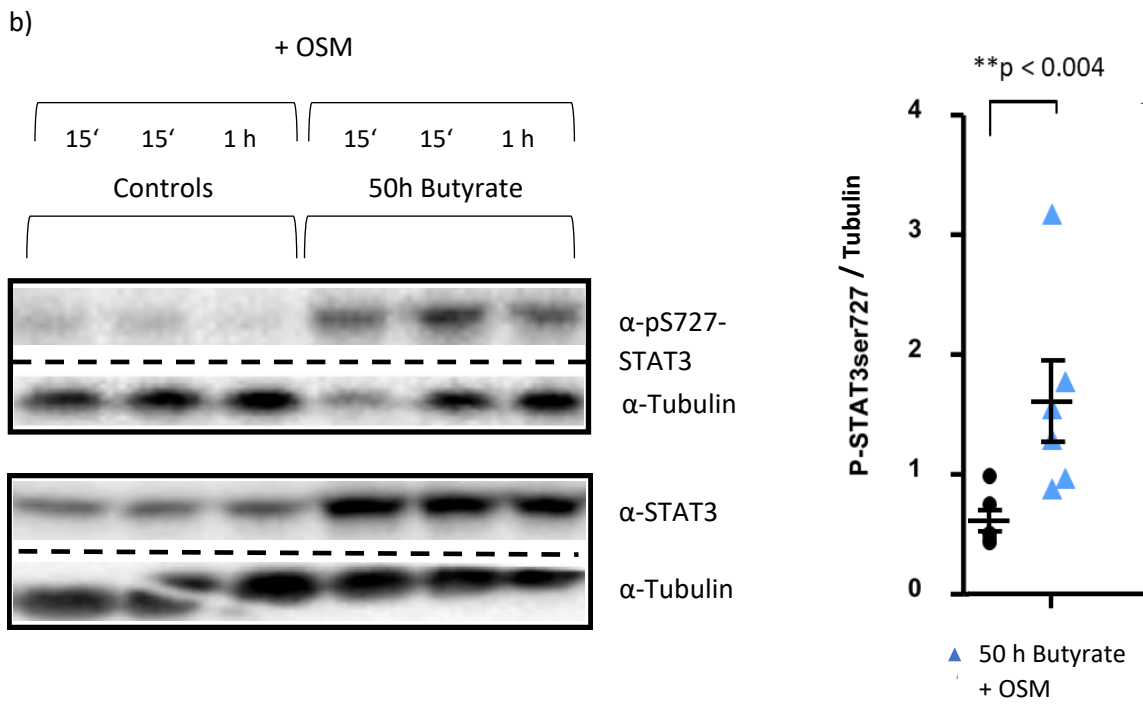
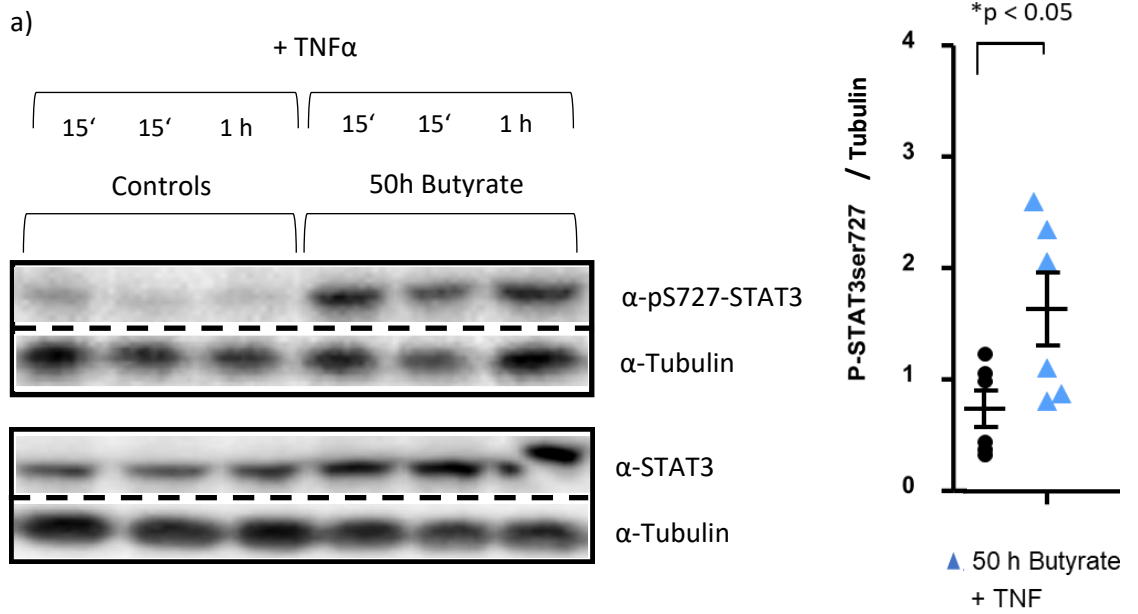
3.2.1. Effects of TNF α and OSM on pS727-STAT3

5 days differentiated cells were either left as unstimulated controls or were incubated with 5 mM sodium-butyrate for 50 hours. Within the last 15 minutes or within the last one hour of the assay, cells were additionally stimulated either with 10 ng/ml TNF α (a strong NF κ B inducer) or Oncostatin M (OSM, a STAT3-activating type-6-cytokine).

Butyrate led to a reliable increase of pS727-STAT3 in CACO-2 cells, despite of an additional cytokine stimulus (Fig. 24a-d).

It was the 2.3 \pm 0.2-fold of the base value under the TNF α /butyrate combination (n = 6; p < 0.05) (vs. 2.2 \pm 0.2-fold in the case of a single-butyrate treatment) (Fig. 24a), and the 2.6 \pm 0.2-fold (vs. 2.2 \pm 0.2-fold) of the controls baseline within the OSM/butyrate-stimulated sample cohort (n = 6; p < 0.004) (Fig. 24b).

Thus, the results lie either within the measurement uncertainties of the singularly butyrate-treated samples (in the case of butyrate/TNF α), or slightly above, but within the second standard deviation of the mean value of the singularly butyrate-stimulated group (in the case of a butyrate/OSM-treatment).



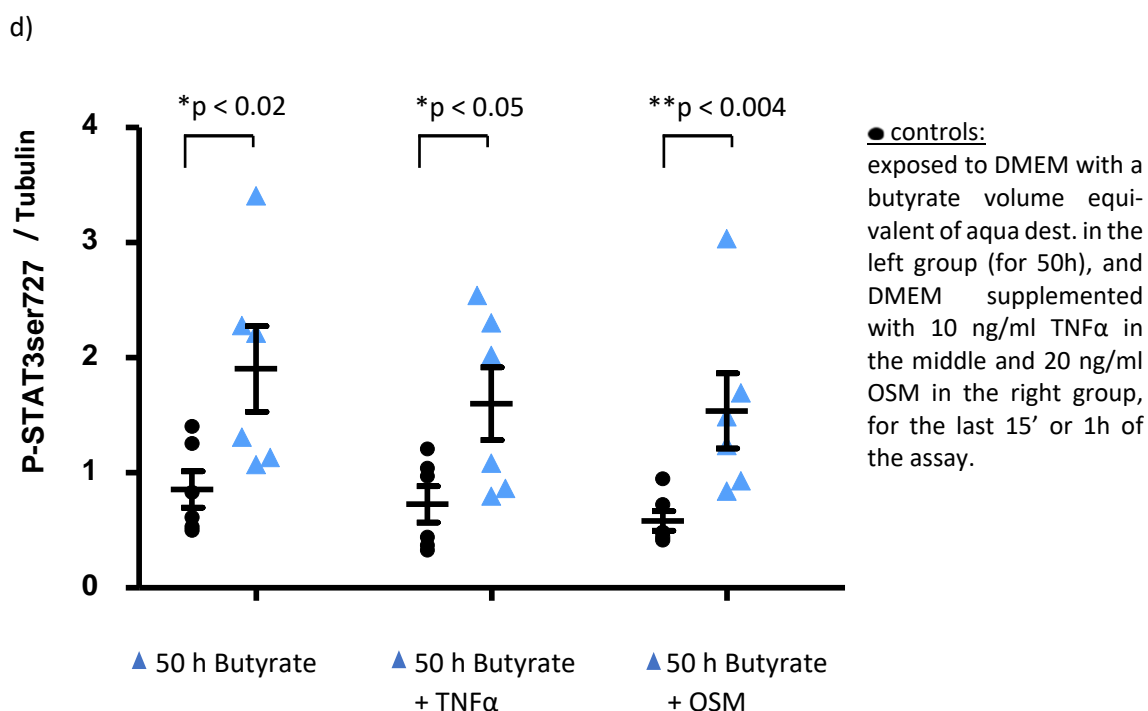


Fig. 24: Effects of TNF α or OSM on pS727-STAT3 and total STAT3 protein.

Fig. 24a + b: 5 days differentiated CACO-2 cells were exposed to the respective cytokine (10ng /ml TNF α or 20 ng/ml OSM) for either 15' or 1h at the end of a 50h-assay. Where indicated, cells had been preincubated with 5 mM sodium butyrate for at least 49h. The Western blot membranes show pS727- and total STAT3 detected proteins in 3 samples of each group ("cytokine" and "cytokine +/- butyrate preincubation"). The shown samples originate from one assay, done in biological triplicates. Tubulin was used as reference protein for the total protein amount. The quantification of the tubulin-normalized light intensity of the pS727-STAT3 signal is displayed in the graphics at the right-hand side. It includes samples of another independently but equally conducted assay, done in triplicates. The black dots represent the reference controls which were exposed to the respective cytokine but lack butyrate preincubation. Samples shown as blue triangles were cytokine-stimulated in conjunction with butyrate preincubation. The mean value and the error of the mean are respectively represented (black bars). The significance was calculated by using the one-tailed Mann-Whitney U test.

Fig. 24c: total STAT3 antibody detected proteins in 5 days differentiated CACO-2 cells which had been left as controls (exposed to DMEM, complemented with aqua dest.) for 50h or were stimulated with either 10 ng/ml TNF α or 20 ng/ml OSM for the last 15' or the last 1h of the assay.

Fig. 24d: Shown is a graphic comparison of the tubulin-normalized pS727-STAT3 quantification between samples which were either exposed to a short-term TNF α /OSM stimulus with (blue triangles) or without (black dots) a 48h-butyrate preincubation. The left group of samples was either left as native controls (carried along with an equal amount aqua dest., black dots) or had been singularly treated with 5 mM sodium butyrate for 50h (blue triangles).

3.2.2. Summary of the effects of TNF α and OSM on total STAT3 protein

As aforementioned in chapter 3.2.1., the singular stimulation of 5 days differentiated CACO-2 cells with 10 ng/ml TNF α or 20 ng/ml OSM for the last 15 minutes or 1 hour of a 50h-observation period did not increase pS727-STAT3 nor total STAT3 protein, compared to the unstimulated controls (compare the Western blot membranes in Fig. 24c and 24d).

On the other hand, likewise to pS727-STAT3, a 50h-butyrate preincubation (5 mM sodium butyrate), accompanying the supplement of 10 ng/ml TNF α or 20 ng/ml OSM both for the last 15 minutes as well as for the last 1 hour of the assay, significantly elevated the total STAT3 protein amount.

The increase was up to the 1.9 +/- 0.2-fold (n= 6; p < 0.002) in the case of the combination butyrate/TNF α , and up to the 1.8 +/- 0.2-fold (n= 6; p < 0.03) of the baseline in the case of butyrate/OSM (referred to the singularly with TNF α , respectively OSM stimulated cell samples).

In synopsis with the results described in chapter 3.1.3., butyrate led to a similar increase of total STAT3 protein in CACO-2 cells after 50(48)h, despite of being accompanied by a short-term cytokine stimulation at the end of the incubation period.

3.2.3. Butyrate significantly increases *hOSMR β* gene expression

We investigated the STAT3 response of CACO-2 cells towards OSM by measuring changes in pY705-STAT3 at the protein level and gained insight to the influence of butyrate in this context. Further, we determined *hOSMR β* expression with and without butyrate exposure.

5 days differentiated CACO-2 cells were either cultured in DMEM (control group) or incubated with 5 mM sodium-butyrate for 24 hours. A cohort of both, control group and butyrate group, was stimulated with 3 different concentrations of OSM (10, 20 or 50 ng/ml) for the last 15' or 1 h of the assay. Whole cell lysates were analyzed by SDS-PAGE/Western blot or were deep frozen for later analysis by qPCR.

10, 20 and 50 ng/ml OSM, added to the cell culture medium for the last 15 minutes or the last 1 hour of a 50h-assay, did not lead to an increase of pY705-STAT3 protein in otherwise unstimulated CACO-2 cells. On the other hand, when having been preincubated with 5 mM sodium-butyrate for 49h, cells reacted to the same amounts of OSM-with an increase of pY705-STAT3 protein, which was reflected by an increase of luminescence intensity at antibody-detected pY705-STAT3 protein bands. Figure 25 shows a representative Western blot membrane for samples of the 10 and 50 ng/ml OSM cohort.

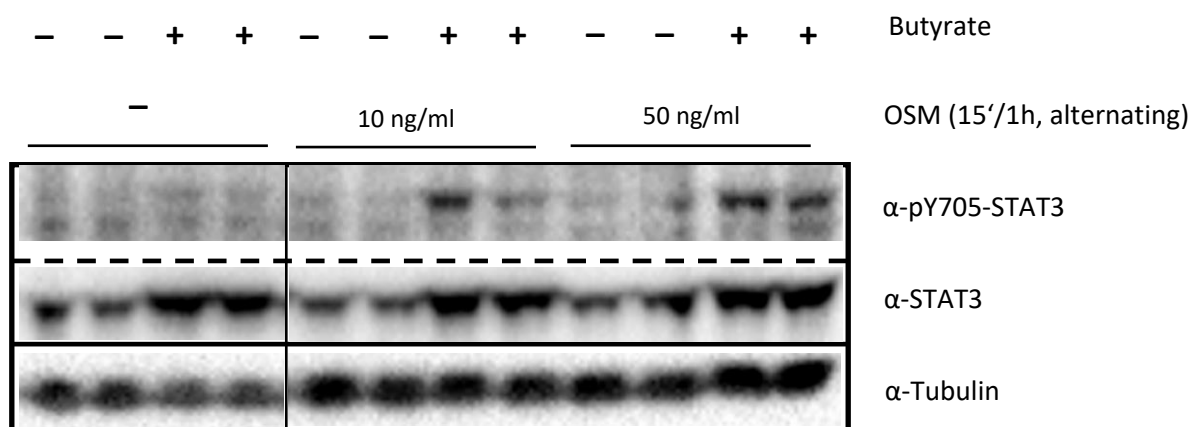


Fig. 25: Butyrate influence on pY705-STAT3 protein in OSM-stimulated CACO-2 cells.

5-days differentiated CACO-2 cells were either left as unstimulated controls or were stimulated with 5 mM sodium butyrate for 24h. Where indicated, cells were additionally stimulated with either 10 ng/ml (the 4 bands in the middle) or 50 ng/ml OSM (the 4 bands on the right-hand side) for the last 15', respectively the last 1h of the assay. Shown are two out of three sample cohorts gained from one assay done in triplicates. The experiment was additionally conducted in triplicates using 20 ng/ml OSM with similar results. While a single OSM-stimulation did not change pY705-STAT3, the combination with a butyrate incubation did.

To locate the mechanism underlying the pY705-STAT3 elevation by a combined treatment of CACO-2 cells with butyrate and OSM, the *hOSMR β* -mRNA expression was evaluated before and after an isolated butyrate exposure for 24 and 48 hours.

Measuring the basic *hOSMR β* mRNA by qPCR revealed a mean CT value of 37 in the 48h- and 35 in the 24h-control group.

The incubation of CACO-2 cells with 5 mM sodium butyrate for 24 hours led to an increase of *hOSMRβ*-mRNA up to the 2.8 +/- 0.7-fold (n= 3; p < 0.05) (Fig. 26a). An incubation with the same concentration of sodium butyrate for 48 hours led to an increase of *hOSMRβ*-mRNA up to the 5.3 +/- 3,7-fold of the mean base value (n= 3; p < 0.05) (Fig. 26b).

Due to the fact, that the *hOSMRβ* expression is low to absent in untreated CACO-2 cells, the error of the mean mRNA increase in 48h-butyrate treated samples was quite high. Thus, although the mRNA increase was statistically significant, the numerical value of the increase factor was uncertain.

Hint:

The sample errors of the mean mRNA increase displayed in Figure 26 are calculated individually for the control- and treated group and are not identical with the error of the mean factor of *hOSMRβ* mRNA increase $E(F)$. Due to error propagation, $E(F)$ is calculated from the ratio of the former two, as it is explained in the methods section.

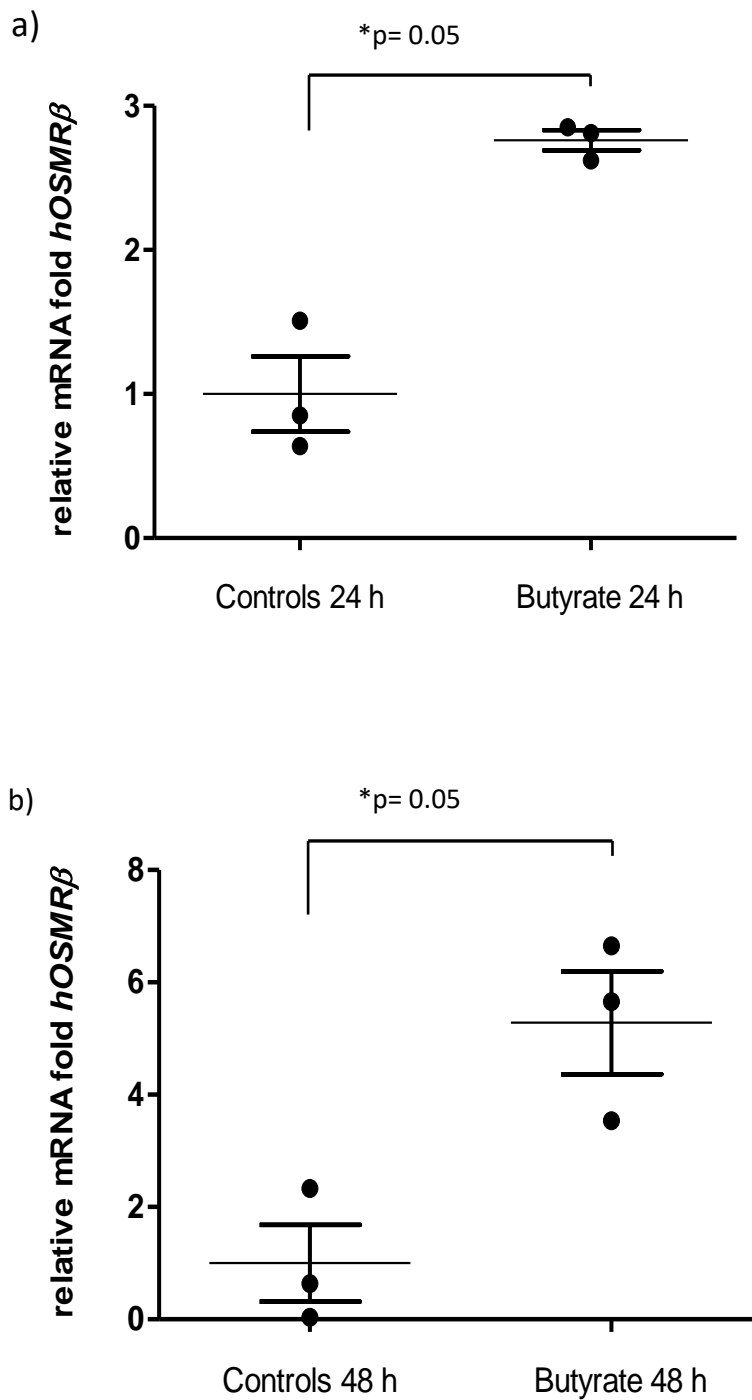


Fig. 26: *hOSMRβ* qPCR results. 5 days differentiated CACO-2 cells were either left as unstimulated controls or were incubated with 5 mM sodium butyrate for 24h (a), respectively 48h (b). Gene expression of *hOSMRβ* was determined by PCR analysis of the cDNA extracts. Displayed are the single, to the mean of the control group related qPCR $2^{-\Delta\Delta CT}$ -values which represent the relative mRNA increase. The black bars represent the mean and the sample error of the mean. Significance was calculated on the basis of the mean ΔCT values by using the one-tailed Mann-Whitney U test.

To estimate the contribution of HDAC-inhibition on the qPCR results, CACO-2 cells were stimulated with TSA instead of butyrate in separate wells of the cell culture plates.

An incubation with 400 nM TSA for 24 h led to an elevation of *hOSMR β* mRNA up to the 8.7 +/- 1.5-fold of the controls mean (n= 3; p < 0.05). An incubation with 400 nM TSA for 48 h increased the *hOSMR β* mRNA up to the 4.1 +/- 1.6-fold of the solvent controls' average (n= 3; p < 0.05) (Fig. 27).

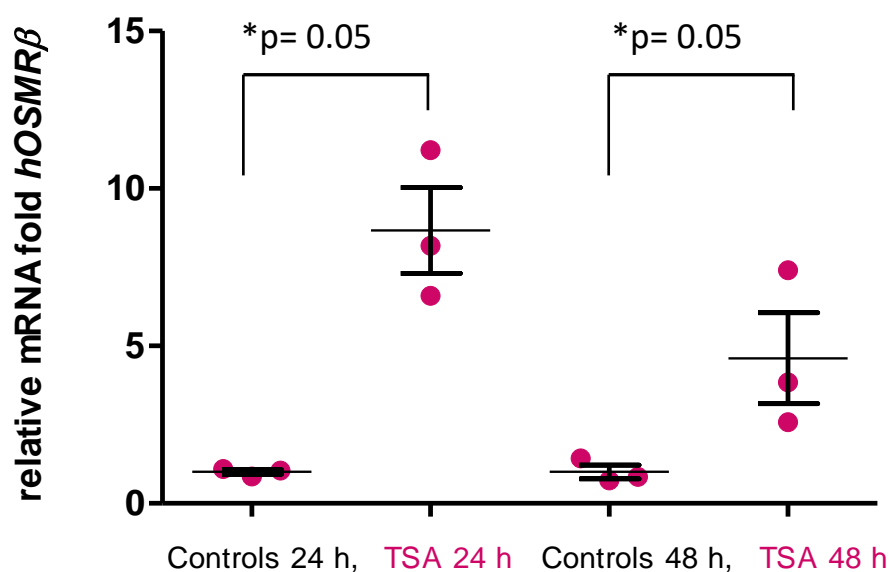


Fig. 27: 5 days differentiated CACO-2 cells were either left as unstimulated controls or were incubated with 400 mM TSA for 24h, respectively 48h. Gene expression of *hOSMR β* was determined by qPCR analysis of the cDNA extracts. Displayed are the single, to the mean of the control group related $2^{-\Delta\Delta CT}$ values (pink dots). The black bars represent the mean and the sample error of the mean separately for the control- and the treated groups. Significancies were calculated based on the mean ΔCT values with the usage of the one-tailed Mann-Whitney-U test of significance.

3.2.4. Butyrate attenuates the susceptibility of CACO-2 cells towards TNF α

In another part of that assay, 10 ng/ml TNF α led to a strong increase of pY705-STAT3 in CACO-2 cells after 1 hour of exposure, whereas this effect was not yet visible after a shorter incubation time of 15 minutes. The pretreatment with 5 mM sodium butyrate for 50 hours attenuated the pY705-STAT3-elevating influence of TNF α on CACO-2 cells (Fig. 28).

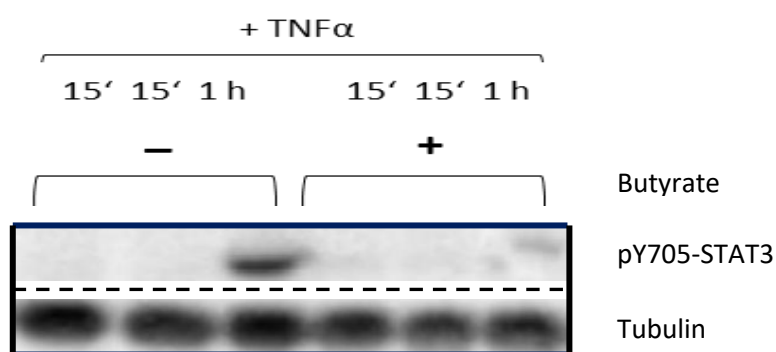


Fig. 28: pY705-STAT3 after TNF α treatment +/- butyrate influence.

5 days differentiated CACO-2 cells were stimulated with 10 ng/ml TNF α for 15 minutes, respectively 1 hour. Where indicated, cells had been pretreated with 5 mM sodium butyrate for 48 hours. Full cell lysates underwent Western blot analysis. Proteins were detected with indicated antibodies. Shown is one 1h-sample out of two independently conducted assays, done in triplicates.

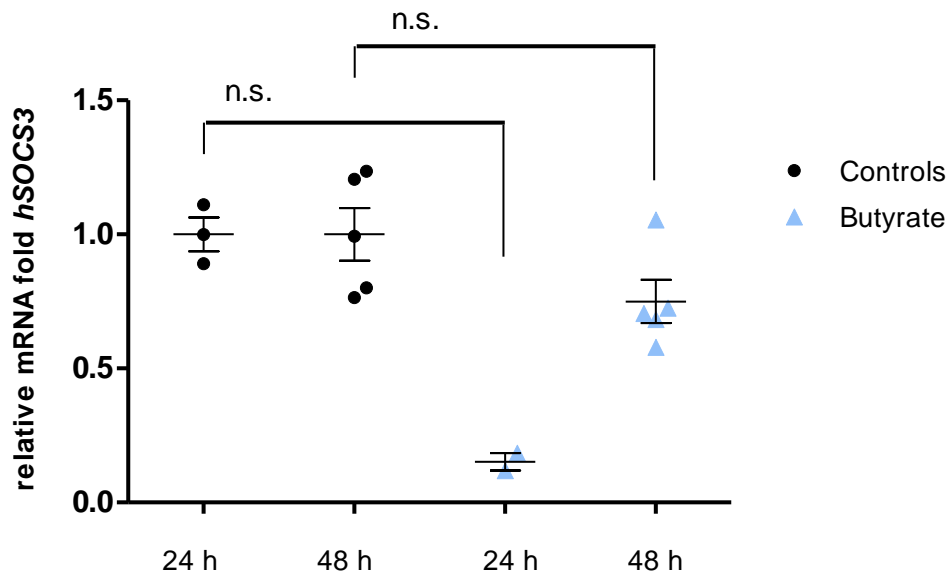
3.3. Butyrate's effects on *hSOCS3* expression

3.3.1 Butyrate downregulates *hSOCS3* mRNA expression in CACO-2 cells after 24h

To investigate the influence of the butyrate-caused pS727-STAT3 elevation on the transcriptional activity of STAT3, we quantified the changes in the human (*h*)*SOCS3* target gene expression by qPCR. In a second step, we repeated the analysis of *hSOCS3* expression with the TSA treated samples to investigate the impact of HDAC inhibition on the results. Suppressor of cytokine signaling 3 (*SOCS3*) is a negative regulator of JAK/STAT associated receptor signaling [119]. The induction of *hSOCS3* gene expression reflects STAT3's transcriptional activity.

The incubation of CACO-2 cells with 5 mM sodium butyrate for 24 hours led to a reduction of *hSOCS3* mRNA down to 15 +/- 3.4 % of the base value (n=2, n.s.) (Fig. 29a). Likewise, the incubation of CACO-2 cells with 400 nM TSA for 24 hours significantly decreased *hSOCS3*-mRNA down to 15.8 +/- 2.4 % of the solvent controls (n = 3, p < 0.05) (Fig. 29b). After a 48h butyrate incubation (5 mM), *hSOCS3* mRNA in butyrate-treated CACO-2 cells was nearly restored to base levels: in one assay the quantitative *hSOCS3* mRNA was 66.3 +/- 1.6 %, in another assay 88 +/- 2.8 % of the controls mean (Fig. 29a). The control samples had been exposed to an equal volume of aqua dest. for 48 hours as a solvent control. Contrarily to that, the *hSOCS3* mRNA of CACO-2 cells which had been treated with 400 nM TSA for 48 hours stayed at low levels, only reaching 25.2 +/- 4 % of the base value (Fig. 29b).

a)



b)

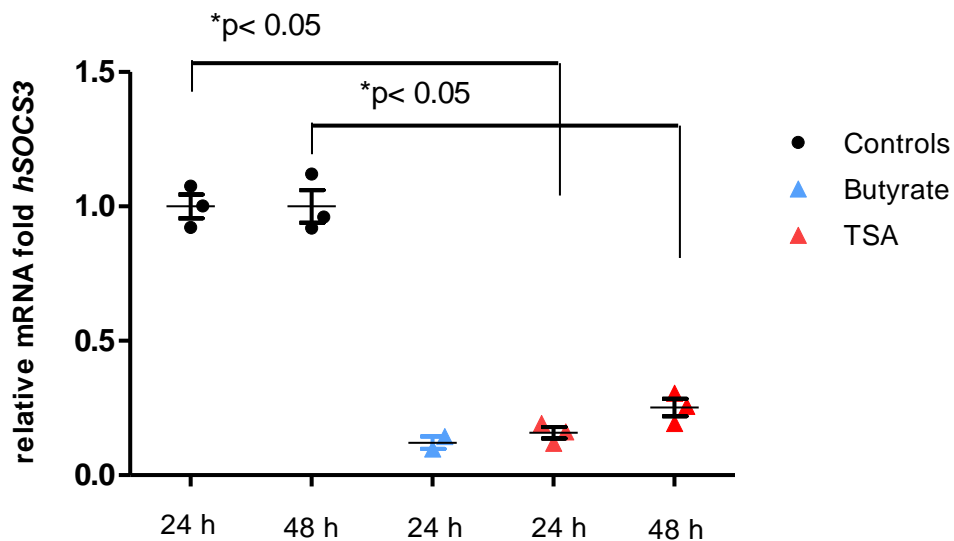


Fig. 29: hSOCS3 qPCR results in with a) Butyrate or b) TSA treated samples.

5 days differentiated CACO-2 cells were either left as unstimulated controls or were incubated with 5 mM sodium butyrate (a) or 400 nM TSA (b) for 24, respectively 48 h. After cell-harvesting, hSOCS3 expression was determined via qPCR. The results originate from one assay done in triplets. Displayed are the mean $2^{-\Delta\Delta CT}$ values, reflecting the divergence of the single measurements from the mean control CT value. Black lines reflect the mean values, black and blue bars reflect the sample errors of the mean. The significance with which the treated sample groups differ from the control groups was calculated based on the mean ΔCT values with the usage of the one-tailed (TSA-samples) and two-tailed Mann-Whitney-U test.

3.3.2. Butyrate attenuates TNF α -induced *hSOCS3* expression

We also tested the effect of a 48h-lasting butyrate preincubation on *hSOCS3* expression by CACO-2 cells in the context of a short-term TNF α stimulus.

A TNF α stimulus with a concentration of 10 ng/ml for both 1 and 4h led to a significant increase of *hSOCS3* mRNA in 5 days differentiated CACO-2 cells. It was up to the 2.8 +/- 0.4-fold of the base value after 1h (n = 3, p < 0.05) and further raised up to the 8.3 +/- 2.1-fold of the solvent controls mean after 4h of exposure (n = 3, p < 0.05). The preincubation with 5 mM sodium butyrate attenuated or even reversed this *hSOCS3* mRNA elevation (Fig. 30a). The mean *hSOCS3* mRNA value under the condition "48h butyrate + 10 ng/ml TNF α for the last 1h" was the 0.8 +/- 0.1-fold of the controls' mean (n= 3) and it was the 3.4 +/- 1.0-fold (n= 3) under the condition "48h butyrate + 10 ng/ml TNF α for the last 4h". This corresponds to an inhibition of the TNF α -caused *hSOCS3* mRNA elevation of about 50 % in both cases, which was significant at the basis of a 95%-confidence interval, using the one-tailed Mann-Whitney U test of significance (Fig. 30a).

3.3.3 OSM has no influence on *hSOCS3* expression after 1 and 4h of exposure

An OSM stimulus by 20 ng/ml OSM, added to the cell culture medium for the last 1h of the 48h assay, did not lead to significant changes in the *hSOCS3* mRNA expression in CACO-2 cells, irrespective of being accompanied by a 48h-butyrates treatment. OSM being the only stimulus led to a mean *hSOCS3* mRNA expression of the 1.2 +/- 0.1- fold of the base value (n=3). In combination with a butyrate pretreatment, the *hSOCS3* mRNA expression was the 0.9 +/- 0.1-fold of the base value (n= 3). Likewise, an exposure of CACO-2 cells to 20 ng/ml OSM for the last 4h of the cell culture assay did not remarkable change *hSOCS3* mRNA expression. The increase was at the most the 0.4 +/- 0.3-fold of the base value, which was not significant using the two-tailed Mann-Whitney U test of significance (n=3). A combination of the 4h-OSM stimulus with a 48h- sodium butyrate pretreatment dampened the slight OSM effect. The *hSOCS3* mRNA expression under this condition was the 1.1 +/- 0.3-fold of the controls mean (n = 3). The results are summarized in Figure 30b.

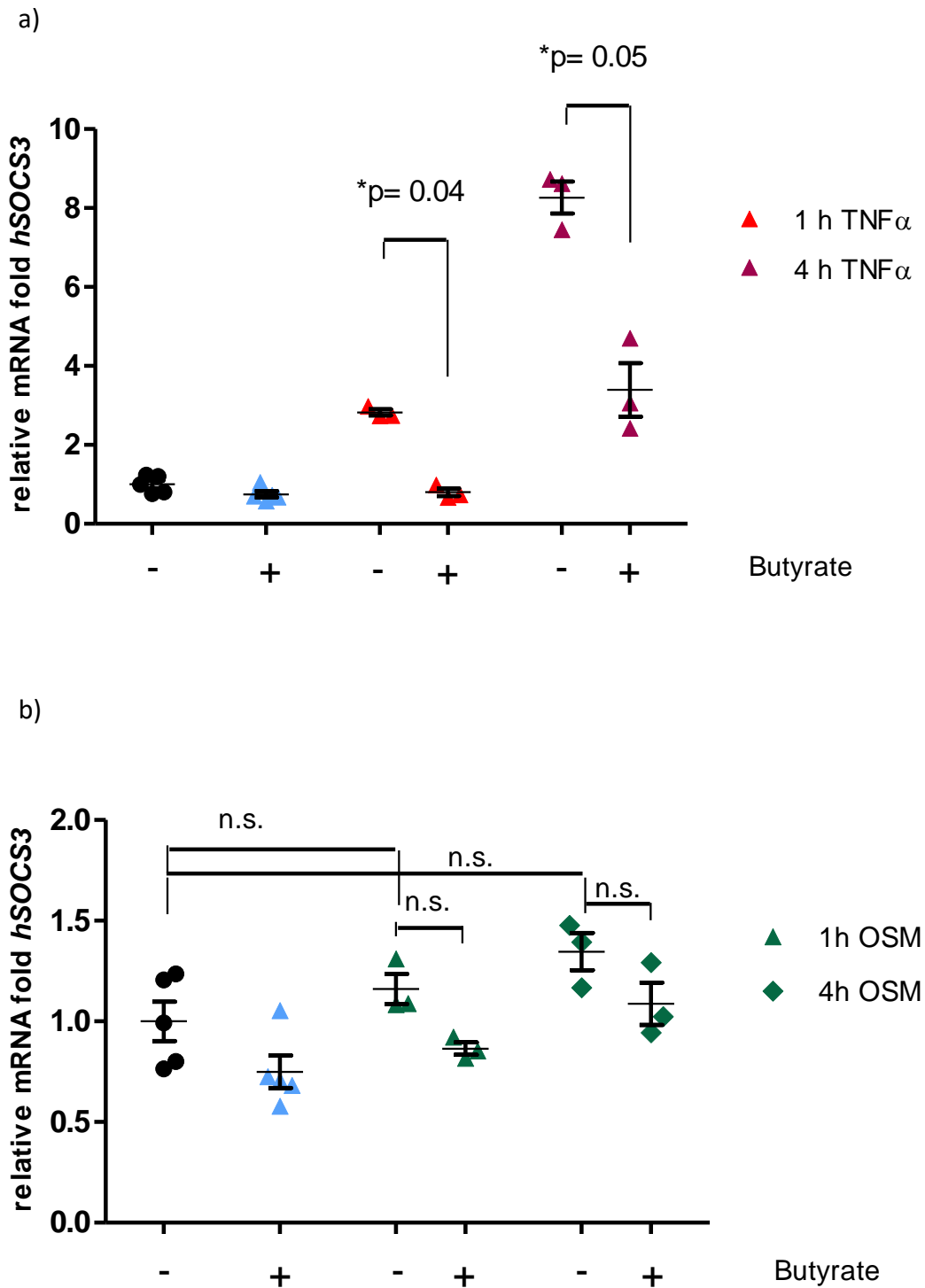


Fig. 30: *hSOCS3* qPCR results in with $TNF\alpha$ or OSM (+/- butyrate) treated samples. 5 days differentiated CACO-2 cells were either left as unstimulated controls or were incubated with 5 mM sodium butyrate for 48h. Where indicated, cells were additionally stimulated with 10 ng/ml $TNF\alpha$ (Fig. 30a) or 20 ng OSM (Fig. 30b) for the last 1, respectively 4h of the 48h-assay. The black lines represent the sample mean values, the black error bars represent the sample error of the mean. The significance was calculated based on the mean Δ CT values with the usage of the one-tailed (Fig. 30a), respectively two-tailed (Fig. 30b) Mann-Whitney-U test. Additional abbreviations: n.s.= not significant.

3.4 Comparison of the GPR109A receptor- and leucocyte attracting cytokine mRNA expression between a 2D and a 3D cell culture system

In this section we investigated the cytokine- and GPR109A mRNA expression of CACO-2 cells in response to a 4h-lasting apical TNF α -(10 ng/ml) stimulus and its dependency on a long-term butyrate preincubation.

In the second part of this section (chapters 3.4.4. to 3.4.5.) the named effects are, again, evaluated with special focus on the influence of the novel 3D setting. A description of this 3D cell culture system with its special features is given in chapter 2.1.4. and will be referred to as “3D environment” or “3D setting” in the following.

3.4.1. Butyrate increases *hCXCL-8*- and decreases *hCCL-2*-expression

The incubation of CACO-2 cells with 5 mM sodium-butyrate for 48 hours significantly increased the expression of the neutrophils-attracting chemokine CXCL-8 mRNA up to the 5.1 +/- 0.1-fold of the controls' mean (n=6, p < 0.001) (Fig. 31a).

The treatment of CACO-2 cells with 5 mM sodium-butyrate for 48 hours decreased the monocytes and lymphocytes attracting cytokine CCL-2 mRNA expression down to 45 +/- 0,2% of the base value (n = 6, p < 0.001) (Fig. 31b).

The results include 3 samples which were additionally treated with 20 ng/ml OSM during the last 4h of the assay. The qPCR results concerning the *hCCL-2* or *hCXCL-8* expression, both of the control samples as well as the butyrate pretreated samples, did not diverge within the standard error of the mean when being compared to the not OSM-treated sample group (see Figure 34, chapter 3.4.5.). Thus, the additionally OSM-treated samples could be included into the total evaluated cohort. The significance was calculated with the usage of the one-tailed Student's t-test.

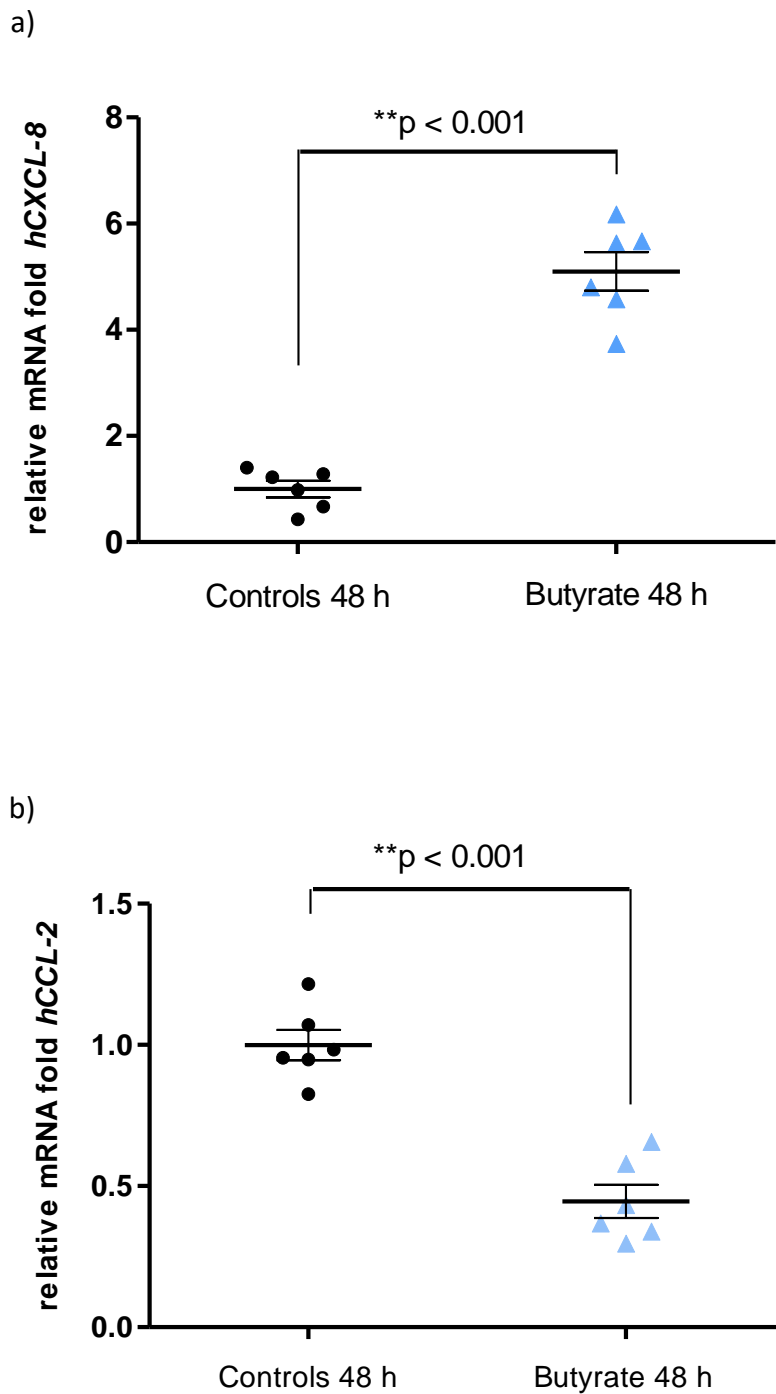


Fig. 31: *hCXCL-8*- (a) and *hCCL-2*- (b) qPCR results in 48h-butyrate-treated samples.

5 days differentiated CACO-2 cells were either left as control (the qPCR results are represented in the black dots) or were stimulated with 5 mM sodium-butyrate for 48h (blue triangles). Included are results of 3 samples which were additionally stimulated with 20 ng/ml OSM for the last 4h of the assay. The error bars represent the sample error of the mean. The significance was calculated based on the mean Δ CT values with the usage of the one-tailed Student's t-test.

3.4.2. Butyrate attenuates TNF α -induced cytokine expression and reduces I κ B protein

An incubation of 5 days differentiated CACO-2 cells with 10 ng/ml TNF α for the last 4h of a 48h-lasting assay led to an increase of the *hCCL-2* expression up to the 14.5 +/- 1.3-fold and to an increase of *hCXCL-8* mRNA up to the 280 +/- 51.8-fold of the controls' mean. A peri-incubation with 5 mM sodium butyrate for 48h (starting 44 hours previous to TNF α exposure), significantly attenuated the *hCCL-2* mRNA increase down to the 3.1 +/- 0.6-fold (n = 3; p < 0.04) and the *hCXCL-8* increase down to the 114.7 +/- 22.8 -fold (n = 3; p < 0.05). The results are depicted in Figure 33.

Western blot analysis revealed a reduction of I κ B protein after a 48h-butyrate incubation in comparison to the controls as well as a butyrate-caused inhibited reappearance of I κ B protein after a 1h-TNF α stimulus (Fig. 32).

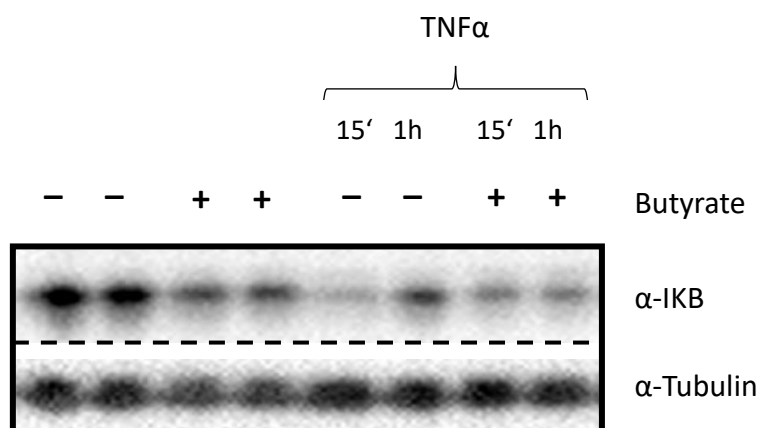


Fig. 32: α -I κ B protein results. 5 days differentiated CACO-2 cells were either left as unstimulated controls or were incubated with 5 mM sodium-butyrate for 48h. Where indicated, cells were additionally stimulated with 10 ng/ml TNF α for the last 15' or the last 1h of the assay. Full cell lysates underwent Western blot analysis of indicated targets. Depicted is one of two independently conducted assays.

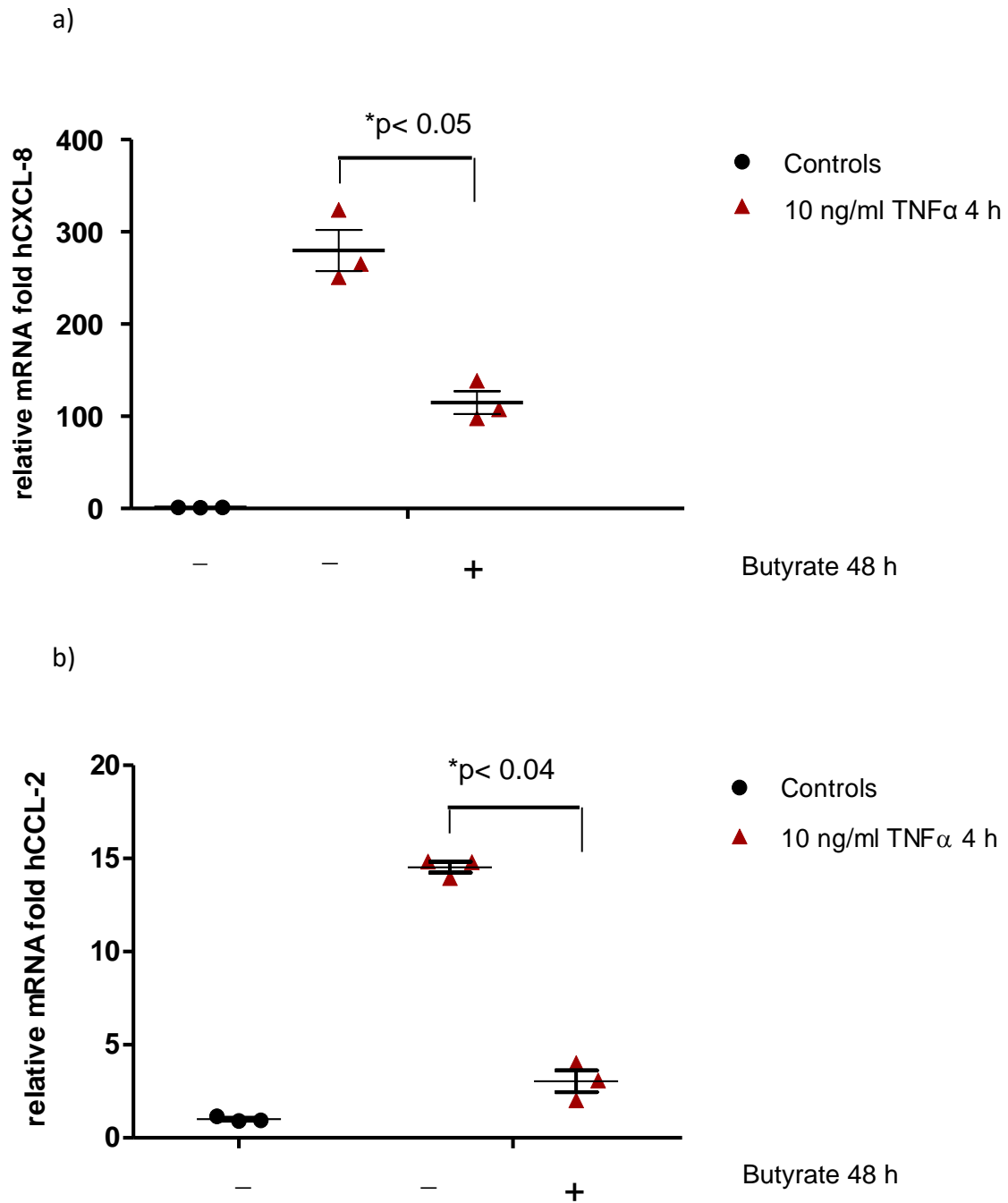


Fig. 33: hCXCL-8 and hCCL-2 qPCR results in dependency of TNF α .

Displayed are the results of one assay done in biological triplicates. 5 days differentiated CACO-2 cells were either left as unstimulated controls or incubated with 5 mM sodium-butyrate for 48h. Where indicated, cells were additionally stimulated with 10 ng/ml TNF α for 4h. Cell lysates underwent qPCR analysis of indicated targets. The error bars represent the sample error of the mean. The significance was calculated based on the mean Δ CT values with the usage of the one-tailed Mann-Whitney-U test.

3.4.3. OSM has no effect on *hCXCL-8* and *hCCL-2* expression after 4h in 2D

Upon an OSM stimulus (20 ng/ml) for the last 4 hours of the 48h-lasting assay, there was neither a change in the *hCXCL-8* nor in the *hCCL-2* expression, compared to the controls mean value. There was also no change of the results in 48h-sodium butyrate pre-treated samples by OSM. The CACO-2 cells reacted with the same expression changes as they had been observed in the situation when butyrate acted as a single agent, as it can be seen in Figure 34.

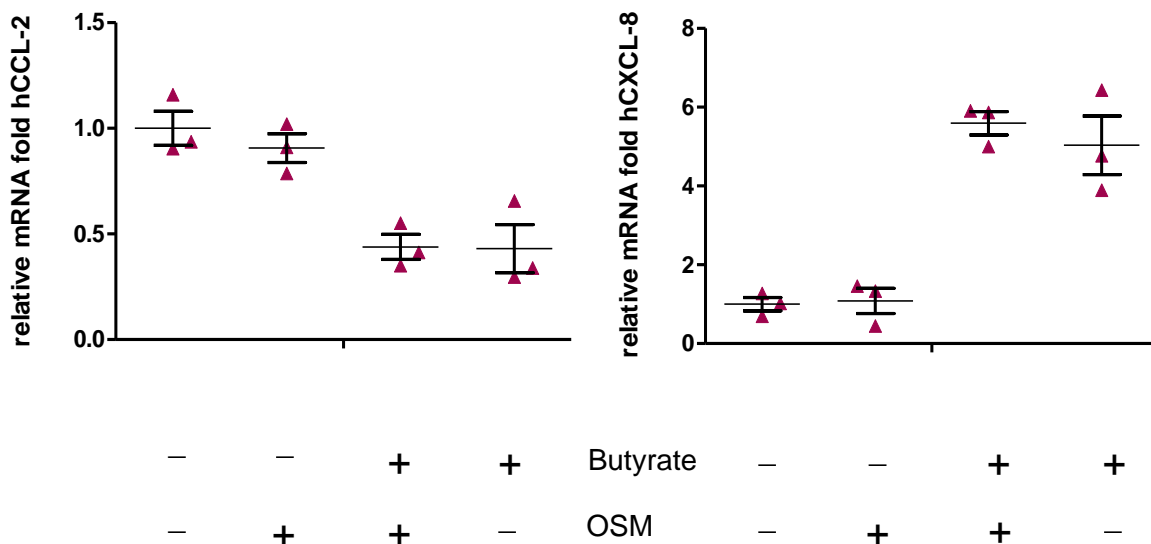


Fig. 34: *hCXCL8*- and *hCCL-2*- qPCR results in dependency of OSM.

5 days differentiated CACO-2 cells were either left as unstimulated controls or were incubated with 5 mM sodium butyrate for 48h. One sample cohort was additionally stimulated with 20 ng/ml OSM for the last 4h of the assay, either in conjunction or without the butyrate-preincubation.

3.4.4. Increase of *GPR109A* mRNA expression in a 3D cell culture

The original issue that inspired to the 3D approach (see chapter 2.1.4.) was the relative underrepresentation of butyrate receptors such as GPR109A in tumor cell lines like CACO-2. This is mainly due to a genetic silencing and therefore low expression of the receptor DNA [158] and affects the butyrate influence on these cells. Compared to a common cell culture on a culture plate (which reflects the “2D-setting”), in 3D-cell culture settings, an increased differentiation of several types of intestinal epithelial cells can be reached and this is ordinarily accompanied by the reactivation of formerly silenced genes [160]. A maturing effect on IECs could be also ascribed to the two-chamber situation [161], which is also given in the 3D-cell culture model used in our study. It offers a high similarity to the physiological, vascularized situation, in which small serum contained molecules like cytokines and growth factors retroact on IECs via basal and basolateral located receptors [162].

CACO-2 cells were either seeded in the 3D- or in the 2D-culture system as described in chapter 2.1.4. in the methods section. After a maturation of 21 days, cells were apically incubated with 5 mM sodium butyrate for 48h. To set a short-term inflammatory stimulus which e.g. resembles the cross-talk between reactive neutrophils with the epithelium, the butyrate pretreatment in one part of the samples was combined with an apical TNF α -stimulus (10 ng/ml) for the last 4h of the assay. TNF α is a prototype of a proinflammatory cytokine which can strongly activate the intracellular NF κ B signaling pathway in IECs. This is typically followed by an increased expression of proinflammatory genes. The transcription factor NF κ B is introduced in chapter 1.3.4.

Subsequently to stimulation, we investigated the expression of mRNA sequences which encode the butyrate receptor GPR109A and the myeloid cell-attracting cytokines CXCL-8, CCL-20, TNF α and CCL-2 by CACO-2 cells (the cytokine mRNA results are summarized in chapter 3.4.5.).

Although the basic expression of the butyrate receptor GPR109A as well as its expression after a 48h-butyrate incubation did not differ between the 2D- and the 3D-maintained CACO-2 cells, the results diverged in the situation when the additional TNF α -stimulus had been applied:

In the 2D-setting, there was no increase of the receptor mRNA detectable both after a 4h-TNF α -stimulus as well as when the 4h-TNF α -stimulus terminated a 48h-butyrate treatment.

In 3D instead, the butyrate receptor GPR109A mRNA increased up to the 2.1 +/- 1.0 - fold of the 2D-base value after the single TNF α -stimulus (the CT-value was 34.9 in the average under TNF α vs. 37.1 in the case of the unstimulated controls). It even further increased up to the 4.1 +/- 1.0 -fold of the 2D-base value, when TNF α was combined with the 48h-butyrate incubation (the mean CT-value was 32.2 under this condition).

Thus, despite of the high CT-values in general, the GPR109A receptor mRNA increased in CACO-2 cells upon the TNF α -stimulus exclusively in the 3D-setting. The difference of the *hGPR109A* mRNA under the condition "TNF α and butyrate" between the two cell culture models was significant, based on the mean Δ CT values ($p < 0.05$, $n = 3$) (Fig. 35).

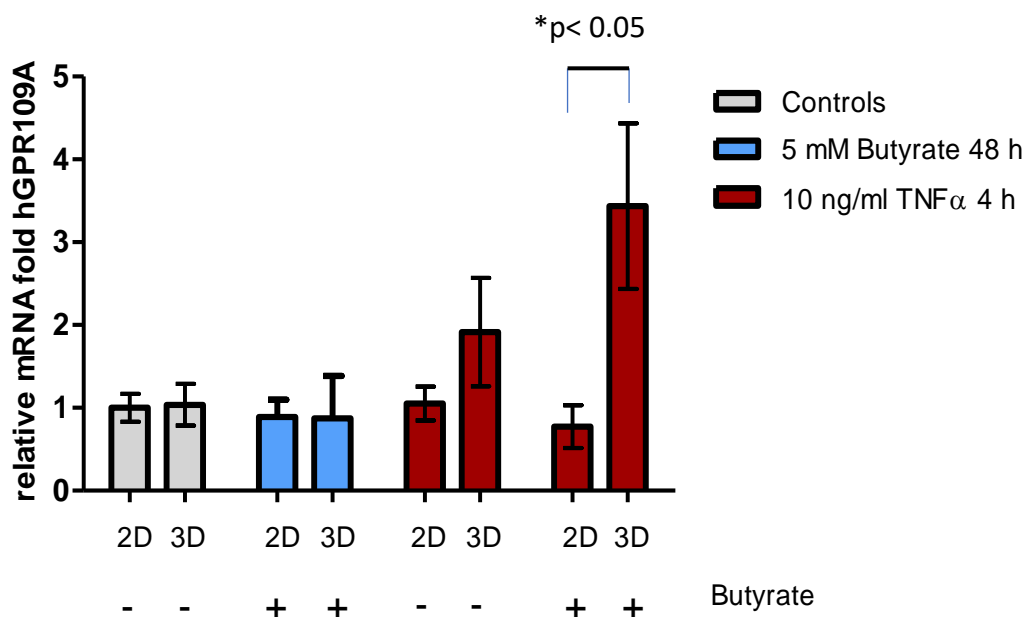


Fig. 35: hGPR109A qPCR results in 2D vs. 3D.

Displayed are the changes in gene expression relative to the mean value of the 2D-control samples. The top of each column reflects the mean value, the error bars reflect the error of the mean. $N = 3$. The significance was calculated on the basis of the mean Δ CT values, using the one-tailed Mann-Whitney U test.

3.4.5. Differential cytokine mRNA expression in a 2D versus a 3D setting

Differences in the basic cytokine expression between the 2 culture systems

The basic expression of *hCCL-2*, *hCXCL-8* and *hTNF α* was lower in the 3D-setting. It was 20 % (*hCCL-2*), 50 % (*hTNF α*), and 72 % (*hCXCL-8*) of that in the 2D-model. In contrast to that, the *hCCL20* basic expression was the 4-fold in 3D- CACO-2, in relation to that in 2D-seeded cells.

Butyrate differentially influences the cytokine expression by CACO-2 cells in 2D vs. 3D

Butyrate as a single agent remarkably increased the cytokine mRNA expression of *hCXCL-8* and *hCCL-20* in 2D- maintained CACO-2 cells, which was not the case in the 3D-environment.

However, the generation of *hTNF α* mRNA by an isolated butyrate treatment was intensified in the 3D- rather than in the 2D-cell culture system.

The *hCCL-2* expression was decreased by butyrate incubation in both cell culture systems.

2D-cultured CACO-2 cells are more susceptible to a TNF α stimulus.

Upon an apical TNF α -stimulus (10 ng/ml for 4h), 21 days-differentiated CACO-2 cells which were seeded in wells of a common cell culture plate (reflecting the 2D-setting), tended to react with a stronger elevation of the myeloid cells-attracting cytokine mRNAs tested, namely *hCXCL-8*, *hCCL-20*, *hTNF α* and *hCCL-2*, compared to CACO-2 cells in the 3D-cell culture system.

The cytokine expression under a combined butyrate/TNF α stimulus differs between the 2D and 3D environment.

In the 2D setting, the cytokine mRNA expression was attenuated by a 48h-peri-incubation with 5 mM sodium butyrate in all of the cases. On the contrary, within the 3D-cell culture model, the same butyrate treatment led to a significant further increase of *hCXCL-8* and *hCCL-20* mRNAs and did not attenuate *hTNF α* expression. *hCCL-2* expression, instead, was similarly attenuated as in the 2D-system.

hCXCL8

Besides the higher base value of *hCXCL8* mRNA expression in the 2D-culture system, a 48h-butyrate incubation led, in contrast to the 3D-setting, to a significant increase of *hCXCL-8* mRNA up to the 3.1 +/- 0.7-fold in 2D (n = 3; p < 0.05) (Fig. 36a).

Upon the TNF α stimulus, 2D- cultured cells reacted with a strong elevation of *hCXCL-8* mRNA up to the 29.6 +/- 8.0-fold (n = 3; p < 0.05) of the base value. The TNF α -caused *hCXCL8* mRNA induction was much lesser expressed in 3D-cultivated CACO-2 cells (4.8 +/- 1.6-fold; n = 3; p < 0.05). The relative *hCXCL-8* mRNA amount in 3D-cultured cells after the TNF α -stimulus was 12% of that in 2D-cultured cells.

Intriguingly, while a butyrate incubation attenuated the TNF α -caused elevation of *hCXCL-8* mRNA in 2D-maintained CACO-2 cells (down to the 17.1 +/- 2.3 -fold of the base value), the same butyrate treatment accelerated it in the 3D setting (up to the 11.3 +/- 3.0 -fold), which was significant related to both, control cells and butyrate treated cells (p < 0.05; n = 3) (Fig. 36b).

Albeit the relative *hCXCL-8* mRNA amount in 3D-cultivated CACO-2 cells under the dual treatment (butyrate and TNF α) was only about the half of that in the 2D-setting.

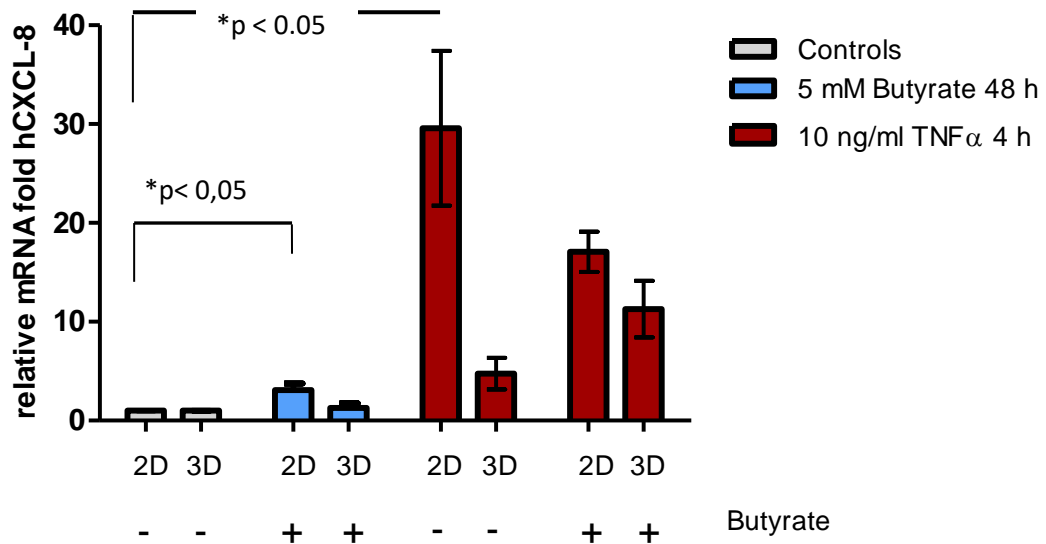
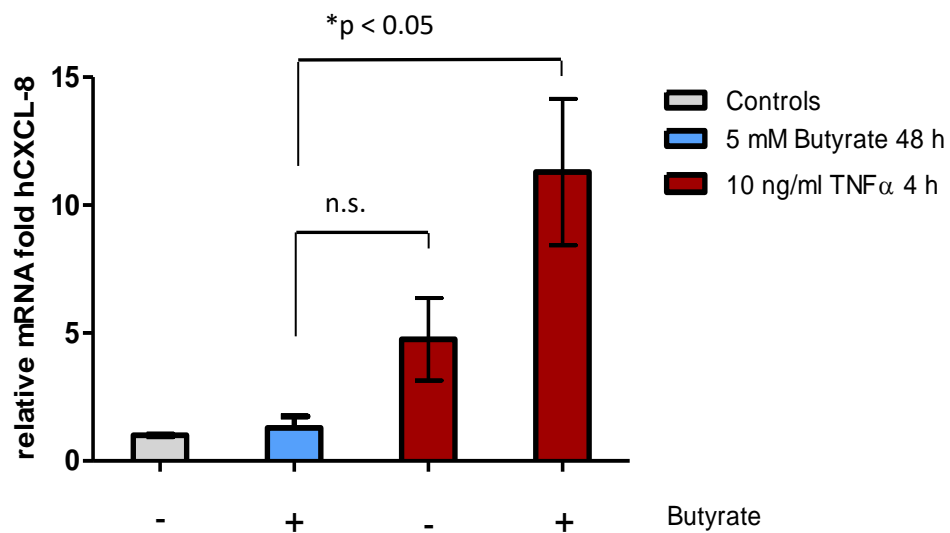
a) Development of the *hCXCL-8* mRNA separate for the 2D and 3D cell cultureb) Development of *hCXCL-8* mRNA in the 3D environment

Fig. 36: *hCXCL-8* qPCR results in 2D vs. 3D.

Displayed are the changes in gene expression relative to the respective 2D or 3D control samples. The top of each column reflects the respective mean value, the error bars reflect the error of the mean.

$n = 3$. The significance was calculated using the one-tailed Mann-Whitney U test, based on the mean $\Delta\Delta CT$.

hCCL-20

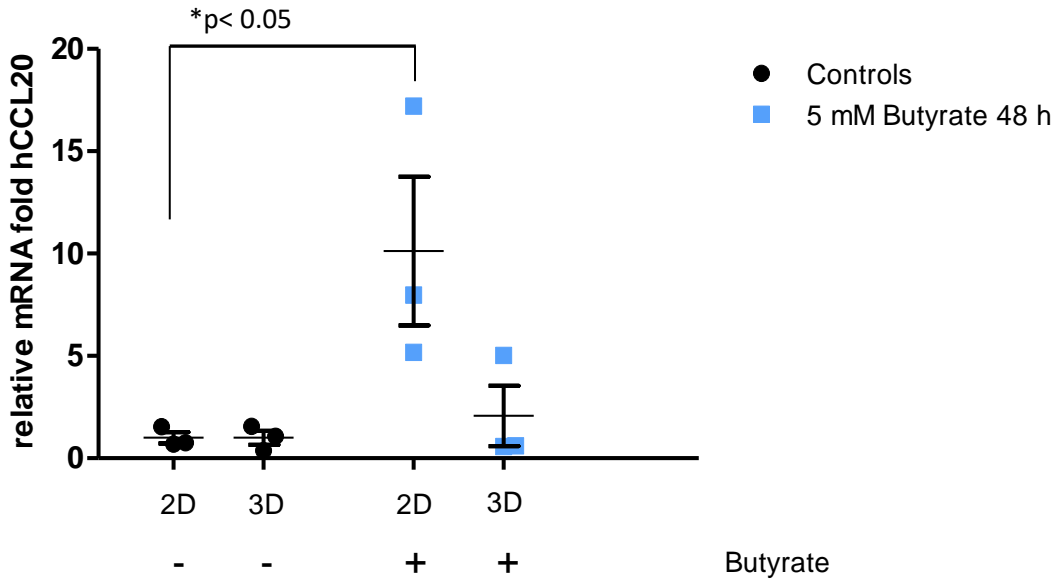
Despite of the 4-fold higher basic expression in the 3D-environment, an incubation with butyrate led to a significant increase of CCL-20 mRNA only in the 2D-cell culture (up to the 10.1 +/- 4.5-fold; $p < 0.05$; $n = 3$). It is worth to mention that one of the three 3D samples showed an increase of *hCCL-20* expression (until the 6-fold), whereas in the two other cell samples, the CCL-20 mRNA amount was decreased down to about 59 % of the base value (Fig. 37a).

The *hCCL-20*-mRNA expression showed a stronger elevation after the TNF α stimulus in the 2D- in opposition to the 3D-setting. It was up to the 71.3 +/- 24.7-fold in 2D ($p < 0.05$; $n = 3$). The increase in 2D was significant, despite of the high variance between the single results.

Intriguingly, while a peri-incubation with butyrate did not markable change the high level of TNF α -induced *hCCL-20* mRNA expression in 2D-maintained cells, the combined treatment with TNF α and butyrate further elevated *hCCL-20* mRNA in the 3D-setting:

In the 3D setting, CACO-2 cells reacted upon a 4h-lasting TNF α stimulus (10ng/ml) with an increase of *hCCL-20* mRNA up to the 18.1 +/- 11,8-fold ($n = 3$; $p < 0.1$; n.s.) which was further accelerated after a combined butyrate/TNF α treatment up to the 44.1 +/- 18.9-fold of the 3D controls mean value ($n = 3$; $p < 0.05$). The results are displayed in Figure 37b.

a)



b)

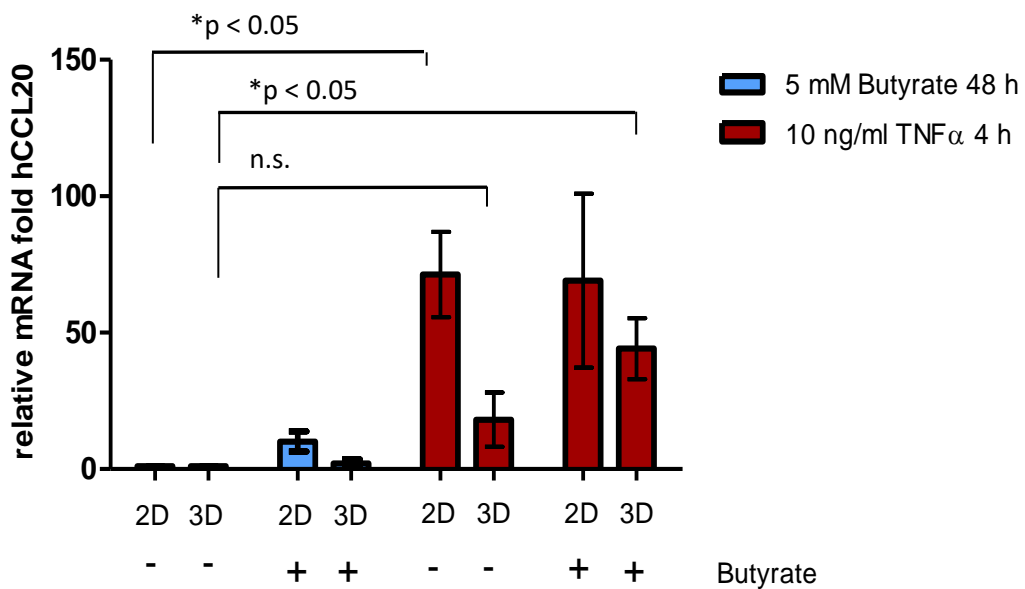


Fig.37: hCCL20- qPCR results in 2D vs.3D.

Displayed are the changes in gene expression relative to the respective 2D or 3D control values. The top of the column reflects the mean value, the error bars the error of the mean. The significance was calculated based on the mean Δ CT values, using the one-tailed Mann-Whitney U test. n.s. = not significant. n= 3.

hTNF α

The base expression of *hTNF α* mRNA was lower (about 50%) in 3D versus 2D- CACO-2 cells. Unlike the development of *hCXCL-8* and *hCCL-20*, *hTNF α mRNA increased rather in 3D- than in 2D maintained CACO-2 cells after a 48h-butyrate exposure*. The elevation of *hTNF α* mRNA was up to the 11.4 +/- 3.9-fold ($p < 0.05$; $n = 3$). This equates to a relative *hTNF α* mRNA amount of about 1.6-fold in 3D-, referring to the 2D-situation (Fig. 38b). After the TNF α stimulus (10 ng/ml TNF α for 4h), the *hTNF α* mRNA expression significantly increased in both cell culture systems. In 2D, the increase was up to the 24,5 +/- 11.8-fold, in 3D it was 27,0 +/- 14.1 of the respective base value ($p < 0.05$; $n = 3$). Significance occurred despite of the high variance of the single measurements (Fig. 38a). A peri-incubation with butyrate in addition to the TNF α stimulus led to a similar development as it was observed with *hCXCL8* mRNA: While butyrate attenuated the TNF α -caused increase of its own mRNA down to the 9.8 +/- 4.4-fold in the 2D-setting, it had no such weakening effect in the 3D-cell culture model (33,4 +/- 16.8) (Fig. 38a). Although the high variance of the single *hTNF α* mRNA measurements in 3D does not allow the statement, that butyrate led to a further increase of the *hTNF α* induction, as it could made for *hCXCL-8* mRNA in this setting (Fig. 36b).

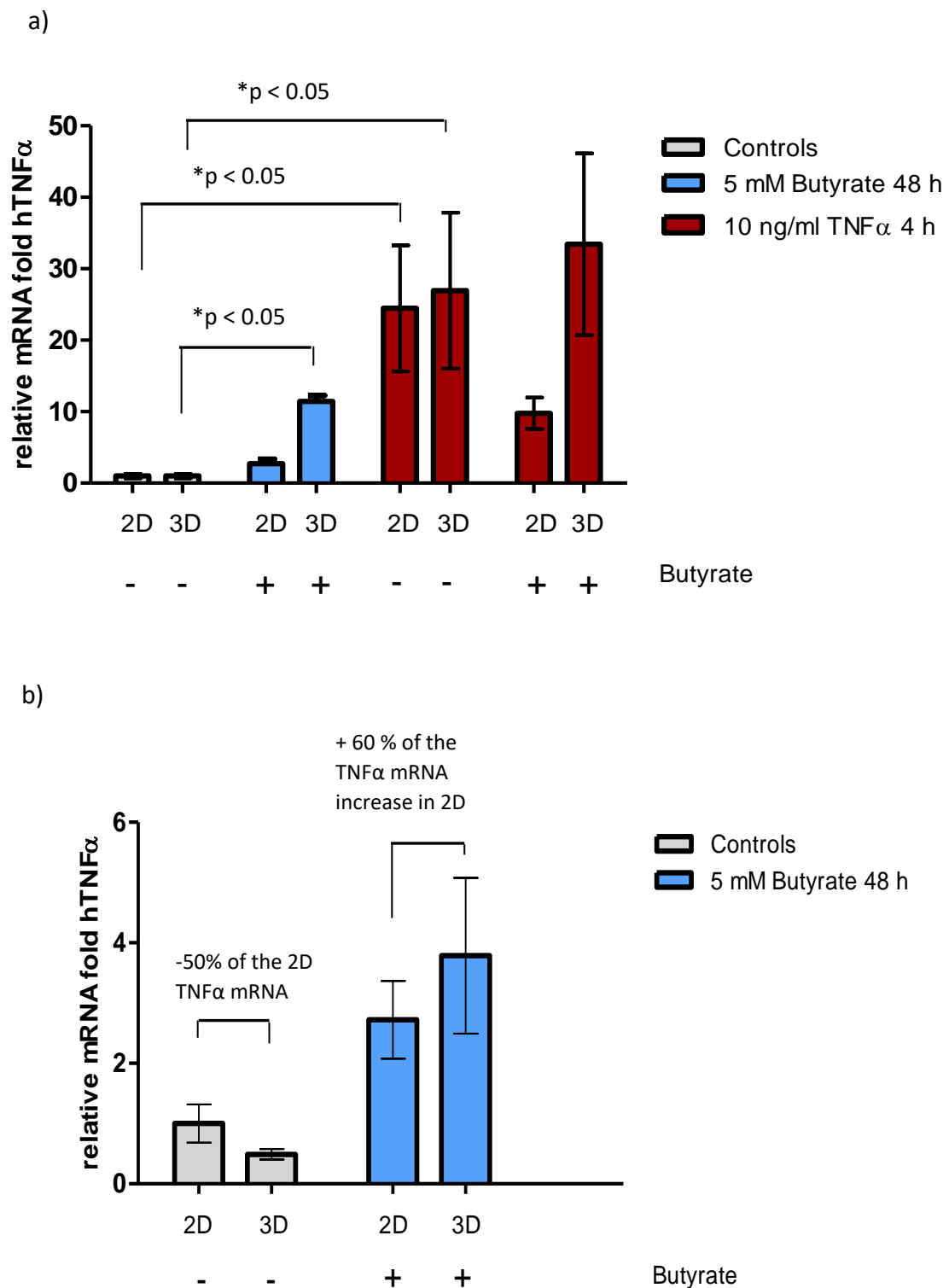


Fig. 38: hTNF α -qPCR results in 2D vs. 3D. Displayed are the changes in gene expression relative to the 2D control samples (b) and relative to the respective controls (a). The error bars reflect the error of the mean. The basic expression of TNF α mRNA in 3D-cultivated CACO-2 cells was about the half of that in the 2D cell culture. The mRNA amount in 3D after the butyrate exposure equates to the 1.6-fold of that in the 2D setting after the butyrate treatment. The height of the columns represents the mean value of the culture condition cohort. The error bars reflect the error of the mean. The significance was calculated based on the mean Δ CT values, using the one-tailed Mann-Whitney U test. n= 3.

hCCL2

The *hCCL2* basic expression in CACO-2 cells seeded in the 3D environment was about 20% of that in the 2D-maintained cells. An incubation with 5 mM sodium butyrate for 48h decreased the *hCCL2* mRNA in both cell culture systems, with a pronunciation of the 2D setting. More precisely, a 48h-butyrate treatment decreased *hCCL2* mRNA down to 67 +/- 40 % in the 3D- and down to 24 +/-7% of the base value in the 2D setting.

Upon a TNF α stimulus (10 ng/ml TNF α for 4h), the *hCCL2* mRNA was upregulated in CACO-2 cells of both culture systems. Relative to the respective base value, the elevation was up to the 11.1 +/- 4.5-fold (n = 3; p < 0.05) in 2D, and up to the 8.9 +/- 4.1-fold (n = 3; p < 0.05) in the 3D setting. The relative *hCCL2* mRNA amount in the 3D situation after the TNF α stimulus equated to about 15 % of that in the 2D setting. A peri-treatment with sodium butyrate abolished the TNF α -caused increase of *hCCL2* mRNA expression within both cell culture systems into negative digits. In the 2D setting, the decrease was down to 0,4 +/- 0,2, in the 3D setting it was down to the 1.4 +/- 0.6-fold of the respective controls' mean, both n = 3; p < 0,05 (Fig. 39).

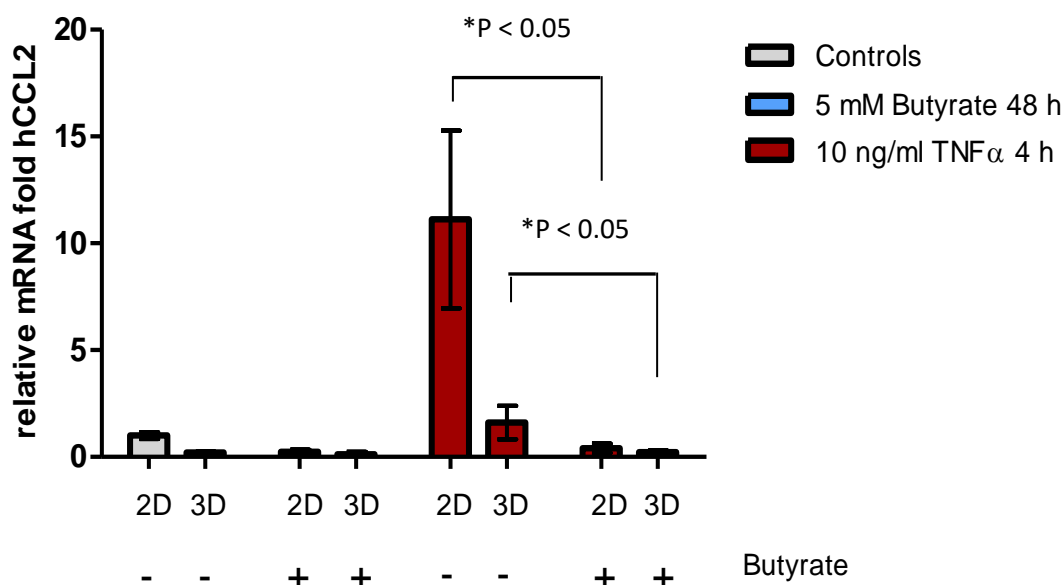


Fig. 39: hCCL2-qPCR results in 2D vs. 3D. Displayed are gene expression changes within the 3D samples, relative to the 2D control samples. The error bars reflect the error of the mean. The significance was calculated on the basis of the mean Δ CT values, using the one-tailed Mann-Whitney U test. n = 3.

4. Discussion

Butyrate is a bioactive molecule produced by the colonic microbiota. It affects the physiology of intestinal epithelial cells (IECs), including cell renewal and cytokine production. A key aspect of this study was to investigate butyrate effects on the expression and regulation of STAT3, a central transcription factor in the immunoregulation and cell maturation of IECs.

In this study, a longterm butyrate incubation (24 to 50h) increased the expression of the STAT3 encoding gene *hSTAT3* in CACO-2 cells and also elevated both total STAT3 protein as well as its activated form pY705-STAT3 (the latter after a butyrate/OSM co-stimulation). Butyrate's increasing effect on OSM-induced pY705-STAT3 was accompanied by an elevation of the *hOSMR β* gene expression.

Furthermore, it was shown for the first time that the serine727-phosphorylated form of STAT3 (pS727-STAT3) is significantly enhanced by a 20 to 50h-butyrate incubation in CACO-2 cells. The increase of pS727-STAT3 is dependent on HDAC inhibition and p38 MAPK activation by butyrate. Intriguingly, Butyrate's effects on pS727-STAT3 did not go along with an increase of the STAT3 target gene *hSOCS3*.

The second part of the discussion deals with the results of gene expression measurements of STAT3/NF κ B-regulated genes. Genes which encode myeloid cell-attracting cytokines and the butyrate receptor gene *hGPR109A* are investigated. The specific usage of a 3D-cell culture model thereby changed several qPCR results significantly. In retrospect, a change in the GPR109A receptor profile in the 3D-setting could have been one reason for that.

4.1. Butyrate increases pS727-STAT3 in CACO-2 cells via HDAC inhibition

In the first part of our study, we investigated butyrate's effects on STAT3-phosphorylation, with special focus on its serine727-phosphorylation (pS727-STAT3). In three independently conducted assays in triplicates, a long-term incubation of CACO-2 cells with a physiological butyrate concentration of 5 mM led to a significant elevation of pS727-STAT3 protein, determined by Western blot analysis. In timeline experiments,

this increase was reproducibly detectable after 20 to 24 hours of butyrate incubation. Especially see the 2.8-fold induction of pS727-STAT3 protein after a 24h- incubation with butyrate depicted in Figure 16b.

As we know, this is the first time, that a pS727-STAT3 elevation by butyrate is shown in a human intestinal epithelial cancer cell line.

The reproducibility of the pS727-STAT3 elevation after the replacement of butyrate by the known HDAC inhibitor Trichostatin A (TSA) after the same incubation period allows the conclusion that HDAC inhibition is the main mechanism by which butyrate increased pS727-STAT3 in our assays.

Already in former *in vitro* assays, STAT3's transcriptional activity was influenced by HDAC inhibition, at least in cancer cell lines [117, 144, 163]. E.g. Bachmann et al. [163] found a prolonged binding of IL-22 induced STAT3 at the promotor region of the *hSOCS3* gene locus in CACO-2 cells which had been stimulated with 3 mM sodium butyrate for 8h. They reproduced this by using TSA. The prolonged promotor binding was accompanied by an elevated *hSOCS3* gene expression. SOCS3 is a STAT3 target gene product and an important negative regulating protein of STAT3 signaling [119].

Accordingly, a study conducted by Togi et al. [164] found a pS727-STAT3 protein elevation by TSA in HeLa cells (a cervix carcinoma cell line). This research group investigated the influence of a pretreatment with both 100 and 200 ng/ml TSA for 12 to 16h previous to a stimulation with the STAT3-activating cytokine LIF (100 ng/ml for 30') on pS727-STAT3 in HeLa cells. This amount of TSA corresponds to 300 or 600 nM, which was approximately the TSA concentration used in our study (400 nM).

From the two main phosphorylation sites at STAT3 (Y705 and S727), the tyrosine705 (Y705)-phosphorylation is supposed to be important for the dimerization and DNA-binding of STAT3 to pro-survival gene subclusters, summarized in a review by Jarnicki et al. [165]. The serine727 (S727)-phosphorylation typically follows tyrosine phosphorylation as cellular response to several cytokines and growth factors [120], but also occurs independently [121, 122]. Both transcription-supporting as well as -inhibiting effects have been ascribed to pS727-STAT3 [121, 123]. Considering the role of STAT3 in cancer progression as well as in functions of the intestinal epithelium, it is of interest to

elucidate the molecular mechanisms by which butyrate, as a nutritional factor, increases pS727-STAT3.

In the following, we address four possible molecular pathways by which HDAC inhibition by butyrate could contribute to the increased serine727-phosphorylation of STAT3.

4.1.1. An elevation of total STAT3 protein contributes to the pS727-STAT3 fraction

We questioned whether a contemporaneous upregulation of total STAT3 protein production could have contributed to the increased pS727-STAT3 fraction. Our results reveal an elevation of total STAT3 protein in response to butyrate both at the transcriptional as well as at the protein level which was reproducible by the usage of TSA instead of butyrate, at least after a 24h-incubation. This confirms the influence of HDAC inhibition on the results. The calculated increase was relatively mild compared to the visible increase in light intensity at the α -STAT3-detected Western blot bands (Fig. 18a and b). This was due to a simultaneous elevation of the housekeeping protein tubulin. The Western blot results were not consistent during different assays (e.g. one of three assays done in triplicates did not show an elevation of the α -STAT3 chemiluminescence signal, see Fig. 18c). In the positive examples, the proportion by which total STAT3 contributed to the butyrate-induced pS727-STAT3 was calculated to be about 30%, and about 17% in the case of TSA-induced pS727-STAT3 (after 50, respectively 24h of exposure).

STAT3 elevation could be a direct effect by butyrate or a cell reaction to overcome a possible inhibition of pY705-STAT3 by butyrate, respectively an inhibition of STAT3's transcriptional activity. In this context, preliminary observations done during this study referring to the STAT3-target gene *hSOCS3* are discussed in chapter 4.3.

4.1.2. Possible role of phosphatase inhibition by HDAC inhibitors

Togi et al. [164] found a pS727-STAT3 protein elevation by TSA in HeLa cells. Furthermore, they implied a dependency of pS727-STAT3 dephosphorylation on the activity of a PP2A/HDAC3/STAT3 complex. Precisely, they concluded that a complex

generation between HDAC3, the serine-/threonine phosphatase PP2A and STAT3 mediates the dephosphorylation of STAT3 at serine727-residues by PP2A in HeLa cells. Transfection of the cells with HDAC3 *siRNA* (*small interfering RNA*) constructs, a cell culture technique to bind and degrade HDAC3 mRNA and, hence, deprive the protein expression of the enzyme, demonstrated that inhibition of the class I histone deacetylase HDAC3 enhances pS727-STAT3 in this cell line. Furthermore, an artificially overexpression of PP2A in HeLa- and in 293T cells (an immortalized embryonic kidney cell line) caused a significant drop of pS727-STAT3. Focusing on STAT3's transcriptional activity, the usage of HDAC3 siRNA as well as the simultaneous abrogation of HDAC3 and PP2A expression by means of RNA interference led to an enhancement of LIF-induced STAT3 luciferase activity at the α 2-macroglobulin promoter in HeLa cells, reflecting an improved STAT3 transcriptional activity at this STAT3 target promoter.

A physical interaction between HDAC3 and STAT3 was also confirmed by Kato et al., both in 293T and Hep3B (hepatoma) cells [166].

But, unlike the conclusions driven by Togi et al. regarding the role of HDAC(3) activity in pS727-STAT3 generation, Kato et al. resumed that the HDAC3/STAT3 complex was promotive for STAT3's phosphorylation at serine727, at least in Hep3B cells.

In detail, they observed that the HDAC3/STAT3 complex not only improved the IL-6 mediated STAT3 phosphorylation at tyrosine705 in HepB3 cells (after 30' and 1h of IL-6 stimulation), but also led to a basic increase of pS727-STAT3 protein in this cell line, which was determined by Western blot analysis, 48h after the transfection with a PML siRNA.

Kato et al. showed that the "promyelocytic leukemia protein" (PML) normally disrupts the HDAC3/STAT3 interaction in the cell lines Hep3B and 293T. The complex formation was, thus, only detectable, when the expression of PML was artificially blocked by siRNA constructs.

Thus, the conclusion of Kato et al. regarding the significance of HDAC3 activity for the serine727 phosphorylation at STAT3, somewhat contradict our findings and those of Togi et al., although an explicit dependency of pS727-STAT3 on HDAC3 or PP2A activity was not shown in the study. pS727-STAT3 protein was rather constitutively enhanced in

the PML-knockdown situation (see Fig. 1D in the paper by Kato et al. [166]), which could rely on mechanisms different from the STAT3/HDAC3 interaction. Different to our study Kato et al. conducted a 2h-lasting serum starvation before starting the IL-6 stimulation, which could have led to cell stress and to STAT3 serine727-phosphorylation via the p38 MAPK/PKC δ pathway, as it is described in the following chapter 4.1.3.

Additionally, the diverging results could be explained by the use of cell lines. Perhaps the role of PP2A differs between the cell types. Although Choi et al. showed a PP2A activation in the context of IL-6 signaling especially for Hep3B cells [167], an influence on pS727-STAT3 by PP2A in this cell line remains elusive.

The distribution of HDAC 1-3 could, as well, vary among different cell types and their respective activity could have a mutual influence. Western blot results by Kato et al. revealed an increase of HDAC1 protein expression after the experimental reduction of HDAC2 or after a combined PML/HDAC2 or PML/HDAC3 knockdown (see Fig. 2D in [166]).

Furthermore, HDACs combine both, enzymatic as well as adaptor functions affecting the transcription machinery. Thus, both transcription inhibiting as well as promoting effects of HDAC inhibition could exist simultaneously as shown by Nguyen et al. for cells of the innate immune system [168].

Apart from that, due to alternative splicing, at least 2 isoforms of the STAT3 protein exist [124]: The α -form is regulated by serine727 phosphorylation, whereas the β -form lacks this phosphorylation site in the molecule, but could, despite of this, still interact with HDACs to form ternary complexes.

In summary, the effects of HDACs on STAT3's transcriptional activity could vary, dependent on cell-type, activation mode and experimental setting. Both positive as well as negative effects may occur simultaneously. A constitutive hyperphosphorylation of STAT3 on serine727, rather than on tyrosine705, is observed in myeloproliferative diseases and CLL, which correlates with the level of autocrine IL-6 production [169]. In colon cancer, on the other hand, a serine727/tyrosine705 phosphorylated STAT3 is constitutively expressed due to hyperactive receptor tyrosine kinases (growth factor receptors) and src/Ras mutations [170, 171].

The observations made by Kato et al. may reflect a special situation in an IL-6-stimulated hepatic cell line with additional PML knockdown. PML silencing as well as HDAC inhibition might affect pS727-STAT3 at additional levels apart from the HDAC3/PP2A/STAT3 complex. E.g., the role of p38 MAPK activation by HDAC inhibitors which occurred in our study (see chapter 4.1.4.) was not addressed by Kato et al.

4.1.3. Possible apoptosis induction including PKC δ activation

When comparing the two main points in time of butyrate incubation (24h versus 50h), the serine727-phosphorylation of STAT3 was more pronounced after a 24h-incubation period. This likewise counts for the TSA-treated CACO-2 cells. Furthermore, after a 48h-incubation with 400 nM TSA, *hSTAT3* expression dropped below the level of the untreated control cohort, despite the initial significant increase after 24h (Fig. 22). 48h-TSA-treated cells showed light microscopic signs of cell destruction (Fig. 21).

This leads to the assumption that pS727-STAT3 could be a marker that accompanies the butyrate- and TSA-caused apoptosis induction in CACO-2 cells, whereas the advanced process could negatively affect pS727-STAT3 generation. Since TSA earlier than butyrate led to cell destruction, this could also explain the lower end-value of pS727-STAT3 induction by TSA in comparison to butyrate after 24h (1.8 vs. 2.8-fold).

HDAC inhibitors such as butyrate or TSA are known to induce apoptosis in cancer cell lines. This goes along with a reactivation of formerly epigenetically silenced tumor suppressor genes [172] like p21 [78], as well as with proteasome inhibition [173]. These effects are also used in cancer therapy [174-176].

Apart from gene transcriptional functions, pS727-STAT3 is suggested to play an important role in cell metabolism, improving energy production via supporting the mitochondrial oxidative chain [125]. This seems to be decisive in situations of metabolic or oxidative stress, at least in cancer cells. In this context, functions of pS727-STAT3, which regulate the release of the important second messenger Ca²⁺, have been discovered [124]. pS727-STAT3's relevance for the cancer-cellular outcome seems to be cell type-dependent since cancer cell types are differentially specialized on varying survival strategies. For instance, Ras-mutated cells seem to profit by a higher proportion

of mitochondrial pS727-STAT3 [126, 127] whereas, in src-mutated cells like CACO-2 cells, the dual phosphorylation of STAT3 both, at Y705 and S727 residues, seems to have major priority for cell stress survival [128, 129].

In the literature, the serine727-phosphorus group is often assumed to promote the transcriptional activity of intranuclear tyrosine phosphorylated STAT3 [130]. A subpanel of STAT3's target genes encode cell survival proteins like survivin, c-myc, Bcl-2 and Bcl-xl which counteract apoptosis. Also positively regulated are VEGF and HIF1 α , which are important for neovascularization and to overcome oxidative stress.

A central protein kinase which is activated upon cell stress is p38 MAPK. We could show its essential activation in butyrate-caused pS727-STAT3 elevation, which is discussed in the next chapter 4.1.4.

A study conducted by McMillan et al. revealed the co-activation of p38 MAPK, caspase 3 and PKC δ during butyrate-caused induction of apoptosis in the colorectal carcinoma cell line AA/C1. The phosphorylation of STAT3 was not addressed in this study [177].

4.1.4. An activation of p38 MAPK is essential for the pS727-STAT3 elevation

The serine727-phosphorylation of STAT3 is cell type- and situation-dependently ascribed to different members of the serine-/threonine kinase family [132].

To address this, we investigated the dependency of pS727-STAT3 elevation on p38 MAPK activity. A subset of CACO-2 cell/butyrate incubation assays, thus, included the preincubation with the p38 MAPK blocker SB202190 or SB203580, starting 30 minutes before butyrate exposure.

As the major result, the usage of SB202190 or SB203580, which are known to block the catalytic center of the p38 MAPK isoforms α and β , reproducibly attenuated the butyrate-induced increase of pS727-STAT3 in CACO-2 cells during our assays (Fig. 23 b-d). This proves the essential role of p38 MAPK activation in the butyrate-caused pS727-STAT3 elevation in the studied CACO-2 cell line.

The induction of p38 MAPK by butyrate was confirmed by the western blot detection of the phosphorylated α -isoform of p38 MAPK protein (pp38) which emerged after 75 minutes of butyrate exposure and remained until the end of the 48h-observation period

(Fig. 17). This went along with an increase of p38 MAPK's enzymatic activity, reflected in the increased phosphorylation of the known p38 MAPK substrate MK2 at the threonine222 residue (pT222-MK2). pT222-MK2 is increased after butyrate incubation and MK2-phosphorylation is decreased by the usage of the p38 MAPK blocker SB203580 (Fig. 23a).

An activation of p38 MAPK by butyrate was also found in former studies by other investigators who studied the *in vitro* effects of HDAC inhibitors in intestinal cancer cell lines.

Daniel et al. [80] and Qi et al. [178] found the p38 MAPK pathway involved in the butyrate-mediated Vit.D-receptor upregulation in CACO-2 cells. Daniel et al. confirmed the essential role of p38 MAPK in Vit.-D receptor elevation in CACO-2 cells by applying the p38 activator arsenate and the p38 blocker SB203580. According to the findings of our assays, the research group observed a significant elevation of phosphorylated p38 MAPK already after 1 hour of butyrate incubation which remained until the end of the 24h-incubation period and showed a peak after 6 hours of incubation with butyrate [80].

Whether p38 MAPK directly phosphorylates STAT3 at serine727-residues in CACO-2 cells or whether it primarily phosphorylates other serine-/threonine kinases such as mTOR, PKC δ or ERK, which subsequently are responsible for the final S727-phosphorylation, is not answered by the study conducted here. One way to address this question would be the utilization of other pharmacological inhibitors blocking possible kinases during butyrate incubation. However, the increase of pS727-STAT3 is detected after 20 hours of butyrate incubation at the earliest (see Fig. 17), whereas the phosphorylation of p38 MAPK is already detectable after 75 minutes, as aforementioned. This makes it unlikely, that this early inducible form of p38 MAPK directly phosphorylates STAT3 at serine727 residues. It might be more probable, that a subsequent intensification of p38 MAPK induction by butyrate's secondary effects, e.g. by the activation of additional signaling pathways (e.g. TNF- α , IL-31) and cofactors (e.g. AP-1, CREB) occurs. An increase of *hTNF α* expression in CACO-2 cells is shown in our assays. An increase of IL-31 was shown in the

case of butyrate-incubated HCT116 colon carcinoma cells [144]. An increase of AP-1 was seen in butyrate-incubated HT-29-colon adenoma- and CACO-2 cells [179].

With respect to the mechanisms by which butyrate can activate the p38 MAPK several aspects need to be discussed:

- 4.1.4.1. The induction of upstream kinases (MKKK-1 or MEK 3/6),
- 4.1.4.2. The support of p38 MAPK-activating signaling pathways,
- 4.1.4.3. The activation of AMP-kinase,
- 4.1.4.4. The decreased dephosphorylation of p38 MAPK,
- 4.1.4.5. The signaling via GPR43 or GPR109A.

4.1.4.1. Possible activation of a p38 MAPK upstream kinase

The inhibition of p38 MAPK activity by SB202190 led to an intensification of the chemiluminescence signal at α -pp38-detected protein bands in our assays (Fig. 23). This was somewhat expected, since the inactive p38 MAPK presumably accumulates in the cytoplasm, where it can be still phosphorylated by upstream kinases.

The pronounced α -pp38 chemiluminescence signal under the combined butyrate/SB202190 influence in comparison to that received from not butyrate- but SB202190-treated samples (Fig. 23 b-d) could further indicate either an active induction of a p38-phosphorylating upstream kinase or an inhibition of the pp38 dephosphorylation by butyrate.

In a human breast cancer cell line, Qi et al. described the transactivation of p38 MAPK and JNK after butyrate incubation [180]. Likewise, Ding et al. found a p38 MAPK activation in CACO-2 cells after a 24 and 48h-incubation with 5 mM butyrate, which was combined with an inhibition of ERK1 activity after the same incubation period and a JNK activation after 8 hours of butyrate exposure [181]. The combined p38 MAPK/JNK activation would confirm the assumption of a MKK upstream kinase (MKKK) being actively induced by butyrate. In accordance with that, Cho et al. could show an increase

of both MEK3 and MEK4 by butyrate in a prostate cancer cell line [182]. MEK3 is thereby known to phosphorylate p38 and MEK4 to phosphorylate JNK.

4.1.4.2. Possible support of p38 MAPK activating signaling pathways

The acceleration of LPS-induced antibacterial reactions via increasing the TLR4 expression by butyrate was shown by Xiao et al. in the human colon cancer cell line SW480 [183]. The activation of TLR4 is known to activate the p38 MAPK and NFκB pathway, subsequently strengthening the innate immune system, e.g. by increasing the myeloid cell-attracting CXCL-8 cytokine expression of IECs [184]. But this way of p38 MAPK activation is not of relevance in our study, since LPS delivering pathogens were absent.

Adam et al. found butyrate being promotive for the expression of TNFα-inducible genes in HeLa cells. Both 5 mM sodium butyrate as well as 450 nM TSA, supplemented for 22 hours to the culture medium, prolonged NFκB's DNA binding at promotor regions of several genes, e.g. *hCXCL-8* and *hIL-6*. Both sodium butyrate and TSA alone led to an increase of the gene transcription at those gene loci, determined by the measurement of a luciferase construct. The combined stimulation with TNFα even further increased transcription [84]. This could also indicate that p38 MAPK activation by butyrate or TSA subsequently leads to the activation of NFκB. Additionally, it could be a sign for the collaboration of pS727-STAT3 and NFκB under HDAC inhibition [145].

It is also possible, that the expression of those cytokines-encoding genes in IECs after butyrate exposure secondarily led to an intensified p38 MAPK activation. Other cytokines, which have the potential to activate p38 MAPK and were shown to be upregulated in IECs after butyrate exposure are e.g. TGFβ (shown for HT-29 colon adenocarcinoma cells [185]) and IL-31 [133, 144].

The study conducted by Dambacher et al. [144] revealed an increased *hIL-31* gene expression in HCT116 cells after a 48h-butyrate incubation, which would be the timeframe used in our study as well. The expression of IL-31, however, was not addressed by us.

In our study with CACO-2 cells, butyrate as a single agent increased the *hTNF α* gene expression, but this was only confirmed for a 48h-incubation period (see Figure 38).

Of importance is the fact that an incubation of 50h-butyrated-preincubated CACO-2 cells with TNF α for 15' or 1h did not lead to a further increase of pS727-STAT3 and at best slightly pronounced the elevation of total STAT3 protein compared to singularly 50h-butyrated-treated samples. Blockade of putatively induced cytokines by antagonistic antibodies could clarify their contribution to the observed p38 MAPK activation by butyrate.

4.1.4.3. Possible role of AMPK activation

AMP-activated protein kinase (AMPK) is a lack-of-energy sensitive kinase in mammalian cells which, when activated, inhibits anabolic processes like cell proliferation and promotes catabolic pathways. Thus, it is implicated in anti-cancerous mechanisms. This was e.g. shown by the identification of the AMPK-activating liver kinase B1 (LKB1) that is loss-of-function mutated in hereditary Peutz Jeghers syndrome, which is associated with an increased risk to develop intestinal cancer [186]. It is also reflected in AMPK's activation by several naturally occurring anti-cancerous compounds, which is picked up in an *in vitro* study on different types of intestinal cancer cell lines by Lea et al. 2014. This research group also mentioned the AMPK-activation by butyrate and determined synergistic anti-proliferative effects of butyrate in combination with A-76992, a known AMPK-activating substance [187]. One major pathway which is regulated by AMPK is the mTOR pathway. The inhibition of mTOR by AMPK e.g. leads to the activation of p53 and p27 which are important tumor suppressor proteins [188]. These processes can be accompanied by a p38 MAPK activation, as it was shown by Sengupta et al. in cells of acute leukemia [189].

4.1.4.4. Possible inhibition of p38 MAPK dephosphorylation

Togi et al. proved a scaffolding role of HDAC3 in the dephosphorylation of pS727-STAT3 by PP2A in 293T cells and HeLa cells [164]. Alvarado-Kristensson et al. found a role for

PP2A in p38 MAPK dephosphorylation in neutrophils [190]. Whether this can be projected on intestinal epithelial cells, and whether here a similar function of histone deacetylases as scaffolds for phosphatases exists, remains elusive.

On the other hand, serine/threonine phosphatases like PP2A also dephosphorylate ERK [191]. Specifically for CACO-2 cells, Ding et al. showed that butyrate-mediated cell differentiation and apoptosis was dependent on the activation of JNK and presumably p38 MAPK, and the concomitant inhibition of ERK [181]. Therefore, the evaluation of the cross-talk between ERK and p38 MAPK might be important to address.

4.1.4.5. Possible activation via GPR signaling

At the first view, receptor mediated signaling by butyrate via its receptors GPR43 or GPR109A, which are present in the apical membrane of normal intestinal epithelial cells and would be capable of transactivating ERK- and p38 MAPK pathways after ligand binding [110, 192], is very unlikely to be responsible for the observed pS727-STAT3 elevation, at least in the 2D-setting. Besides their generally low expression in CACO-2 cells, these receptors are not markedly upregulated at the gene transcription level after a 48h-butyrates exposure (see Figure 35). Apart from that, receptor-mediated signaling would transport information to connected kinases within minutes and secondary effects would occur after one to two hours, whereas pS727-STAT3 elevation occurs the earliest after 20h after butyrate exposure. On the other hand, p38 MAPK phosphorylation is pronounced after 75' of butyrate exposure in timeline assays (Fig. 17). This does not exclude a possible influence of GPR-signaling on the STAT3 results. It is possible, that p38 MAPK activation is a reaction that follows the receptor-mediated suppression of other kinases like ERK, although an early activation of ERK by Niacin-mediated GPR109A receptor activation shown in a human epidermoid cell line would contradict this hypothesis [193]. Also secondary pathways like a receptor- induced cytokine production could link GPR-activated p38 MAPK to pS727-STAT3 elevation by butyrate in CACO-2 cells. To explore this context, the results could be compared with those in the 3D-setting, in which GPR109A is higher expressed under TNF α influence (Fig. 35). GPR109A could be further artificially blocked by the usage of Pertussis toxin.

4.2. Butyrate effects on *hOSMR β* expression

Since STAT3 is supposed to play an important role in immune reactions of IECs during inflammation, we also investigated whether a short-time stimulus with 10 ng/ml TNF α (a strong NF κ B inducer) or 20 ng/ml OSM (a STAT3-activating type-6-cytokine) in the last 15 minutes or in the last one hour of the assay would influence the effect that a 48h-butyrates incubation had on pS727-STAT3- and total STAT3 protein. Or, vice versa, whether the presence of butyrate could affect the tyrosine705-phosphorylation status of cytokine-induced STAT3.

No markable difference was detected regarding total STAT3 protein and the serine727 phosphorylation of STAT3 when CACO-2 cells were short-time stimulated with one of the two cytokines, despite of a butyrate pre-incubation (see chapter 3.2.2.). However, a clear enhancement of pY705-STAT3 protein was measured if OSM-stimulation followed butyrate pretreatment, which was not the case in the absence of butyrate (Fig. 25).

The gene which encodes the OSMR subunit OSMR β is often silenced by hypermethylation in colon cancer cell lines, which is even used for diagnostic purpose [143]. This is the case in CACO-2 cells as well [142] and was likely the reason why pY705-STAT3 showed no difference between OSM-treated and -not-treated samples in the absence of butyrate. On the other hand, both a 24h- and 48h-butyrates incubation significantly increased *hOSMR β* mRNA expression in CACO-2 cells in our assays.

Due to the fact, that the *hOSMR* expression is low to absent in untreated CACO-2 cells, the error of the mean mRNA-increase in 48h-butyrates treated samples was quite high. Thus, the numerical value of the increase factor in the 48h-group was uncertain. A solution for this technical problem could lie in the repetition of the measurement with using the undiluted cDNA instead of the commonly used 1:3 dilution, in order to increase PCR sensitivity.

The *hOSMR β* -increase was reliably reproducible by using TSA instead of butyrate, suggesting that HDAC inhibition is the underlying mechanism. To confirm that in prospective, the pY705-STAT3 protein results should be verified under the TSA- instead of the butyrate influence. However, the *hOSMR β* expression in 24h-butyrates-treated

CACO-2 cells was nearly the 3-fold, in 24h-TSA-treated cells the 7-fold of the base value in our assays.

Looking at the 48h-treated samples, the TSA-induced *hOSMR β* expression was regressive, whereas it seemed even more pronounced in the case of a butyrate incubation. Fitting these findings, 48h-butyrate-treated HCT116 colon cancer cells reacted with a 12-fold-increase of *hOSMR β* expression in a study by Dambacher et al [144]. The role of HDAC inhibition was not specifically investigated by this research group. However, another study by Lacreusette et al. [194] revealed the reactivation of both the *hOSMR β* expression and the pY705-STAT3 inducibility by OSM in a before OSM-resistant melanoma cell line after a 24h-treatment with TSA.

In consumption with other receptor inductions (e.g. IL31R [144], IL22R [163]), butyrate could contribute to the improved responsiveness of colon cancer cells towards OSM and other STAT3-activating cytokines, thereby promoting STAT3-mediated immune reactions, wound healing processes [113, 134] and cell differentiation [142].

On the other hand, butyrate potentially attenuates the induction of STAT3-activating secondary cytokines by TNF α , at least in the 2D-setting in our assays. TNF α increased pY705-STAT3 after one hour of exposure, implying that TNF α induces cytokines which are able to activate STAT3 via their respective receptors, like IL-31 [133]. This was shown to be upregulated by a 48h-butyrate incubation in HCT116 colon cancer cells [144], but was not further investigated by us. However, the pY705-STAT3-increasing effect of TNF α was attenuated by a 48h-butyrate preincubation in the 2D-cell culture assay (Fig. 28).

4.3. Butyrate effects on *hSOCS3* expression

To determine the functional relevance of butyrate-induced pS727-STAT3 elevation and OSM-sensitization in CACO-2 cells *in vitro*, we investigated the mRNA expression of the STAT3-regulated target gene *hSOCS3* in cell lysates after 24 and 48h of butyrate incubation.

As explained in the chapter 1.5., *hSOCS3* is a target gene product of cytokine-activated STAT3. It functions as a negative feedback regulator in IL-6-and IL-10-type-cytokine-mediated STAT3 signaling [119, 163]. In the CACO-2 *in-vitro* assays conducted by us and

those by Bachmann et al. [163], as well as in *in-vitro* studies using other cell lines [166, 195], changes in *hSOCS3* mRNA expression served as reference for the transcriptional activity of STAT3.

To study the STAT3 stimulation via the cytokine receptor pathway, we took advantage of the IL-6 type cytokine Oncostatin M (OSM). OSM would normally lead to a strong pY705-STAT3 induction via the binding to the GP130/OSMR β complex, as it is described in Figure 8b. According to the low basic expression of OSMR β in CACO-2 cells (see chapter 4.2.), OSM at a concentration of 20 ng/ml did not increase *hSOCS3* gene expression in otherwise native CACO-2 cells, neither after 1h nor after 4h of incubation (Fig. 30b). This was underlined by the missing induction of pY705-STAT3 protein by the OSM-treatment in non-butyrate stimulated CACO-2 cells, determined via Western blot analysis of full cell lysates, 15' and 1h after the beginning of OSM stimulation (Fig. 25). Despite of the butyrate-mediated elevation of *hOSMR β* -expression which went along with an induction of pY705-STAT3 by OSM (see chapter 4.2.), qPCR analysis of *hSOCS3* mRNA in 1h and 4h-OSM-stimulated CACO-2 cells (20 ng/ml OSM) revealed no stimulation of the *hSOCS3* gene expression by OSM in the presence of a minimum 44h-butyrate preincubation (Fig. 30b). This was despite of a low basic expression of *hSOCS3* (CT value = 30). Furthermore, an isolated 24h-butyrate incubation even decreased *hSOCS3* expression, at least in 2 biological replicates (Fig. 29a). This drop of *hSOCS3* expression was likewise measured via qPCR in cell lysates after a 24h-TSA exposure (Fig. 29b). While *hSOCS3* mRNA was restored after a 48h-butyrate incubation, it stayed at low levels in the case of a TSA treatment (400 nM TSA for 48h).

Facing the small size of the investigated 24h-butyrate-treated cohort (n=2), conclusiveness of our data is somewhat limited and awaits validation.

If the results can be confirmed in equally conducted assays, one possible explanation for the failed inducibility of *hSOCS3* expression could lie in a possible transcription-inhibiting function of pS727-STAT3, at least at certain gene subclusters, including *hSOCS3*.

However, in a study conducted by Bachmann et al. [163], a 24h-incubation of CACO-2 cells with 3 mM butyrate did not change *hSOCS3* mRNA base expression.

4.4. Butyrate effects on cytokine- and GPR109A expression – the significance of a 3D environment

Comparing the cytokine expression in butyrate-treated versus untreated cells is another way to evaluate the functional relevance for butyrate-caused changes of STAT3. In our assays, we could confirm former observations concerning butyrate effects on the CXCL-8 and CCL-2 expression in 2D-cultured CACO-2 cells. Like in a study conducted by Fusunyan et al. [30], butyrate as a single agent increased the CXCL-8- and decreased the CCL-2 expression after 48 hours in a 2D-cell culture. In our assays, this also counted for the 3D-situation. Also the *hTNF α* - and *hCCL-20* expression was induced by butyrate in both cell culture settings. For CXCL-8- and TNF α , an mRNA-stabilization by p38 MAPK/MK-2 activity has been shown [112], so butyrate could additionally increase these cytokines via the p38 MAPK activation shown in our assays.

Compared to *hCXCL-8*, the CCL-2-encoding gene *hCCL-2* was basically high expressed in the 2D-setting (the mean base CT value was 26,5 (*hCCL-2*) versus 31 (*hCXCL-8*)). A high base expression of CLL-2 was also measured in the study by Fusunyan et al., determined by protein ELISA [30], which was ascribed to a basic activation of NF κ B in CACO-2 cells. Thus, the reduction of CCL-2 by butyrate was partly explained by butyrate's capability to inhibit the transcriptional activity of NF κ B.

Accordingly, butyrate pre-incubation attenuated TNF α -induced cytokine expression for all of the investigated cytokines in the 2D-cell culture in our assays.

In the 2D setting, several investigators formerly showed, as well, a reduced TNF α -mediated cytokine production in different cell types under a butyrate preincubation, also in CACO-2 cells [196]. Luhrs et al. described an inhibition of nuclear translocation of NF κ B by butyrate in the context of a TNF α stimulation of SW480, SW620, and HeLa229 cells which coincided with an inhibition of I κ B degradation [52]. But, apart from a decreased I κ B degradation, a reduced reappearance of I κ B to the cytoplasm, coinciding with a prolonged DNA-binding of NF κ B has also been described [84]. In our assays with CACO-2 cells, the reappearance of I κ B protein was also delayed after a 1h-lasting TNF α stimulus when cells had been pretreated with 5 mM sodium butyrate for 48h (Fig. 32).

Although this could be partly explained by a prolonged I κ B kinase activity [84], the inhibition of NF κ B at the I κ B gene promoter does also come into consideration. In this context, the interference of pY705/pS727-STAT3 and acetylated NF κ B/p65 (= RelA) at the cytokine promoter regions has to be taken into account [145].

Many genes which encode cytokines are co-regulated by NF κ B and STAT3, and additional transcription co-factors [145]. Depending on posttranslational phosphorylation- and acetylation status, these factors interfere or cooperate at promoter regions of gene subpanel [90, 145].

Interestingly, the TNF α -induced cytokine expression was not inhibited by butyrate in the 3D-cell culture. The gene expression of *hCXCL-8* was even significantly further increasable by the costimulation with TNF α and butyrate in the 3D-setting, which was not the case in the 2D environment (Fig. 36).

In the following, some aspects considering the diverging results gained from the 2D-versus the 3D-setting are discussed:

The maturation of intestinal epithelial cells in the 3D-*in vitro* setting might be deciding for their immune reactions. For instance, EGFR-signals lose some of their significance when cells mature or are 3-dimensional connected, as it is the case in physiological, more-dimensional cell networks [160]. This may have an influence on the basic phosphorylation of STAT3, i.e. the tyrosine705-phosphorylation might be affected.

Butyrate itself is known to increase the maturation of intestinal epithelial cells, partly via an upregulation of TGF β 1 [185] which was also observed in CACO-2 cells [197]. Moreover, via its receptor GPR109A, butyrate may be capable to strengthen the TGF β /SMAD signaling pathway, since it was shown that the artificial knockout of GPR109a in mice increased intraplasmatic SMAD6 and SMAD7, which are inhibitors of the TGF β signaling pathway [57].

In our assays, 5 days-differentiated CACO-2 cells showed a higher basic expression as well as a much higher peak of TNF α -induced *hCXCL-8* expression in comparison to 21 days-differentiated ones (the 30 vs. the 5-fold of the base value in the 2D-setting). This

implies an influence of the cell maturation on the immune reactivity. Furthermore, CACO-2 cells within the 2D-environment reacted upon a TNF α -stimulus with a much higher elevation of cytokine expression in comparison to 3D-seeded cells.

The original issue that led to the 3D approach was the low representation of butyrate receptors such as GPR109A in tumor cell lines like CACO-2, which is mainly due to a genetic silencing and therefore low expression of the receptor RNA in tumor cells [158, 198, 199]. In the 3D-cell culture setting, the combined treatment of CACO-2 cells with 48h-butyrates and an additional TNF α stimulus (10 ng/ml TNF α for the last 4h of the 48h-lasting assay) led to an increase of the GPR109A mRNA to about 5 CT values in the qPCR analysis (Fig. 35). Although the preliminary results await reproduction, the higher GPR109A expression under an TNF α -stimulus within the 3D environment could be useful concerning prospective investigations which aim to elucidate the signaling pathways in the inflamed mucosa.

An activation of SCFA receptors like GPR109A by butyrate could influence MAPK- and NF κ B pathways in IECs. Thus, the signaling via GPR109A might play a role in butyrate-caused effects on the STAT3-phosphorylation and on the cytokine expression in intestinal epithelial cells. One aspect could lay in an early GPR-mediated activation of p38 MAPK [111] (also see chapter 4.1.4.), which could have several subsequent effects. Among them, a stabilization of cytokine mRNA [112], an increased cell maturation [80] and a possible NF κ B activation are to mention.

Apart from that, the activatability of the TNF α receptor could be shown to differ between cells in a 3D and a 2D environment, e.g. in experiments with fibroblasts [200]. In the case of a 3D-environment, the activatability of the TNF α receptor was preserved for higher TNF α concentrations, whereas it became refractory in 2D-cultured cells.

4.5. Conclusions and Outlook

Butyrate as an abundant nutritional and microbial factor represents an interesting agent for the supplemented treatment of dysbiosis-associated diseases. This is mainly due to butyrate's capability to modulate the signal transduction and immunoregulation in intestinal epithelial cells by HDAC inhibition.

In a CACO-2 cell-based *in vitro* model of the intestinal epithelium we showed an increased pS727-STAT3 generation which was dependent on butyrate's function as an HDAC inhibitor and essentially included a p38 MAPK activation. HDAC inhibition by butyrate additionally increased *hOSMR β* expression in CACO-2 cells which fitted the results of formerly conducted assays by other investigators [144]. This was accompanied by pY705-STAT3 inducibility in response to OSM which was not detectable without the butyrate treatment.

It is limiting to mention that the cancer cell line used in our study (in line with several other investigators) cannot fully replace the examination at native colon cell lines. Several genes including *hOSMR β* are known to be silenced in cancer cells. Thus, the first future aim would be the repetition of the assays by using native cell lines.

In another step, we used a 3D-cell culture setting with CACO-2 cells seeded on a connective tissue matrix of a porcine small intestine. The presumed better differentiation and more physiological accessibility of the cells for soluted substances was reflected by a higher expression of the butyrate receptor GPR109A mRNA and a different cytokine mRNA expression pattern under the combined butyrate/TNF α influence, compared to the 2D-situation.

The generation of pS727-STAT3 is possibly an apoptosis concomitant feature of CACO-2 cells either to avoid or to support regularly apoptosis in response to HDAC inhibition.

Despite often being supposed to support the transcriptional activity of pY705-STAT3, the significance of the serine727-STAT3 in STAT3 signaling is controversially discussed in literature. At least a subcluster of STAT3-regulated genes could be inhibited by pS727-STAT3.

This subcluster might include the STAT3 target gene *hSOCS3*, which was found to be not induced in response to a stimulation with 20 ng/ml OSM for 1 and 4h, although pY705-

STAT3 was upregulated owing to butyrate preincubation and a strong *hOSMR* upregulation.

HDAC inhibition by substances like butyrate and TSA, which were exchangeable regarding the observed effects in our study, presumably initiate apoptosis via both the reactivation of before silenced tumor suppressor genes as well as by the interruption of STAT3/NFκB-dependent survival pathways. An inhibition of NFκB functions by butyrate could be shown in our assays as well, e.g. by the decreased detection of IκB protein 1h after a TNFα stimulus. IκB is normally simultaneously induced as negative feedback regulator of NFκB, transporting it back to the cytoplasm after nuclear activity.

pS727-STAT3 in our study could also be generated by a p38 MAPK-subsequent kinase (e.g. PKCδ) as a result of apoptosis induction, perhaps by a loss of function of pY705-STAT3, at least at a subpanel of genes including *hSOCS3*. This could be further investigated, e.g. by a blocking of PKCδ previous to the butyrate incubation and by determining anti-apoptotic proteins like Bcl-2, Bcl-xl and survivin [201].

Whether the raising pS727-STAT3 mainly occurs in the nucleus or rather in the cytoplasm cannot be answered with the results of our study. One would have to separate the nucleus proteins from the plasmatic ones before protein analysis to be able to distinguish this.

To investigate whether our butyrate-based results in CACO-2 cells fit the TSA results made by Togi et al. in HeLa cells regarding the role of HDAC(3) inhibition in pS727-STAT3 elevation [164], our assays await replication with adaptation of the conditions. E.g. by using HDAC3 siRNA constructs in the CACO-2 cell assays as it was performed by Togi et al. Since this research group only took usage of TSA as stimulating agent, one would have to treat HeLa cells also with 5 mM butyrate to be really able to compare the results. It is likely that the effects of butyrate, including those based on HDAC inhibition, depend on the cell type used in the assays.

To even out differences between the study by Kato et al. [166] and our study, one could try a PML knockdown in CACO-2 cells combined with serum starvation before starting the butyrate incubation or treat Hep3B cells with sodium butyrate as it was used in our assays to compare the pS727-STAT3 results. The role of PML should also be further

investigated. Does it have other side effects in addition to the interference with the STAT3/HDAC3 interaction?

Altogether, the functional outcome of CACO-2 cells after a long-term butyrate incubation of at least 24h is controversial and needs further investigation. Limiting to mention is also the, in some cases small sample cohort tested. For example, the measurement of *hSOCS3* expression after 24h butyrate should be repeated in a higher amount of equally conducted assays. This also applies to the qPCR results concerning *hGPR109A* and cytokines encoding genes gained by us in both 2D- and 3D cell culture approaches in order to broaden the statistical basis of the results. At the end, the 3D-cell culture approach tested by us in this context could be a useful supplement for further investigations, since the influence of GPR109A signaling might be better represented. The increased expression of *hGPR109A* in the situation of a combined butyrate/TNF α treatment in the 3D setting (when being compared to the 2D situation) could be even more pronounced by using primer with a higher efficiency.

As a perspective for the future, the observations of this study contribute to a more detailed picture of butyrate's effects on IECs and will be a basis for further investigation. To date, JAK/STAT inhibitors, HDAC inhibitors and specific proteasome inhibitors (e.g. Bortezomib, Vorinostat) are partly delineated from naturally occurring agents like Resveratrol, Curcumin or Capsaicin. Their effects are explored in clinical trials or they are already in usage for the therapy of some forms of cancer [33]. JAK/STAT inhibitors are also developed for the therapy of diabetes mellitus type 2, psoriasis, rheumatoid arthritis, atherosclerosis and chronic intestinal bowel disease [32].

The present study confirms a molecular basis for the clinically beneficial effects of butyrate concerning dysbiosis-associated diseases. In particular, butyrate's newly observed capacity to increase pS727-STAT3 could be an interesting issue in the discussion of butyrate effects at the intestinal barrier and on the physiology of intestinal cancer. Furthermore, the p38 MAPK pathway is located as a possible signaling pathway to target. The 3D-model was used for the first time in the observation of molecular butyrate effects on IECs and is an interesting approach for further studies in a humanified *in vitro* milieu.

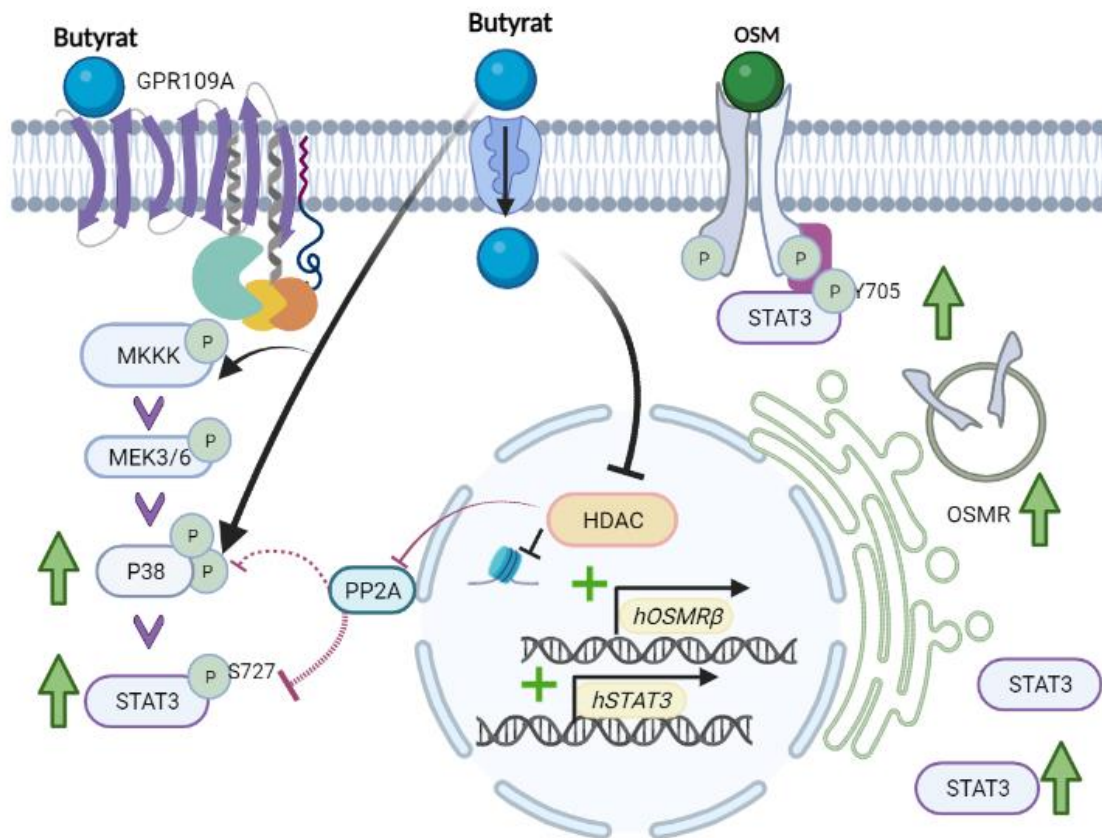


Fig. 40: Summary of effects and hypotheses.

Displayed are the main examined and hypothesized signaling pathways leading to the increase of pS727- and pY705-STAT3 protein by incubating CACO-2 cells with 5 mM sodium butyrate for minimum 20h. While some of the shown enzymes are hypothesized to be involved (e.g. MKKK-1, MEK-3/6, PP2A), the contribution of others (p38 MAPK, HDACs) is proven in this thesis. Green arrows indicate a proven increase of the protein or its phosphorylation status, the green plus shows a proven increase of gene transcription. PP2A phosphatase inhibition could contribute to both p38- as well as pS727-STAT3 phosphorylation. It would link HDAC inhibition and p38 MAPK activation. Apart from that, the MKKK/MEK/p38 signaling cascade could be induced by butyrate, binding to its receptors like GPR109A. Also cytokine receptors like the OSM-receptor might induce this cascade after ligand binding.

Butyrate enters cytoplasm and nucleoplasm via butyrate transporters or free diffusion. In the nucleus, butyrate inhibits the deacetylation of histones by HDACs which leads to an improved accessibility of several genes like hOSMRβ and hSTAT3 for gene transcription. Hence, total STAT3 protein and the OSM-receptor subunit OSMR(β) are higher produced. Subsequently, the binding of the receptor ligand OSM results in an increase of pY705-phosphorylated STAT3 by the OSMR complex.

5. Summary

A disturbance in the symbiotic mutualism between the intestinal microbiome and the human host's organism (syn. dysbiosis) accompanies the development of a variety of inflammatory and metabolic diseases that comprise the Metabolic Syndrome, chronic inflammatory gut diseases like Crohn's disease, Non-alcoholic fatty liver disease (NAFLD) and cardiovascular diseases, among others. The changed uptake and effectiveness of short chain fatty acids (SCFAs) as well as an increase of the intestinal permeability are common, interdependent disease elements in this regard. Short chain fatty acids are end-products of intestinal bacterial fermentation and affect the mucosal barrier integrity via numerous molecular mechanisms.

There is evidence to suggest, that SCFAs have a modulating influence on Signal transducer and activator of transcription 3 (STAT3) in intestinal epithelial cells. STAT3 is a central gene-transcription factor in signaling pathways of proliferation and inflammation. It can be activated by growth factors and other intercellular signaling molecules like the cytokine Oncostatin M (OSM). The mode of STAT3's activation exhibits, finally, a decisive influence on the immunological balance at the intestinal mucosa. Therefore, the posttranslational modification of STAT3 under the influence of SCFAs is likely to be a very important factor within the development and -progression of dysbiosis-associated diseases.

In this study, a clear positive in vitro-effect of the short chain fatty acid butyrate on the posttranslational serine727-phosphorylation of STAT3 and its total protein amount in the human adenocarcinoma cell line CACO2 is verified. Moreover, an increased gene expression of the OSM-receptor subunit OSMR β can be observed after butyrate incubation. Histone deacetylase inhibition is shown to have a predominant role in these effects. Furthermore, a subsequent p38 MAPK-activation by Butyrate is found to be a key molecular mechanism regarding the STAT3-phosphorylation at serine727-residues. To consider the portion of butyrate receptor signaling in this context in future assays, a CACO-2 cell 3D-culture model is introduced in which an improvement of the GPR109A-receptor expression in CACO-2 cells is accomplished.

5. Zusammenfassung

Eine Störung der symbiotischen Wechselbeziehung zwischen dem Darmmikrobiom und dem Wirtsorganismus (syn. Dysbiose) begleitet die Entwicklung vieler verschiedener entzündlicher und metabolischer Erkrankungen. Zu ihnen zählen unter anderem das Metabolische Syndrom, chronisch entzündliche Darmerkrankungen wie M. Crohn, die Nicht-alkoholische Fettlebererkrankung (NAFLD) und kardiovaskuläre Erkrankungen. Eine veränderte Aufnahme und Wirkung von kurzkettigen Fettsäuren (Short-chain fatty acids = SCFAs) und eine Schwächung der Darmbarriere bedingen sich in diesem Zusammenhang gegenseitig. Kurzkettige Fettsäuren sind Endprodukte des bakteriellen Stoffwechsels und beeinflussen die Integrität der Darmbarriere über eine Vielzahl molekularer Mechanismen.

Es gibt Hinweise darauf, dass kurzkettige Fettsäuren einen modulierenden Einfluss auf „Signal transducer and activator of transcription 3“ (STAT3) in intestinalen epithelialen Zellen ausüben. STAT3 ist hier ein zentraler Gentranskriptionsfaktor in proliferations- und entzündungsregulierenden Zellsignalwegen. Er kann durch Wachstumsfaktoren und andere interzelluläre Botenstoffe, wie beispielsweise das Zytokin Oncostatin M (OSM), aktiviert werden. Die Art der Aktivierung von STAT3 wirkt sich nicht zuletzt entscheidend auf die immunologische Balance an der Darmbarriere aus. Die Modifikation von STAT3 durch kurzkettige Fettsäuren ist aufgrund dessen mit hoher Wahrscheinlichkeit ein sehr wichtiger Faktor im Hinblick auf Entstehung und Progression der im Zusammenhang mit einer Dysbiose stehenden Erkrankungen.

In dieser Arbeit kann eine klare Steigerung der posttranslationalen Phosphorylierung von STAT3 an den Serin-Molekülendungen der Position 727 sowie eine Steigerung der Gesamtproteinmenge von STAT3 in der humanen Karzinomzelllinie CACO2 *in vitro* durch Butyrat-Inkubation gezeigt werden. Weiterhin wird unter Butyrat-Einfluss auch die Genexpression der OSM-Rezeptor-Untereinheit OSMR β gesteigert. Diese Effekte können größtenteils auf den Mechanismus der Histondeacetylase-Hemmung durch Butyrat zurückgeführt werden. Die in der Folge erhöhte P38 MAPK-Phosphorylierung durch Butyrat ist in Bezug auf die Serin727-Phosphorylierung an STAT3 entscheidend

beteiligt. Um in künftigen Assays auch den möglichen Einfluss der Butyrat-Rezeptor-Wirkung in diesem Zusammenhang besser zu erfassen, wird ein 3D-Zellkultur Ansatz getestet und in diesem eine verbesserte Expression des Butyrat-Rezeptors GPR109A in CACO-2-Zellen erreicht.

6. List of references

1. García-Montero, C., et al., *Nutritional Components in Western Diet Versus Mediterranean Diet at the Gut Microbiota-Immune System Interplay. Implications for Health and Disease*. *Nutrients*, 2021. **13**(2): p. 699.
2. Qin, J., et al., *A metagenome-wide association study of gut microbiota in type 2 diabetes*. *Nature*, 2012. **490**(7418): p. 55-60.
3. Wainwright, P. and C.D. Byrne, *Bidirectional Relationships and Disconnects between NAFLD and Features of the Metabolic Syndrome*. *Int J Mol Sci*, 2016. **17**(3): p. 367.
4. Aqel, B. and J.K. DiBaise, *Role of the Gut Microbiome in Nonalcoholic Fatty Liver Disease*. *Nutr Clin Pract*, 2015. **30**(6): p. 780-6.
5. Laurell, A. and K. Sjöberg, *Prebiotics and synbiotics in ulcerative colitis*. *Scand J Gastroenterol*, 2017. **52**(4): p. 477-485.
6. Arai, M., K. Matsuoka, and T. Kanai, *[Gut Microbiota and Internal Diseases: Update Information. Topics: 1. The role of the gut microiota on inflammatory bowel disease (IBD) and irritable bowel syndrome (IBS)]*. *Nihon Naika Gakkai Zasshi*, 2015. **104**(1): p. 35-41.
7. Matsuoka, K., et al., *Fecal microbiota transplantation for gastrointestinal diseases*. *Keio J Med*, 2014. **63**(4): p. 69-74.
8. Basson, A., et al., *Mucosal Interactions between Genetics, Diet, and Microbiome in Inflammatory Bowel Disease*. *Front Immunol*, 2016. **7**: p. 290.
9. Ng, S.C., et al., *Worldwide incidence and prevalence of inflammatory bowel disease in the 21st century: a systematic review of population-based studies*. *Lancet*, 2018. **390**(10114): p. 2769-2778.
10. Xu, X., et al., *Research advances in the relationship between nonalcoholic fatty liver disease and atherosclerosis*. *Lipids Health Dis*, 2015. **14**: p. 158.
11. Bultman, S.J., *Interplay between diet, gut microbiota, epigenetic events, and colorectal cancer*. *Mol Nutr Food Res*, 2017. **61**(1).
12. Ren, Z., et al., *Gut microbiome analysis as a tool towards targeted non-invasive biomarkers for early hepatocellular carcinoma*. *Gut*, 2019. **68**(6): p. 1014-1023.
13. Ley, R.E., D.A. Peterson, and J.I. Gordon, *Ecological and evolutionary forces shaping microbial diversity in the human intestine*. *Cell*, 2006. **124**(4): p. 837-48.
14. Nash, A.K., et al., *The gut mycobiome of the Human Microbiome Project healthy cohort*. *Microbiome*, 2017. **5**(1): p. 153.
15. Nicholson, J.K., et al., *Host-gut microbiota metabolic interactions*. *Science*, 2012. **336**(6086): p. 1262-7.
16. Kelly, C.R., et al., *Update on Fecal Microbiota Transplantation 2015: Indications, Methodologies, Mechanisms, and Outlook*. *Gastroenterology*, 2015. **149**(1): p. 223-37.
17. Geurts, L., et al., *Gut microbiota controls adipose tissue expansion, gut barrier and glucose metabolism: novel insights into molecular targets and interventions using prebiotics*. *Benef Microbes*, 2014. **5**(1): p. 3-17.
18. Wikoff, W.R., et al., *Metabolomics analysis reveals large effects of gut microflora on mammalian blood metabolites*. *Proc Natl Acad Sci U S A*, 2009. **106**(10): p. 3698-703.
19. Dodd, D., et al., *A gut bacterial pathway metabolizes aromatic amino acids into nine circulating metabolites*. *Nature*, 2017. **551**(7682): p. 648-652.
20. Grice, E.A. and J.A. Segre, *The human microbiome: our second genome*. *Annu Rev Genomics Hum Genet*, 2012. **13**: p. 151-70.

21. Di Domenico, M., et al., *The Intestinal Microbiota May Be a Potential Theranostic Tool for Personalized Medicine*. J Pers Med, 2022. **12**(4).
22. Blacher, E., et al., *Microbiome-Modulated Metabolites at the Interface of Host Immunity*. J Immunol, 2017. **198**(2): p. 572-580.
23. Sealy, L. and R. Chalkley, *The effect of sodium butyrate on histone modification*. Cell, 1978. **14**(1): p. 115-21.
24. Levy, M., et al., *Microbiota-Modulated Metabolites Shape the Intestinal Microenvironment by Regulating NLRP6 Inflammasome Signaling*. Cell, 2015. **163**(6): p. 1428-43.
25. Shapiro, H., et al., *The cross talk between microbiota and the immune system: metabolites take center stage*. Curr Opin Immunol, 2014. **30**: p. 54-62.
26. Peterson, L.W. and D. Artis, *Intestinal epithelial cells: regulators of barrier function and immune homeostasis*. Nat Rev Immunol, 2014. **14**(3): p. 141-53.
27. Smith, P.M., et al., *The microbial metabolites, short-chain fatty acids, regulate colonic Treg cell homeostasis*. Science, 2013. **341**(6145): p. 569-73.
28. Li, G., et al., *Microbiota metabolite butyrate constrains neutrophil functions and ameliorates mucosal inflammation in inflammatory bowel disease*. Gut microbes, 2021. **13**(1): p. 1968257-1968257.
29. Scheppach, W., et al., *Histological changes in the colonic mucosa following irrigation with short-chain fatty acids*. Eur J Gastroenterol Hepatol, 1997. **9**(2): p. 163-8.
30. Fusunyan, R.D., et al., *Butyrate switches the pattern of chemokine secretion by intestinal epithelial cells through histone acetylation*. Mol Med, 1999. **5**(9): p. 631-40.
31. Vanhoutvin, S.A., et al., *Butyrate-induced transcriptional changes in human colonic mucosa*. PLoS One, 2009. **4**(8): p. e6759.
32. Salas, A., et al., *JAK-STAT pathway targeting for the treatment of inflammatory bowel disease*. Nat Rev Gastroenterol Hepatol, 2020. **17**(6): p. 323-337.
33. Chai, E.Z., et al., *Targeting transcription factor STAT3 for cancer prevention and therapy*. Pharmacol Ther, 2016. **162**: p. 86-97.
34. David, L.A., et al., *Diet rapidly and reproducibly alters the human gut microbiome*. Nature, 2014. **505**(7484): p. 559-63.
35. De Filippo, C., et al., *Impact of diet in shaping gut microbiota revealed by a comparative study in children from Europe and rural Africa*. Proc Natl Acad Sci U S A, 2010. **107**(33): p. 14691-6.
36. Cani, P.D., et al., *Gut microbiota fermentation of prebiotics increases satietogenic and incretin gut peptide production with consequences for appetite sensation and glucose response after a meal*. Am J Clin Nutr, 2009. **90**(5): p. 1236-43.
37. Bäckhed, F., et al., *The gut microbiota as an environmental factor that regulates fat storage*. Vol. 101. 2004. 15718-23.
38. Liu, T.F., et al., *Fueling the flame: bioenergy couples metabolism and inflammation*. J Leukoc Biol, 2012. **92**(3): p. 499-507.
39. Ohira, H., W. Tsutsui, and Y. Fujioka, *Are Short Chain Fatty Acids in Gut Microbiota Defensive Players for Inflammation and Atherosclerosis?* J Atheroscler Thromb, 2017. **24**(7): p. 660-672.
40. Kim, C.H., J. Park, and M. Kim, *Gut microbiota-derived short-chain Fatty acids, T cells, and inflammation*. Immune Netw, 2014. **14**(6): p. 277-88.
41. Coppola, S., et al., *The Protective Role of Butyrate against Obesity and Obesity-Related Diseases*. Molecules (Basel, Switzerland), 2021. **26**(3): p. 682.
42. Roediger, W.E., *Role of anaerobic bacteria in the metabolic welfare of the colonic mucosa in man*. Gut, 1980. **21**(9): p. 793-8.

43. Valenzano, M.C., et al., *Remodeling of Tight Junctions and Enhancement of Barrier Integrity of the CACO-2 Intestinal Epithelial Cell Layer by Micronutrients*. PLoS One, 2015. **10**(7): p. e0133926.
44. Peng, L., et al., *Butyrate enhances the intestinal barrier by facilitating tight junction assembly via activation of AMP-activated protein kinase in Caco-2 cell monolayers*. J Nutr, 2009. **139**(9): p. 1619-25.
45. Wang, H.B., et al., *Butyrate enhances intestinal epithelial barrier function via up-regulation of tight junction protein Claudin-1 transcription*. Dig Dis Sci, 2012. **57**(12): p. 3126-35.
46. Macia, L., et al., *Metabolite-sensing receptors GPR43 and GPR109A facilitate dietary fibre-induced gut homeostasis through regulation of the inflammasome*. Nat Commun, 2015. **6**: p. 6734.
47. Kulkarni, N.N., et al., *Phenylbutyrate induces cathelicidin expression via the vitamin D receptor: Linkage to inflammatory and growth factor cytokines pathways*. Mol Immunol, 2015. **63**(2): p. 530-9.
48. Fernando, M.R., et al., *Butyrate enhances antibacterial effects while suppressing other features of alternative activation in IL-4-induced macrophages*. Am J Physiol Gastrointest Liver Physiol, 2016. **310**(10): p. G822-31.
49. Maslowski, K.M., et al., *Regulation of inflammatory responses by gut microbiota and chemoattractant receptor GPR43*. Nature, 2009. **461**(7268): p. 1282-6.
50. Kim, M.H., et al., *Short-chain fatty acids activate GPR41 and GPR43 on intestinal epithelial cells to promote inflammatory responses in mice*. Gastroenterology, 2013. **145**(2): p. 396-406.e1-10.
51. Elinav, E., et al., *NLRP6 inflammasome regulates colonic microbial ecology and risk for colitis*. Cell, 2011. **145**(5): p. 745-57.
52. Luhrs, H., et al., *Cytokine-activated degradation of inhibitory kappaB protein alpha is inhibited by the short-chain fatty acid butyrate*. Int J Colorectal Dis, 2001. **16**(4): p. 195-201.
53. Singh, N., et al., *Activation of Gpr109a, receptor for niacin and the commensal metabolite butyrate, suppresses colonic inflammation and carcinogenesis*. Immunity, 2014. **40**(1): p. 128-39.
54. Chang, P.V., et al., *The microbial metabolite butyrate regulates intestinal macrophage function via histone deacetylase inhibition*. Proc Natl Acad Sci U S A, 2014. **111**(6): p. 2247-52.
55. Digby, J.E., et al., *Anti-inflammatory effects of nicotinic acid in human monocytes are mediated by GPR109A dependent mechanisms*. Arterioscler Thromb Vasc Biol, 2012. **32**(3): p. 669-76.
56. Le Poul, E., et al., *Functional characterization of human receptors for short chain fatty acids and their role in polymorphonuclear cell activation*. J Biol Chem, 2003. **278**(28): p. 25481-9.
57. Zimmerman, M.A., et al., *Butyrate suppresses colonic inflammation through HDAC1-dependent Fas upregulation and Fas-mediated apoptosis of T cells*. Am J Physiol Gastrointest Liver Physiol, 2012. **302**(12): p. G1405-15.
58. Nagalakshmi, M.L., et al., *Interleukin-22 activates STAT3 and induces IL-10 by colon epithelial cells*. Int Immunopharmacol, 2004. **4**(5): p. 679-91.
59. Cummings, J.H., et al., *Short chain fatty acids in human large intestine, portal, hepatic and venous blood*. Gut, 1987. **28**(10): p. 1221-7.
60. Correa-Oliveira, R., et al., *Regulation of immune cell function by short-chain fatty acids*. Clin Transl Immunology, 2016. **5**(4): p. e73.

61. Goncalves, P. and F. Martel, *Butyrate and colorectal cancer: the role of butyrate transport*. *Curr Drug Metab*, 2013. **14**(9): p. 994-1008.
62. den Besten, G., et al., *The role of short-chain fatty acids in the interplay between diet, gut microbiota, and host energy metabolism*. *J Lipid Res*, 2013. **54**(9): p. 2325-40.
63. Peng, L., et al., *Effects of butyrate on intestinal barrier function in a Caco-2 cell monolayer model of intestinal barrier*. *Pediatr Res*, 2007. **61**(1): p. 37-41.
64. Kumar, A., et al., *Lactobacillus acidophilus counteracts enteropathogenic E. coli-induced inhibition of butyrate uptake in intestinal epithelial cells*. *Am J Physiol Gastrointest Liver Physiol*, 2015. **309**(7): p. G602-7.
65. Thibault, R., et al., *Down-regulation of the monocarboxylate transporter 1 is involved in butyrate deficiency during intestinal inflammation*. *Gastroenterology*, 2007. **133**(6): p. 1916-27.
66. Rau, M., et al., *Fecal SCFAs and SCFA-producing bacteria in gut microbiome of human NAFLD as a putative link to systemic T-cell activation and advanced disease*. *United European Gastroenterol J*, 2018. **6**(10): p. 1496-1507.
67. Sturm, A. and A.U. Dignass, *Epithelial restitution and wound healing in inflammatory bowel disease*. *World J Gastroenterol*, 2008. **14**(3): p. 348-53.
68. Pabst, O. and A.M. Mowat, *Oral tolerance to food protein*. *Mucosal Immunol*, 2012. **5**(3): p. 232-9.
69. Nguyen, P.M., T.L. Putoczki, and M. Ernst, *STAT3-Activating Cytokines: A Therapeutic Opportunity for Inflammatory Bowel Disease?* *J Interferon Cytokine Res*, 2015. **35**(5): p. 340-50.
70. Park, J., et al., *Short-chain fatty acids induce both effector and regulatory T cells by suppression of histone deacetylases and regulation of the mTOR-S6K pathway*. *Mucosal Immunol*, 2015. **8**(1): p. 80-93.
71. Siegmund, B., *Interleukin-18 in intestinal inflammation: friend and foe?* *Immunity*, 2010. **32**(3): p. 300-2.
72. Arts, R.J., L.A. Joosten, and M.G. Netea, *Immunometabolic circuits in trained immunity*. *Semin Immunol*, 2016. **28**(5): p. 425-430.
73. Goto, Y. and Ivanov, II, *Intestinal epithelial cells as mediators of the commensal-host immune crosstalk*. *Immunol Cell Biol*, 2013. **91**(3): p. 204-14.
74. Wells, J.M., et al., *Epithelial crosstalk at the microbiota-mucosal interface*. *Proc Natl Acad Sci U S A*, 2011. **108 Suppl 1**: p. 4607-14.
75. Goncalves, P. and J.P. Di Santo, *An Intestinal Inflammasome - The ILC3-Cytokine Tango*. *Trends Mol Med*, 2016. **22**(4): p. 269-271.
76. Ulrich. Gerke, T., *Inhibition des nukleären Transkriptionsfaktors kappa B (NF-kB) [(NF-kappa-B)] durch die kurzkettige Fettsäure Butyrat*. 2004.
77. Wajant, H., *TRAIL- and TNF-induced signaling complexes-so similar yet so different*. *Embo j*, 2017. **36**(9): p. 1117-1119.
78. Davie, J.R., *Inhibition of histone deacetylase activity by butyrate*. *J Nutr*, 2003. **133**(7 Suppl): p. 2485s-2493s.
79. Gaschott, T. and J. Stein, *Short-chain fatty acids and colon cancer cells: the vitamin D receptor--butyrate connection*. *Recent Results Cancer Res*, 2003. **164**: p. 247-57.
80. Daniel, C., et al., *p38 MAPK signaling pathway is involved in butyrate-induced vitamin D receptor expression*. *Biochem Biophys Res Commun*, 2004. **324**(4): p. 1220-6.
81. Daniel, C., et al., *The TGFbeta/Smad 3-signaling pathway is involved in butyrate-mediated vitamin D receptor (VDR)-expression*. *J Cell Biochem*, 2007. **102**(6): p. 1420-31.
82. Velazquez, O.C., H.M. Lederer, and J.L. Rombeau, *Butyrate and the colonocyte. Production, absorption, metabolism, and therapeutic implications*. *Adv Exp Med Biol*, 1997. **427**: p. 123-34.

83. Lin, M.Y., et al., *Redirection of Epithelial Immune Responses by Short-Chain Fatty Acids through Inhibition of Histone Deacetylases*. *Front Immunol*, 2015. **6**: p. 554.
84. Adam, E., et al., *Potentialiation of tumor necrosis factor-induced NF-kappa B activation by deacetylase inhibitors is associated with a delayed cytoplasmic reappearance of I kappa B alpha*. *Mol Cell Biol*, 2003. **23**(17): p. 6200-9.
85. Glozak, M.A., et al., *Acetylation and deacetylation of non-histone proteins*. *Gene*, 2005. **363**: p. 15-23.
86. Ziesche, E., et al., *The coactivator role of histone deacetylase 3 in IL-1-signaling involves deacetylation of p65 NF-kappaB*. *Nucleic Acids Res*, 2013. **41**(1): p. 90-109.
87. Guilloteau, P., et al., *From the gut to the peripheral tissues: the multiple effects of butyrate*. *Nutr Res Rev*, 2010. **23**(2): p. 366-84.
88. Luo, J., et al., *Acetylation of p53 augments its site-specific DNA binding both in vitro and in vivo*. *Proc Natl Acad Sci U S A*, 2004. **101**(8): p. 2259-64.
89. Lee, H., et al., *Persistently activated Stat3 maintains constitutive NF-kappaB activity in tumors*. *Cancer Cell*, 2009. **15**(4): p. 283-93.
90. Grivennikov, S.I. and M. Karin, *Dangerous liaisons: STAT3 and NF-kappaB collaboration and crosstalk in cancer*. *Cytokine Growth Factor Rev*, 2010. **21**(1): p. 11-9.
91. Wilson, A.J., et al., *Histone deacetylase 3 (HDAC3) and other class I HDACs regulate colon cell maturation and p21 expression and are deregulated in human colon cancer*. *J Biol Chem*, 2006. **281**(19): p. 13548-58.
92. Wang, X., et al., *Histone deacetylases and their inhibitors: molecular mechanisms and therapeutic implications in diabetes mellitus*. *Acta Pharmaceutica Sinica B*, 2012. **2**(4): p. 387-395.
93. Alenghat, T., et al., *Nuclear receptor corepressor and histone deacetylase 3 govern circadian metabolic physiology*. *Nature*, 2008. **456**(7224): p. 997-1000.
94. Whitt, J., et al., *Disruption of Epithelial HDAC3 in Intestine Prevents Diet-Induced Obesity in Mice*. *Gastroenterology*, 2018. **155**(2): p. 501-513.
95. Shakespear, M.R., et al., *Histone deacetylases as regulators of inflammation and immunity*. *Trends Immunol*, 2011. **32**(7): p. 335-43.
96. Alenghat, T., et al., *Histone deacetylase 3 coordinates commensal-bacteria-dependent intestinal homeostasis*. *Nature*, 2013. **504**(7478): p. 153-7.
97. Cousens, L.S., D. Gallwitz, and B.M. Alberts, *Different accessibilities in chromatin to histone acetylase*. *J Biol Chem*, 1979. **254**(5): p. 1716-23.
98. Marks, P.A., *Histone deacetylase inhibitors: a chemical genetics approach to understanding cellular functions*. *Biochim Biophys Acta*, 2010. **1799**(10-12): p. 717-25.
99. Seidel, C., et al., *Histone deacetylase modulators provided by Mother Nature*. *Genes Nutr*, 2012. **7**(3): p. 357-67.
100. Blottiere, H.M., et al., *Molecular analysis of the effect of short-chain fatty acids on intestinal cell proliferation*. *Proc Nutr Soc*, 2003. **62**(1): p. 101-6.
101. Siavoshian, S., et al., *Butyrate and trichostatin A effects on the proliferation/differentiation of human intestinal epithelial cells: induction of cyclin D3 and p21 expression*. *Gut*, 2000. **46**(4): p. 507-14.
102. Schroder, O., et al., *Upregulation of 25-hydroxyvitamin D(3)-1(alpha)-hydroxylase by butyrate in Caco-2 cells*. *World J Gastroenterol*, 2005. **11**(45): p. 7136-41.
103. Gaschott, T., et al., *1,25-Dihydroxycholecalciferol enhances butyrate-induced p21(Waf1/Cip1) expression*. *Biochem Biophys Res Commun*, 2001. **283**(1): p. 80-5.
104. Vander Heiden, M.G., L.C. Cantley, and C.B. Thompson, *Understanding the Warburg effect: the metabolic requirements of cell proliferation*. *Science*, 2009. **324**(5930): p. 1029-33.

105. Cabrero, A., J.C. Laguna, and M. Vazquez, *Peroxisome proliferator-activated receptors and the control of inflammation*. *Curr Drug Targets Inflamm Allergy*, 2002. **1**(3): p. 243-8.
106. Alex, S., et al., *Short-chain fatty acids stimulate angiopoietin-like 4 synthesis in human colon adenocarcinoma cells by activating peroxisome proliferator-activated receptor gamma*. *Mol Cell Biol*, 2013. **33**(7): p. 1303-16.
107. Ang, Z. and J.L. Ding, *GPR41 and GPR43 in Obesity and Inflammation - Protective or Causative?* *Front Immunol*, 2016. **7**: p. 28.
108. Yonezawa, T., Y. Kobayashi, and Y. Obara, *Short-chain fatty acids induce acute phosphorylation of the p38 mitogen-activated protein kinase/heat shock protein 27 pathway via GPR43 in the MCF-7 human breast cancer cell line*. *Cell Signal*, 2007. **19**(1): p. 185-93.
109. Kaiser, M.M.M., et al., *Butyrate Conditions Human Dendritic Cells to Prime Type 1 Regulatory T Cells via both Histone Deacetylase Inhibition and G Protein-Coupled Receptor 109A Signaling*. *Front Immunol*, 2017. **8**: p. 1429.
110. Chai, J.T., J.E. Digby, and R.P. Choudhury, *GPR109A and vascular inflammation*. *Curr Atheroscler Rep*, 2013. **15**(5): p. 325.
111. Ma, L. and G. Pei, *Beta-arrestin signaling and regulation of transcription*. *J Cell Sci*, 2007. **120**(Pt 2): p. 213-8.
112. Winzen, R., et al., *The p38 MAP kinase pathway signals for cytokine-induced mRNA stabilization via MAP kinase-activated protein kinase 2 and an AU-rich region-targeted mechanism*. *Embo j*, 1999. **18**(18): p. 4969-80.
113. Neufert, C., et al., *Activation of epithelial STAT3 regulates intestinal homeostasis*. *Cell Cycle*, 2010. **9**(4): p. 652-5.
114. Schindler, C. and J.E. Darnell, Jr., *Transcriptional responses to polypeptide ligands: the JAK-STAT pathway*. *Annu Rev Biochem*, 1995. **64**: p. 621-51.
115. Yu, H., et al., *Revisiting STAT3 signalling in cancer: new and unexpected biological functions*. *Nature Reviews Cancer*, 2014. **14**(11): p. 736-746.
116. Levy, D.E. and C.K. Lee, *What does Stat3 do?* *J Clin Invest*, 2002. **109**(9): p. 1143-8.
117. Miraglia, E., et al., *Entinostat up-regulates the CAMP gene encoding LL-37 via activation of STAT3 and HIF-1alpha transcription factors*. *Sci Rep*, 2016. **6**: p. 33274.
118. Avalle, L., et al., *STAT3 in cancer: A double edged sword*. *Cytokine*, 2017. **98**: p. 42-50.
119. Heinrich, P.C., et al., *Principles of interleukin (IL)-6-type cytokine signalling and its regulation*. *Biochem J*, 2003. **374**(Pt 1): p. 1-20.
120. Kojima, H., et al., *STAT3 regulates Nemo-like kinase by mediating its interaction with IL-6-stimulated TGFbeta-activated kinase 1 for STAT3 Ser-727 phosphorylation*. *Proceedings of the National Academy of Sciences of the United States of America*, 2005. **102**(12): p. 4524-4529.
121. Chung, J., et al., *STAT3 serine phosphorylation by ERK-dependent and -independent pathways negatively modulates its tyrosine phosphorylation*. *Mol Cell Biol*, 1997. **17**(11): p. 6508-16.
122. Qin, H.R., et al., *Activation of signal transducer and activator of transcription 3 through a phosphomimetic serine 727 promotes prostate tumorigenesis independent of tyrosine 705 phosphorylation*. *Cancer Res*, 2008. **68**(19): p. 7736-41.
123. Woetmann, A., et al., *Inhibition of protein phosphatase 2A induces serine/threonine phosphorylation, subcellular redistribution, and functional inhibition of STAT3*. *Proc Natl Acad Sci U S A*, 1999. **96**(19): p. 10620-5.
124. Avalle, L. and V. Poli, *Nucleus, Mitochondrion, or Reticulum? STAT3 à La Carte*. *International journal of molecular sciences*, 2018. **19**(9): p. 2820.

125. Wegrzyn, J., et al., *Function of mitochondrial Stat3 in cellular respiration*. Science, 2009. **323**(5915): p. 793-7.
126. Gough, D.J., et al., *Mitochondrial STAT3 supports Ras-dependent oncogenic transformation*. Science, 2009. **324**(5935): p. 1713-6.
127. Yu, C., et al., *Mitochondrial STAT3 contributes to transformation of Barrett's epithelial cells that express oncogenic Ras in a p53-independent fashion*. Am J Physiol Gastrointest Liver Physiol, 2015. **309**(3): p. G146-61.
128. Turkson, J., et al., *Requirement for Ras/Rac1-mediated p38 and c-Jun N-terminal kinase signaling in Stat3 transcriptional activity induced by the Src oncoprotein*. Mol Cell Biol, 1999. **19**(11): p. 7519-28.
129. Bromberg, J.F., et al., *Stat3 activation is required for cellular transformation by v-src*. Mol Cell Biol, 1998. **18**(5): p. 2553-8.
130. Wen, Z., Z. Zhong, and J.E. Darnell, Jr., *Maximal activation of transcription by Stat1 and Stat3 requires both tyrosine and serine phosphorylation*. Cell, 1995. **82**(2): p. 241-50.
131. Jain, N., et al., *Protein kinase C delta associates with and phosphorylates Stat3 in an interleukin-6-dependent manner*. J Biol Chem, 1999. **274**(34): p. 24392-400.
132. Decker, T. and P. Kovarik, *Serine phosphorylation of STATs*. Oncogene, 2000. **19**(21): p. 2628-37.
133. Hermanns, H.M., *Oncostatin M and interleukin-31: Cytokines, receptors, signal transduction and physiology*. Cytokine Growth Factor Rev, 2015. **26**(5): p. 545-58.
134. Pickert, G., et al., *STAT3 links IL-22 signaling in intestinal epithelial cells to mucosal wound healing*. J Exp Med, 2009. **206**(7): p. 1465-72.
135. Lovato, P., et al., *Constitutive STAT3 activation in intestinal T cells from patients with Crohn's disease*. J Biol Chem, 2003. **278**(19): p. 16777-81.
136. Willson, T.A., et al., *Deletion of intestinal epithelial cell STAT3 promotes T-lymphocyte STAT3 activation and chronic colitis following acute dextran sodium sulfate injury in mice*. Inflamm Bowel Dis, 2013. **19**(3): p. 512-25.
137. Wittkopf, N., et al., *Activation of intestinal epithelial Stat3 orchestrates tissue defense during gastrointestinal infection*. PLoS One, 2015. **10**(3): p. e0118401.
138. Welte, T., et al., *STAT3 deletion during hematopoiesis causes Crohn's disease-like pathogenesis and lethality: a critical role of STAT3 in innate immunity*. Proc Natl Acad Sci U S A, 2003. **100**(4): p. 1879-84.
139. West, N.R., et al., *Oncostatin M drives intestinal inflammation and predicts response to tumor necrosis factor-neutralizing therapy in patients with inflammatory bowel disease*. Nat Med, 2017. **23**(5): p. 579-589.
140. Beigel, F., et al., *Oncostatin M mediates STAT3-dependent intestinal epithelial restitution via increased cell proliferation, decreased apoptosis and upregulation of SERPIN family members*. PLoS One, 2014. **9**(4): p. e93498.
141. Elks, C.M., et al., *Loss of Oncostatin M Signaling in Adipocytes Induces Insulin Resistance and Adipose Tissue Inflammation in Vivo*. J Biol Chem, 2016. **291**(33): p. 17066-76.
142. Deng, G., et al., *Unique methylation pattern of oncostatin m receptor gene in cancers of colorectum and other digestive organs*. Clin Cancer Res, 2009. **15**(5): p. 1519-26.
143. Kim, M.S., et al., *Promoter DNA methylation of oncostatin m receptor-beta as a novel diagnostic and therapeutic marker in colon cancer*. PLoS One, 2009. **4**(8): p. e6555.
144. Dambacher, J., et al., *Interleukin 31 mediates MAP kinase and STAT1/3 activation in intestinal epithelial cells and its expression is upregulated in inflammatory bowel disease*. Gut, 2007. **56**(9): p. 1257-65.
145. Bollrath, J. and F.R. Greten, *IKK/NF-kappaB and STAT3 pathways: central signalling hubs in inflammation-mediated tumour promotion and metastasis*. EMBO Rep, 2009. **10**(12): p. 1314-9.

146. Daien, C.I., et al., *Detrimental Impact of Microbiota-Accessible Carbohydrate-Deprived Diet on Gut and Immune Homeostasis: An Overview*. Front Immunol, 2017. **8**: p. 548.
147. van Ampting, M.T., et al., *Intestinally secreted C-type lectin Reg3b attenuates salmonellosis but not listeriosis in mice*. Infect Immun, 2012. **80**(3): p. 1115-20.
148. Bluemel, S., et al., *The Role of Intestinal C-type Regenerating Islet Derived-3 Lectins for Nonalcoholic Steatohepatitis*. Hepatol Commun, 2018. **2**(4): p. 393-406.
149. Wang, L., et al., *Intestinal REG3 Lectins Protect against Alcoholic Steatohepatitis by Reducing Mucosa-Associated Microbiota and Preventing Bacterial Translocation*. Cell Host Microbe, 2016. **19**(2): p. 227-39.
150. Takeda, K., et al., *Enhanced Th1 activity and development of chronic enterocolitis in mice devoid of Stat3 in macrophages and neutrophils*. Immunity, 1999. **10**(1): p. 39-49.
151. Gamero, A.M., H.A. Young, and R.H. Wiltrot, *Inactivation of Stat3 in tumor cells: releasing a brake on immune responses against cancer?* Cancer Cell, 2004. **5**(2): p. 111-2.
152. Wang, T., et al., *Regulation of the innate and adaptive immune responses by Stat-3 signaling in tumor cells*. Nat Med, 2004. **10**(1): p. 48-54.
153. Wang, Y., et al., *The role of STAT3 in leading the crosstalk between human cancers and the immune system*. Cancer Lett, 2018. **415**: p. 117-128.
154. Miklossy, G., T.S. Hilliard, and J. Turkson, *Therapeutic modulators of STAT signalling for human diseases*. Nat Rev Drug Discov, 2013. **12**(8): p. 611-29.
155. Kim, B.H., E.H. Yi, and S.K. Ye, *Signal transducer and activator of transcription 3 as a therapeutic target for cancer and the tumor microenvironment*. Arch Pharm Res, 2016. **39**(8): p. 1085-99.
156. Lea, T., *Caco-2 Cell Line*, in *The Impact of Food Bioactives on Health: in vitro and ex vivo models*, K. Verhoeckx, et al., Editors. 2015, Springer Copyright 2015, The Author(s). Cham (CH). p. 103-111.
157. Thangaraju, M., et al., *Sodium-coupled transport of the short chain fatty acid butyrate by SLC5A8 and its relevance to colon cancer*. J Gastrointest Surg, 2008. **12**(10): p. 1773-81; discussion 1781-2.
158. Tang, Y., et al., *G-protein-coupled receptor for short-chain fatty acids suppresses colon cancer*. Int J Cancer, 2011. **128**(4): p. 847-56.
159. Schweinlin, M., et al., *Development of an Advanced Primary Human In Vitro Model of the Small Intestine*. Tissue Eng Part C Methods, 2016. **22**(9): p. 873-83.
160. Luca, A.C., et al., *Impact of the 3D microenvironment on phenotype, gene expression, and EGFR inhibition of colorectal cancer cell lines*. PLoS One, 2013. **8**(3): p. e59689.
161. Ferruzza, S., et al., *A protocol for differentiation of human intestinal Caco-2 cells in asymmetric serum-containing medium*. Toxicology in Vitro, 2012. **26**(8): p. 1252-1255.
162. Yakovich, A.J., et al., *Vectorial TGF β signaling in polarized intestinal epithelial cells*. Journal of Cellular Physiology, 2010. **224**(2): p. 398-404.
163. Bachmann, M., et al., *Cooperation between the bacterial-derived short-chain fatty acid butyrate and interleukin-22 detected in human Caco2 colon epithelial/carcinoma cells*. Biofactors, 2017. **43**(2): p. 283-292.
164. Togi, S., et al., *HDAC3 influences phosphorylation of STAT3 at serine 727 by interacting with PP2A*. Biochem Biophys Res Commun, 2009. **379**(2): p. 616-20.
165. Jarnicki, A., T. Putoczki, and M. Ernst, *Stat3: linking inflammation to epithelial cancer - more than a "gut" feeling?* Cell division, 2010. **5**: p. 14-14.
166. Kato, M., et al., *PML suppresses IL-6-induced STAT3 activation by interfering with STAT3 and HDAC3 interaction*. Biochem Biophys Res Commun, 2015. **461**(2): p. 366-71.

167. Choi, I., et al., *Roles of protein phosphatase 2A in IL-6 signal transduction in Hep3B cells*. Immunol Lett, 1998. **61**(2-3): p. 103-7.
168. Nguyen, H.C.B., et al., *Dichotomous engagement of HDAC3 activity governs inflammatory responses*. Nature, 2020. **584**(7820): p. 286-290.
169. Liu, F.T., et al., *STAT3 and NF-kappaB cooperatively control in vitro spontaneous apoptosis and poor chemo-responsiveness in patients with chronic lymphocytic leukemia*. Oncotarget, 2016. **7**(22): p. 32031-45.
170. Yu, C.L., et al., *Enhanced DNA-binding activity of a Stat3-related protein in cells transformed by the Src oncoprotein*. Science, 1995. **269**(5220): p. 81-3.
171. Yu, H., Jove, R., *STAT signaling as a molecular target for cancer therapy*, in *Molecular Oncology*. 2013, Cambridge University Press. . p. 305-312.
172. Karpf, A.R. and D.A. Jones, *Reactivating the expression of methylation silenced genes in human cancer*. Oncogene, 2002. **21**(35): p. 5496-503.
173. Yin, L., G. Laevsky, and C. Giardina, *Butyrate suppression of colonocyte NF-kappa B activation and cellular proteasome activity*. J Biol Chem, 2001. **276**(48): p. 44641-6.
174. Kiliccioğlu, I., et al., *Apoptotic effects of proteasome and histone deacetylase inhibitors in prostate cancer cell lines*. Genet Mol Res, 2014. **13**(2): p. 3721-31.
175. Auer, B., *Der Einfluss von α - Liponsäure und weiteren HDAC-Inhibitoren auf Tumorwachstum und Angiogenese in der Pankreaskarzinomzelllinie MIA-PaCa-2*, in *Veterinärmedizin*. 2008, Justus-Liebig-Universität Gießen.
176. Abaza, M.S., A.M. Bahman, and R.J. Al-Attayah, *Valproic acid, an anti-epileptic drug and a histone deacetylase inhibitor, in combination with proteasome inhibitors exerts antiproliferative, pro-apoptotic and chemosensitizing effects in human colorectal cancer cells: underlying molecular mechanisms*. Int J Mol Med, 2014. **34**(2): p. 513-32.
177. McMillan, L., et al., *Opposing effects of butyrate and bile acids on apoptosis of human colon adenoma cells: differential activation of PKC and MAP kinases*. British Journal Of Cancer, 2003. **88**: p. 748.
178. Qi, X., et al., *p38 MAPK activation selectively induces cell death in K-ras-mutated human colon cancer cells through regulation of vitamin D receptor*. J Biol Chem, 2004. **279**(21): p. 22138-44.
179. Nepelska, M., et al., *Butyrate produced by commensal bacteria potentiates phorbol esters induced AP-1 response in human intestinal epithelial cells*. PLoS One, 2012. **7**(12): p. e52869.
180. Qi, X., et al., *The p38 and JNK pathways cooperate to trans-activate vitamin D receptor via c-Jun/AP-1 and sensitize human breast cancer cells to vitamin D(3)-induced growth inhibition*. J Biol Chem, 2002. **277**(29): p. 25884-92.
181. Ding, Q., Q. Wang, and B.M. Evers, *Alterations of MAPK activities associated with intestinal cell differentiation*. Biochem Biophys Res Commun, 2001. **284**(2): p. 282-8.
182. Cho, S.D., et al., *Critical role of the c-JunNH2-terminal kinase and p38 mitogen-activated protein kinase pathways on sodium butyrate-induced apoptosis in DU145 human prostate cancer cells*. Eur J Cancer Prev, 2006. **15**(1): p. 57-63.
183. Xiao, T., et al., *Butyrate upregulates the TLR4 expression and the phosphorylation of MAPKs and NK- κ B in colon cancer cell in vitro*. Oncol Lett, 2018. **16**(4): p. 4439-4447.
184. Böcker, U., et al., *Responsiveness of intestinal epithelial cell lines to lipopolysaccharide is correlated with Toll-like receptor 4 but not Toll-like receptor 2 or CD14 expression*. Int J Colorectal Dis, 2003. **18**(1): p. 25-32.
185. Martin-Gallausiaux, C., et al., *Butyrate produced by gut commensal bacteria activates TGF-beta1 expression through the transcription factor SP1 in human intestinal epithelial cells*. Sci Rep, 2018. **8**(1): p. 9742.

186. Shackelford, D.B. and R.J. Shaw, *The LKB1-AMPK pathway: metabolism and growth control in tumour suppression*. Nature reviews. Cancer, 2009. **9**(8): p. 563-575.
187. Lea, M.A., et al., *Growth inhibition of colon cancer cells by compounds affecting AMPK activity*. World J Gastrointest Oncol, 2014. **6**(7): p. 244-52.
188. Kim, I. and Y.-Y. He, *Targeting the AMP-Activated Protein Kinase for Cancer Prevention and Therapy*. Frontiers in oncology, 2013. **3**: p. 175-175.
189. Sengupta, T.K., et al., *Cytotoxic effect of 5-aminoimidazole-4-carboxamide-1-beta-4-ribofuranoside (AICAR) on childhood acute lymphoblastic leukemia (ALL) cells: implication for targeted therapy*. Mol Cancer, 2007. **6**: p. 46.
190. Alvarado-Kristensson, M. and T. Andersson, *Protein phosphatase 2A regulates apoptosis in neutrophils by dephosphorylating both p38 MAPK and its substrate caspase 3*. J Biol Chem, 2005. **280**(7): p. 6238-44.
191. Cseh, B., E. Doma, and M. Baccharini, *"RAF" neighborhood: protein-protein interaction in the Raf/Mek/Erk pathway*. FEBS letters, 2014. **588**(15): p. 2398-2406.
192. Srivastava, A., et al., *Emerging Functional Divergence of beta-Arrestin Isoforms in GPCR Function*. Trends Endocrinol Metab, 2015. **26**(11): p. 628-642.
193. Li, G., et al., *Distinct kinetic and spatial patterns of protein kinase C (PKC)- and epidermal growth factor receptor (EGFR)-dependent activation of extracellular signal-regulated kinases 1 and 2 by human nicotinic acid receptor GPR109A*. J Biol Chem, 2011. **286**(36): p. 31199-212.
194. Lacreusette, A., et al., *Loss of oncostatin M receptor β in metastatic melanoma cells*. Oncogene, 2007. **26**(6): p. 881-892.
195. Dhar, K., et al., *SOCS3 promotor hypermethylation and STAT3-NF- κ B interaction downregulate SOCS3 expression in human coronary artery smooth muscle cells*. Am J Physiol Heart Circ Physiol, 2013. **304**(6): p. H776-85.
196. Böcker, U., et al., *Butyrate modulates intestinal epithelial cell-mediated neutrophil migration*. Clin Exp Immunol, 2003. **131**(1): p. 53-60.
197. Schroder, O., et al., *Mediation of differentiating effects of butyrate on the intestinal cell line Caco-2 by transforming growth factor-beta 1*. Eur J Nutr, 1999. **38**(1): p. 45-50.
198. Bandres, E., et al., *Epigenetic regulation of microRNA expression in colorectal cancer*. Int J Cancer, 2009. **125**(11): p. 2737-43.
199. Thangaraju, M., et al., *GPR109A is a G-protein-coupled receptor for the bacterial fermentation product butyrate and functions as a tumor suppressor in colon*. Cancer Res, 2009. **69**(7): p. 2826-32.
200. Htwe, S.S., et al., *Investigating NF- κ B signaling in lung fibroblasts in 2D and 3D culture systems*. Respiratory research, 2015. **16**: p. 144-144.
201. Ruemmele, F.M., et al., *Butyrate induced Caco-2 cell apoptosis is mediated via the mitochondrial pathway*. Gut, 2003. **52**(1): p. 94-100.
202. Petta, S., et al., *Pathophysiology of Non Alcoholic Fatty Liver Disease*. Int J Mol Sci, 2016. **17**(12).

I List of scientific abbreviations and acronyms

Aqua dest.	distillated water
AP-1	Activator protein 1
β- Arr.	beta – Arrestine
Ca ²⁺	calcium-ion
cAMP	cyclic adenosine – monophosphate
CCL/ CXCL	chemokine-receptor ligand (= chemokine)
CpGs	cytosine-/guanine- dinucleotides, that induce immune reactions
CREB	cAMP response element binding protein
CRP	capsule polysaccharide C reactive protein
CT- value	cycle- threshold- value
cDNA	complementary DNA
DAG	diacyl-glycerol
DC	dendritic cell
DMEM	Dulbecco’s modified eagle medium
DMSO	Dimethylsulfoxid
DNA	deoxyribonucleic acid
DNMT1	DNA – methyltransferase 1
DSS	dextran sulfat sodium
EGFR	epidermal growth factor receptor
ER	endoplasmic reticulum
ERK	extracellular signal reactive kinase
EtOH	ethanol
Gi/o	adenylate-cyclase- inhibiting GTP-binding protein
GP130	Glycoprotein 130 (= Oncostatin M-receptor subunit)
GPR	GTP-binding protein coupled receptor
Gq	(phospholipase C activating) GTP- binding q-protein

GTP	guanosintriphosphate
HATs	histone acetyl transferases
HDACs	histone – deacetylases
HDAC-I.	histone - deacetylase inhibitor
<i>hHPRT</i>	human hypoxanthin-phosphoribosyl-transferase-encoding gene
<i>hRPLP0</i>	human ribosomal protein lateral stalk subunit P0-encoding gene
IBD	inflammatory bowel disease
IECs	intestinal epithelial cells, in the narrower sense: enterocytes (ECs), but also containing goblet cells (GCs), paneth cells, multifold (M-) cells and enteroendocrine cells.
IgA	immunoglobulin A
I κ B α	α - subunit of the inhibitory factor of NF κ B
IKK	I κ B-kinase kinase
IL	interleukin
IL-1 β -R.	interleukin 1-beta receptor
IP3	inositol 1,4,5–triphosphate
JAKs	Janus kinases
JNK	c-Jun-N-terminal kinase
LIF	leukemia inhibitory factor
LIFR	LIF-Receptor (= Oncostatin M -receptor subunit)
LPS	lipopolysaccharide (= membrane component of gram-negative bacteria
MCT-1	monocarboxylate transporter- 1
MEK (=MKK)	mitogen- activated protein kinase (MAPK) kinase
MK2	MAPK-activated protein kinase 2
MKKK	mitogen-activated protein kinase kinase kinase
mRNA	messenger ribonucleic acid

p38 MAPK	mitogen- activated protein kinase p38
Na ⁺	Sodium ion
NFκB	nuclear factor kappa-light-chain-enhancer of activated B-lymphocytes
mTOR	mechanistic target of Rapamycin
OSM	Oncostatin M
OSMR(β)	Oncostatin M receptor (subunit beta)
PBS	phosphate buffered saline
PIAS	protein inhibitor of activated STAT
PI3K	Phosphoinositol-3-kinase
PIP2	phosphatidylinositol 4,5- bisphosphate
PKA	proteinkinase A
PKCδ	proteinkinase C delta
PLC	phospholipase C
PPARγ	peroxisome proliferator activated receptor gamma
PP2A	protein-phosphatase 2 A
PRR	pathogen-recognition receptor
qPCR	quantitative polymerase chain reaction
Raf	rapidly accelerated fibrosarcoma (serine-/threonine- kinase)
Ras	small protein in a complex with Raf
RegIII	regenerating islet-derived protein III
SH2	Src- homology region 2
SHP2	Src- homology region- containing protein tyrosine phosphatase 2
SOCS3	suppressor of cytokine signaling 3
STAT	signal transducer and activator of transcription
TBS-T	tris-buffered saline with Tween20
TCEP	tris-2-carboxyethyl-phosphine
TEMED	Tetramethylethylenediamine
TGF-β	transforming growth factor – beta

TLR	toll – like receptor = one form of pathogen-recognition-receptors
TNF α	tumor necrosis factor alpha
TNFR	TNF α - receptor
TRIS	tris(hydroxymethyl)-aminomethane (buffer substance)
TSA	Trichostatin A
Tyr	tyrosine
VDR	vitamin D3- receptor
Zn ²⁺	zinc ion

Other abbreviations

ChIP	histochemic immunoprecipitation
ELISA	enzyme-linked immunosorbent assay
FACS	fluorescence activated cell sorting
i.a.	inter alia
M.	morbus
n	sample
n.s.	not significant
Phospho-/ p-	phosphorylated
rev.	reviewed
Spp.	species
syn.	synonym
vs.	versus
WT	wild type

II List of figures

	<i>Page</i>
Figure 1: Interdependent dysbiosis-contributing conditions and connected disease susceptibilities - includes an element of Dr. Georg Wittschiers webpage www.wittschier.com , "Magen-Darm-Trakt"; access to website and received permission on 22/04/2018: "...Können sie gerne verwenden." (e-mail@wittschier.com); includes a drawing of the liver, formerly used in a review by S.Petta, F.Bonino et al. in 2016 [202], permission received on 12/04/2021 "We are very pleased to grant you for sure the permission..." (ferruccio.bonino@unipi.it)	4
Figure 2: Molecular structure of a) butyric acid and b) sodium butyrate	6
Figure 3: Homeostasis	8
Figure 4: Acute inflammation and recovery	9
Figure 5: Chronic inflammation Fig.3. includes drawings of intestinal epithelial cells, picked from the paper by Eran Elinav et al. in 2014 [25], received permission on 25/03/2021: "Sure. Enjoy. EE" (e.elinav@dkfz-heidelberg.de)	10
Figure 6: GPR signaling and connections with MAP kinases	16
Figure 7: Structural organization of STAT3	18
Figure 8: Signaling via the JAK/STAT pathway	20
Figure 9: Sodium butyrate incubation assays	30
Figure 10: TSA incubation assays	31
Figure 11: SB202190 and SB203580 incubation assays	33
Figure 12: 2D/3D- cell culture assays for Fig. 12a and 12b, picture permission received on 11/10/2019 from Matthias Schweinlin, TERM Würzburg: "Gerne kannst du die Fotos in deiner Arbeit verwenden. Beste Grüße, Matthias" (matthias.schweinlin@uni-wuerzburg.de)	35 - 36
Figure 13: Measurement of the primer efficacy	40
Figure 14: PCR amplification plot	41
Figure 15: Matching of sample doublets	50
Figure 16: pS727-STAT3 in the butyrate incubation assays	55
Figure 17: Time-dependent, butyrate-caused changes in pS727-STAT3 and pp38 MAPK	56
Figure 18: total STAT3 in the butyrate incubation assays	58
Figure 19: hSTAT3 expression in the butyrate incubation assays	59

Figure 20: pS727-STAT3 and total STAT3 in the TSA incubation assays	60
Figure 21: CACO-2 cell monolayer with or without a butyrate/ TSA treatment.....	62
Figure 22: <i>hSTAT3</i> expression in the TSA incubation assays	63
Figure 23: pS727-STAT3 in the SB202190 and SB203580 incubation assays	65 – 66
Figure 24: Effects of TNF α or OSM on pS727-STAT3 and total STAT3 protein ...	68 – 69
Figure 25: Butyrate influence on pY705-STAT3 protein in OSM-stimulated cells	71
Figure 26: <i>hOSMRβ</i> qPCR results in the butyrate incubation assays	73
Figure 27: <i>hOSMRβ</i> qPCR results in the TSA incubation assays	74
Figure 28: pY705-STAT3 after TNF α treatment +/- butyrate influence	75
Figure 29: <i>hSOCS3</i> qPCR results in with a) Butyrate or b) TSA treated samples	77
Figure 30: <i>hSOCS3</i> qPCR results in TNF α or OSM treated samples (+/- butyrate).....	78
Figure 31: <i>hCXCL-8-(a)</i> and <i>hCCL-2-(b)</i> qPCR results in 48h-butyrate treated samples.....	81
Figure 32: α -I κ B protein results	82
Figure 33: <i>hCXCL-8</i> and <i>hCCL-2</i> qPCR results in dependency of TNF α	83
Figure 34: <i>hCXCL8-</i> and <i>hCCL-2-</i> qPCR results in dependency of OSM	84
Figure 35: <i>GPR109A</i> qPCR results in 2D vs. 3D	86
Figure 36: <i>hCXCL-8</i> qPCR results in 2D vs. 3D	89
Figure 37: <i>hCCL20</i> qPCR results in 2D vs. 3D	91
Figure 38: <i>hTNFα</i> qPCR results in 2D vs. 3D	93
Figure 39: <i>hCCL2</i> -qPCR results in 2D vs. 3D	94
Figure 40: Summary of effects and hypotheses (created in BioRender.com).....	116

III List of tables

	<i>Page</i>
Table 1: Cell culture medium and -agents	28 – 29
Table 2: Cytokines and agents	32
Table 3: Primer sequences	42 - 43
Table 4: Western blot and electrophoresis buffers and reagents	46 - 47
Table 5: Antibodies	48 - 49

IV Danksagung

Ich möchte an erster Stelle meiner Familie, meinen Eltern, Großeltern und meinem Bruder danken,
die mein Interesse für die Vorgänge in der Natur und die Liebe zu den Lebewesen durch ihr Beispiel gefördert haben,
mich bestärkt und unterstützt haben
und bei denen ich stets einen Rückhalt weiß.

Danke!

Weiterhin möchte ich mich bei Frau Dr. Heike Hermanns und Herrn Dr. Daniel Jahn für die Betreuung meiner Arbeit und das Beisteuern wichtiger Ideen, für ihre Hilfestellungen bei der fachlichen und praktischen Umsetzung, für die Bereitstellung der Materialien, für ihre Geduld und ihr Interesse sowie für die inspirierenden Diskussionen recht herzlich bedanken!

Herrn Professor Andreas Geier danke ich sehr für die Möglichkeit, mich mit einem mich sehr interessierenden Themenbereich in seiner Abteilung inhaltlich und praktisch beschäftigen zu dürfen, für textliche Anregungen sowie für seine Motivation zur Teilnahme an Kongressen.

Ich danke Frau Dr. Monika Rau für die Bereitstellung des Themenschwerpunktes und dass sie mich zu einem breiten Literaturstudium motivierte.

Ich danke Frau Dr. Sabine Herterich, Frau Dr. Dorothee Rogoll, Leonhard Wagner, Donata Dorbath, Charel Breier, Julia Wohlfahrt und Philipp Lederer für ihre stete Hilfsbereitschaft und den Austausch sowie Herrn Professor Andreas Beilhack für das Mutmachen in einer schwierigen Phase.

Ich danke Frau Professor Heike Walles, Herrn Dr. Matthias Schweinlin, Frau Christina Fey und weiteren Mitarbeitern des Fraunhofer - Instituts für Tissue Engineering Würzburg für die Einführung in die CACO-2- und 3D-scaffold-Zellkultur-Technik und die Möglichkeit, mit diesem Modell zu arbeiten.

Vielen Dank!